

Functional characterization of two genes of the GDSL hydrolase gene family

Dissertation

der Mathematisch-Naturwissenschaftlichen Fakultät

der Eberhard Karls Universität Tübingen

zur Erlangung des Grades eines

Doktors der Naturwissenschaften

(Dr. rer. nat.)

vorgelegt von

Ritwika Kar

aus Bankura, Indien

Tübingen

2020

Tag der mündlichen Qualifikation: 19.06.2020

Dekan: Prof. Dr. Wolfgang Rosenstiel

1. Berichterstatter: Prof. Dr. Christopher Grefen

2. Berichterstatter: Prof. Dr. Klaus Harter

Acknowledgements

First of all, I would like to express my gratitude to my mentor and PhD supervisor Prof. Dr. Christopher Grefen who helped me to grow as a scientist. His encouragement, support and critical advices enriched me with motivation over the years. I would like to thank Emmy Noether fellowship of the DFG (GR425/1-1) for funding and supporting the project.

I am greatly obliged to Prof Dr. Klaus Harter and Dr. Martin Bayer for being members of my thesis committee. Their valuable suggestions and advices helped me throughout the PhD. I would like to thank Prof. Dr. Claudia Oeking and Dr. Sabine Müller for being the examiner in my examination committee.

For the great working environment and collegiality, I would like to thank entire Grefen lab. Doing research in such an amazing and helpful atmosphere was truly inspiring. I am especially grateful to Lisa Asseck, Dietmar Mehlhorn, Niklas Wallmeroth, Dr. Shuping Xing, Dr. Martiniano Ricardi and Eva Schwörzer for their constant help, motivation and support. I would also like to thank members of Müller lab, with whom I shared my lab space, specially Dr. Sabine Müller, Theresa Lauster, Dr. Arvid Herrmann, Steffi Zimmermann and Dr. Pantelis Livanos. I would like to thank Dr. Pantelis

Livanos for great discussions about different aspects of stomata and his help in some of the experiments. I would also like to thank the whole department of developmental genetics in ZMBP, University Tübingen. The open floor structure provided a great opportunity for communication, discussion and collaboration with other research scientists in the institute. I would like to thank specially Ulrike Hiller, Dr. Manoj Singh, Dr. Misoon Park and Dr. Sandra Richter for the great support scientifically.

I am also thankful to Prof. Dr. Gabriel Schaaf and his team for their support during my early days in Germany. Especially Dr. Debabrata Laha and Dr. Nargis Parvin for constant motivation scientifically and personally and Dr. Marilia Campos for being my first supervisor.

I would like to thank all collaborators, Dr. Martin Bayer (Max Planck Institute, Tübingen), Prof. Dr. Markus Schwarzländer (University of Münster), Prof. Dr. Dominik Begerow (Ruhr-University, Bochum), Dr. Minou Nowrousian (Ruhr-University, Bochum), Dr. Arun Sampathkumar (Max Planck Institute, Golm), Central facilities of ZMBP, especially Dr. Mark Stahl, Dr. Joachim Kilian, Bettina Stadelhofer, Dr. York Stierhof and Dieter Steinmetz (ZMBP, Tübingen), Dr. Farid El Kasmi (ZMBP, Tübingen), Prof. Dr. Tilman Schäffer (Institute of Applied Physics, Tübingen) and CeGaT GmbH (Tübingen).

My deepest thanks belong to my loving family, my mother Swastika Kar, my father Rup Kumar Kar and my mother-in-law Susanne Pfeffer for their constant support, understanding and love every day, every situation. Without you nothing would be possible. I want to thank my mother for being my pillar of strength. Her constant love, care and

motivation allow me to grow up as a strong, independent person. Being a daughter of a Professor in Plant Physiology, my father is always my role model, which is an inspiration to walk into the world of science. His motivation and guidance, scientifically and personally, shaped me as a scientist and as a better human being. I would also like to thank my mother-in-law for her support and love. Thank you for being there in ups and downs and supporting me with positivity and trust in life.

A big gratitude goes to my two pet dogs, Ziko and Tarsky for their unconditional love and affection. Their company brought a great comfort to life. Thank you Tarsky for sitting next to me during my writing phase.

Finally, a special thanks to my loving husband, Dr. Franz Krah for being an amazing companion and a great support. Thank you for the regular scientific discussions and technical as well as personal support. Thanks for getting equally excited about world of stomata and not getting bored with molecular biology talks. Thanks for being there as a source of my strength and inspiration. Without your motivation, this PhD thesis would not have been possible. Ich liebe dich!

Abstract

Hydrolases are an important class of enzymes in living organisms. They include GDSL hydrolase, a family of hydrolytic enzymes with a broad range of substrates whose members are characterized by a distinct GDSL amino acid motif. In *Arabidopsis thaliana*, the GDSL hydrolase family contains 100 members, but the majority of the respective genes remain uncharacterized. Thus, the aim of this study is to characterize two homologous members of GDSL hydrolase, CGM3 and CGM4 (“Contains GDSL Motif”).

The full-length CGM3 and CGM4 proteins were localized in the apoplast. Although CGM3 and CGM4 share high sequence similarity, CGM3 was expressed in imbibed seeds, and CGM4 in the early lineage of stomatal development. However, in the absence of CGM4, CGM3 was expressed in the early stomatal lineage cells, suggesting that these homologous genes are, at least in part, functionally redundant. This thesis explores the function of the homologous genes CGM3 and CGM4, based on the results of anatomical, physiological, biophysical and biochemical experiments using *cgm3cgm4* T-DNA insertion lines.

A comparison of the stomatal patterning and index of *cgm3cgm4* and wild type showed no obvious differences, but the ultrastructure of the stomata included an appar-

ently thicker stomatal ledge in *cgm3cgm4* than in the wild type. Physiological experiments showed that, in response to various abiotic and biotic stimuli, *cgm3cgm4* plants had a tendency of a decreased width to length ratio of the stomatal pore (aperture index) and a transpiration rate lower than that of wild type plants. A transcriptome analysis showed no obvious differences in ABA-induced gene expression between *cgm3cgm4* and wild type plants. According to a biophysical analysis (atomic force microscopy) of the stiffness at the stomatal pore area, there was a tendency towards an increased stiffness in the stomata of the *cgm3cgm4* mutants but not in those of the wild type. Additionally, a biochemical analysis of the cell wall composition of the mutant plants suggested a reduction in the abundance of polyphenol derivatives compared to the wild type.

These results indicated that the *cgm3cgm4* plants have a mechanical defect in the opening-closing dynamics of their mature stomata, independent of ABA signaling. A mature stoma consists of two guard cells surrounding the stomatal pore. During the developmental process, stomatal precursors undergo symmetric cell division, giving rise to guard cells. At a later stage of development, the stomatal pore is formed between the guard cells. The guard cell wall facing the pore is a crucial site for the establishment of a typical, unevenly thickened, cell wall architecture and stomatal ledge, which influences the opening-closing dynamics of stomata. The research described in this thesis provides that the GDSL hydrolase genes *CGM3* and *CGM4* play roles in cell wall biogenesis, influencing stomatal opening-closing dynamics.

Zusammenfassung

Hydrolasen bilden eine wichtige Klasse von Enzymen in allen lebenden Organismen. Zu ihnen gehören die GDSL-Hydrolasen, eine Familie von hydrolytischen Enzymen mit einem breiten Substratspektrum, deren Mitglieder ein ausgeprägtes GDSL-Aminosäuremotiv beinhalten. Die Modellpflanze *Arabidopsis thaliana* umfasst 100 Mitglieder der GDSL-Hydrolase Familie, allerdings ist die Mehrheit der Gene noch nicht charakterisiert. Diese Arbeit zielt daher darauf ab, zwei homologe Mitglieder der GDSL-Hydrolasen, CGM3 und CGM4 ("Contains GDSL Motif") zu charakterisieren.

Die Proteine CGM3 und CGM4 wurden, in voller Länge, im Apoplast lokalisiert. Obwohl CGM3 und CGM4 eine hohe Sequenzähnlichkeit aufweisen, wurde CGM3 in gequellten Samen und CGM4 in der frühen Entwicklungslinie der Spaltöffnungen exprimiert. In Abwesenheit von CGM4 wurde CGM3 jedoch in den Zellen der frühen Entwicklungslinie der Spaltöffnungen exprimiert, was darauf hindeutet, dass diese homologen Gene zumindest teilweise funktionell redundant sind. Die vorliegende Arbeit benutzt anatomische, physiologische, biophysikalische und biochemische Experimente mit *cgm3cgm4* T-DNA-Insertionslinien, um die Funktion der homologen Gene CGM3 und CGM4 zu untersuchen.

Ein Vergleich der Spaltöffnungsstruktur und des Spaltöffnungsindex von *cgm3cgm4* und dem Wildtyp, zeigte keine offensichtlichen Unterschiede. Jedoch ergab eine Un-

tersuchung der Ultrastruktur der Spaltöffnungen im Falle von *cgm3cgm4* eine deutlich verdickte Spalt-öffnungsleiste im Vergleich zum Wildtyp. Physiologische Experimente zeigten, dass *cgm3cgm4* Pflanzen als Reaktion auf verschiedene abiotische und biotische Stimuli tendenziell ein geringeres Verhältnis von Breite zu Länge der Spaltöffnungsporen (Aperturindex) hatten und eine geringere Transpirationsrate als beim Wildtyp. Eine Transkriptomanalyse zeigte keine offensichtlichen Unterschiede in der ABA-induzierten Genexpression zwischen *cgm3cgm4*-Pflanzen und dem Wildtyp. Auf Grund einer biophysikalischen Analyse (Rasterkraftmikroskopie) der Steifigkeit im Bereich der Spaltöffnungsporen, zeigte sich eine tendenziell erhöhte Steifigkeit der *cgm3cgm4*-Mutanten, im Vergleich zum Wildtyp. Eine biochemische Analyse der Zellwand-zusammensetzung der mutierten Pflanzen, deutete zudem auf eine Verringerung der Häufigkeit von Polyphenol-Derivaten im Vergleich zum Wildtyp hin.

Diese Ergebnisse deuteten darauf hin, dass die *cgm3cgm4*-Pflanzen einen mechanischen Defekt, unabhängig von der ABA-Signalisierung, in der Öffnungs- und Schließdynamik ihrer reifen Spaltöffnungen aufweisen. Eine reife Spaltöffnung besteht aus zwei Schließzellen, die die Spaltöffnungspore umgeben. Während des Entwicklungsprozesses unterziehen sich die Vorläufer der Spaltöffnung einer symmetrischen Zellteilung, wodurch Schließzellen entstehen. In einem späteren Entwicklungsstadium wird die Spaltöffnungspore zwischen den Schließzellen gebildet. Die der Pore zugewandte Schließzellenwand ist eine entscheidende Stelle für die Bildung einer typischen, ungleichmäßig verdickten Zellwandarchitektur und einer Spaltöffnungsleiste, welche die Öffnungs- und Schließdynamik der Spaltöffnung beeinflusst. Die in dieser Arbeit beschriebene Forschung liefert Hinweise darauf, dass die GDSL-Hydrolase-Gene CGM3 und CGM4 eine wichtige Rolle in der Zellwandbiogenese spielen und die Öffnungs- und Schließdynamik der Spaltöffnungen beeinflussen.

Contents

1	Introduction	1
1.1	GDSL lipase/esterase, a family of hydrolases	1
1.2	Large GDSL hydrolases family	2
1.3	Phylogenetic analysis of GDSL hydrolases family	3
1.4	Localization of GDSL hydrolases family	5
1.5	Stomata	7
1.6	Developmental pathway of Stomata	9
1.7	Stomatal patterning and receptor like kinases	11
1.8	Stomatal function	12
1.9	Mechanical properties of stomata	15
1.10	Seed germination	19
1.11	Known GDSL hydrolases in cell wall modification	20
2	Material and Methods	23
2.1	Molecular biology	23
2.1.1	Polymerase chain reaction (PCR)	23
2.1.2	Restriction digestion reaction	24
2.1.3	Plasmid extraction protocol	24

2.1.4	Gateway cloning techniques	25
2.1.5	BP clonase reaction	25
2.1.6	LR clonase reaction	26
2.1.7	<i>Escherichia coli</i> mediated transformation	26
2.1.8	<i>Agrobacterium tumefaciens</i> mediated transformation	27
2.1.9	Colony PCR for positive transformants	28
2.1.10	<i>Agrobacterium tumefaciens</i> mediated floral dipping	29
2.1.11	<i>Nicotiana benthamiana</i> infiltration for transient expression assay	29
2.1.12	Quantitative Real-Time PCR (qRT-PCR) analysis	30
2.1.13	Transcriptome analysis using RNAseq	31
2.2	Cloning of different expression vectors	32
2.2.1	Cloning of GW-nls-eGFP vector	32
2.2.2	Cloning of Promoter of interest(POI)/p35S-mScarlet-3xHA . . .	33
2.2.3	Cloning of CGM3 and CGM4 promoter construct	33
2.3	Plant growth	34
2.3.1	Plant growth condition	34
2.3.2	T-DNA insertion lines	34
2.3.3	Vapor phase seed sterilization	35
2.4	Plant physiology	36
2.4.1	Stomatal aperture analysis	36
2.4.2	Gas exchange analysis	36
2.4.3	Drought stress evaluation	37
2.4.4	Growth assay under differential light regimes	38
2.4.5	Reactive oxygen species (ROS) accumulation assay	38
2.4.6	Germination assay	39

2.5	Microscopy	40
2.5.1	Confocal microscopy	40
2.5.2	Scanning electron microscopy (SEM)	40
2.5.3	Atomic force microscopy (AFM)	41
2.6	Biochemical assay of cell wall	42
2.6.1	Cell wall extraction	42
2.6.2	Metabolomics analysis	42
2.6.3	Immunostaining with the pectin epitopes	43
2.6.4	Apoplastic sap extraction	44
2.6.5	Pectate lyase assay with commercial kit	45
3	Results	47
3.1	Subcellular localization of CGM3 and CGM4	47
3.2	Tissue-specific expression of CGM4	52
3.3	Tissue-specific expression of CGM3	55
3.4	Overall phenotype of <i>cgm3cgm4</i> plants	60
3.5	Stomatal index and patterning in <i>cgm3cgm4</i>	61
3.6	Stomatal aperture index in <i>cgm3cgm4</i> and CGM4ox under different abiotic stimuli	63
3.7	Reactive oxygen species (ROS) accumulation assay in <i>cgm3cgm4</i> and wild-type Col-0	67
3.8	Gas exchange in <i>cgm3cgm4</i> and CGM4ox in response to different abiotic stimuli	70
3.9	Response of <i>cgm3cgm4</i> and CGM4ox to pathogens	73
3.10	Effects of drought stress in <i>cgm3cgm4</i> and CGM4ox	75

3.11	ABA-induced gene transcription in <i>cgm3cgm4</i> and wild-type Col-0 . . .	78
3.12	Growth of <i>cgm3cgm4</i> and CGM4ox under different light regimes	82
3.13	Biochemical assay of cell wall composition of <i>cgm3cgm4</i> and CGM4ox leaves	85
3.14	Immunolabelling of stomatal cell wall with pectin epitopes	89
3.15	Scanning electron microscopy of the stomata of wild type Col-0 and <i>cgm3cgm4</i>	91
3.16	Transverse views of stomatal structure as revealed using confocal mi- croscopy	93
3.17	The abundance of unsaturated pectin products in cell wall extracts . . .	95
3.18	Quantification of stomatal pore area stiffness using atomic force mi- croscopy (AFM)	97
3.19	CGM4 expressed under the guard cell specific promoter	100
3.20	Germination of <i>cgm3cgm4</i> and CGM4ox	104
3.21	Effect of Abscisic Acid (ABA) and Gibberellic acid (GA3) on germination	106
3.22	Co-expression of other GDSL hydrolases with CGM4 in the stomatal lineage	108
4	Discussion	111
4.1	CGM4 and CGM3 are extracellular proteins	111
4.2	CGM4 expressed during the stomatal lineage development	114
4.3	CGM4 influences the mature stomatal function	116
4.4	CGM4 involved in cell wall biosynthesis of the guard cell	122
4.5	CGM3 involved in seed germination process	126

4.6	Potential involvement of other GDSL hydrolases in stomatal development and function	128
5	Conclusion and Conceptual Model	129
6	Future directions	133
6.1	Stage-specific expression of CGM4	133
6.2	Subcellular localization of CGM3 and CGM4 with an organelle-retaining motif	134
6.3	Standardization of protein extraction protocol from apoplastic sap . . .	135
6.4	Extensive immunolabeling with multiple cell-wall-related epitopes and high-resolution microscopy	136
6.5	Standardization of the cell wall extraction protocol for assays of the cell wall composition	136
6.6	Atomic Force Microscopy for measuring stomatal stiffness	137
6.7	Ultrastructure of imbibed seeds and fatty acid content	137
6.8	Multiple knock-out lines of other GDSL candidates with <i>cgm3cgm4</i> . .	138
A	Appendices	141
	Bibliography	157

List of Figures

1.1	Conserved sequence blocks of GDSL hydrolases in prokaryotic and eukaryotic genomes	2
1.2	Phylogenetic tree of <i>Arabidopsis thaliana</i> GDSL hydrolases.	5
1.3	Conventional protein secretory pathway in plants	6
1.4	<i>Arabidopsis thaliana</i> stomata	8
1.5	Developmental pathway of stomata	11
1.6	Receptor-like kinases and proteins involved in stomatal development . .	12
1.7	Stomatal opening	14
1.8	Stomatal closing	14
1.9	Simple outline of Plant cell wall composition	18
1.10	Known GDSL hydrolase functions in <i>Arabidopsis thaliana</i>	21
3.1	Signal peptide prediction in CGM3 and CGM4	49
3.2	Subcellular localization of CGM4 transiently expressed in <i>Nicotiana benthamiana</i> leaves	50
3.3	Subcellular localization of CGM4 in root epidermis of <i>Arabidopsis thaliana</i>	51
3.4	Tissue specific expression of CGM4	53
3.5	Expression of CGM4 in <i>spch</i> and <i>fama</i>	54

List of Figures

3.6	Expression of CGM3 in imbibed seeds	56
3.7	Transcript analysis of CGM3 by semiquantitative RT-PCR in imbibed seeds	57
3.8	Expression pattern of CGM3 in wild type Col-0 and <i>cgm4</i>	58
3.9	Tissue specific expression of CGM3 in <i>cgm4</i>	59
3.10	Phenotype of <i>cgm3cgm4</i>	60
3.11	Stomatal patterning and stomatal index in <i>cgm3cgm4</i>	62
3.12	Stomatal aperture index in <i>cgm3cgm4</i>	65
3.13	Stomatal aperture index in CGM4ox and CGM4 ^{dSP} ox	66
3.14	Reactive oxygen species (ROS) accumulation in <i>cgm3cgm4</i> stomata . .	68
3.15	Reactive oxygen species (ROS) accumulation in <i>cgm3cgm4</i> stomata under ABA and DPI treatment	69
3.16	Gas exchange measurement of <i>cgm3cgm4</i> and CGM4ox under different light conditions	71
3.17	Gas exchange measurement of <i>cgm3cgm4</i> and CGM4ox under different CO ₂ concentrations	72
3.18	Pathogen assay with <i>Pseudomonus syringae</i> pv. Tomato DC3000 on <i>cgm3cgm4</i> and CGM4ox leaves	74
3.19	Drought stress assay on <i>cgm3cgm4</i> and CGM4ox	76
3.20	Water loss assay on <i>cgm3cgm4</i> and CGM4ox leaves over time	77
3.21	Transcriptome analysis in <i>cgm3cgm4</i> and wild type Col-0 leaves treated with and without ABA	79
3.22	Transcriptome analysis of ABA induced genes in <i>cgm3cgm4</i> and wild type Col-0 leaves treated with and without ABA	80

3.23	Growth of wild type Col-0 and <i>cgm3cgm4</i> plants under different light regime	84
3.24	Sugar composition in cell wall of <i>cgm3cgm4</i> and CGM4ox	87
3.25	Metabolomics assay of <i>cgm3cgm4</i> and CGM4ox leaf cell wall	87
3.26	Metabolomics assay in the apoplastic fluid from transiently expressed CGM4	88
3.27	Immunolabelling of stomatal cell wall with pectin epitopes in <i>cgm3cgm4</i> and CGM4ox	90
3.28	Scanning electron microscopy of individual stomate of wild type Col-0 and <i>cgm3cgm4</i>	92
3.29	Transverse section of stomata using confocal microscopy in <i>cgm3cgm4</i>	94
3.30	Pectate lyase assay for abundance of unsaturated products in cell wall extract of <i>cgm3cgm4</i> and CGM4ox	96
3.31	Topography of stoma in wild type Col-0 and <i>cgm3cgm4</i> using AFM	98
3.32	Median stiffness of stoma and surrounding leaf tissues of wild type Col-0 and <i>cgm3cgm4</i>	99
3.33	Differences in relative stomatal stiffness in wild type Col-0 and <i>cgm3cgm4</i>	99
3.34	Expression and localization of pGC1:CGM4-GFP	101
3.35	Gas exchange measurement of pGC1:CGM4-GFP	102
3.36	Stomatal aperture index of pGC1:CGM4-GFP with or without ABA treatment	103
3.37	Germination assay of <i>cgm3cgm4</i> and other mutant lines	105
3.38	Effect of GA3 on germination of <i>cgm3cgm4</i> and other mutant lines	107
3.39	Effect of ABA on germination of <i>cgm3cgm4</i> and other mutant lines	107

List of Figures

3.40	Co-expression analysis of other GDSL lipase with CGM4 using ATTED-II	109
3.41	Promoter localization of the other GDSL lipases	109
5.1	Conceptual model	131
6.1	Genotyping of <i>cgm3cgm4cgm19cgm21</i>	139
A.1	Scanning electron microscopy of individual stomate of wild type Col-0 and <i>cgm3cgm4</i>	142

List of Tables

1.1	Known GDSL hydrolases in plants	3
1.2	Known GDSL hydrolases in <i>Arabidopsis thaliana</i>	4
2.1	T-DNA insertion lines (seeds)	35
3.1	Transcriptome analysis of ABA-induced genes in ABA-treated Col-0 vs Col-0	80
3.2	Transcriptome analysis of ABA-induced genes in ABA-treated <i>cgm3cgm4</i> vs Col-0	81
3.3	Transcriptome analysis of ABA-induced genes in ABA-treated <i>cgm3cgm4</i> vs ABA-treated Col-0	82
A.1	Entry clones	143
A.2	Destination clones	144
A.3	Chemicals	145
A.4	Primer sequences	147

Chapter 1

Introduction

1.1 GDSL lipase/esterase, a family of hydrolases

Hydrolases comprise a class of enzymes that cleave bonds by hydrolysis. Their broad substrate specificity includes esters, lipids, peptides, triglycerides, amides and halides (Fojan *et al.*, 2000; Akoh *et al.*, 2004; Ding *et al.*, 2019). Historically, hydrolases have been classified according to their specific substrate. Two broad classes are esterases, which break down ester bonds of short-chain fatty acids, and lipases, which target the long-chain fatty acids (Verger, 1997; Carrière *et al.*, 1998; Fojan *et al.*, 2000). Most esterases contain the highly conserved sequence motif GxSxG, with serine as the active site of the enzymes (Winkler *et al.*, 1990; Brzozowski *et al.*, 1991; Schrag *et al.*, 1991; Akoh *et al.*, 2004).

A subfamily of these hydrolytic/lipolytic enzymes is characterized by a different conserved motif, consisting of a GDSL sequence (Upton, 1995; Akoh *et al.*, 2004). Unlike the common lipases, members of this GDSL lipase/esterase subfamily (hereafter GDSL hydrolases) lack the so-called nucleophilic elbow and instead have a flexible active site.

The conformation of the flexible active site can change according to the available substrate, thus allowing binding to different substrates (Mølgaard *et al.*, 2000; Chepyshko *et al.*, 2012). GDSL hydrolases contain four important Ser, Gly, Asn and His catalytic residues located within four conserved sequence blocks: I, II, III and V. GDSL hydrolases are found in both the eukaryotic and the prokaryotic kingdom, with the five consensus sequence blocks highly conserved in both (Brick *et al.*, 1995; Upton, 1995; Mølgaard *et al.*, 2000; Akoh *et al.*, 2004; Ding *et al.*, 2019) (Fig.1.1).

	Block-I	Block-II	Block-III	Block-IV	Block-V
<i>Streptomyces rimosus</i>	yVAlGDSYsSgv	-----GsvDsss	-tdLVsitiGgND-	GesacL-----aria	wlhS--vTlPve
<i>Vibrio parahaemolyticus</i>	VVALGDSLSDtG	npnswFlchFSnGf	aNtLftLefGlnDF	GAknfmLmtLPDatkaP	Fvf-WDvThPTT
<i>Aeromonas hydrophila</i>	IVmFGDSLSDtG	sSPpyYeGrFSnGp	-ddLViLwvGaNdy	GAKeiLLfnLPDLGQnP	F---WDqvhPTT
<i>Pseudomonas putida</i>	MivFGDSLSDaG	vSPmilgSglgvnp	-NaLyyLtgGgNDF	GARYimvwlLPDLGQtP	waiSWqqvlpST
<i>Populus trichocarpa</i>	FFIFGDSfLDAG	PTGRFSdGRlapDfi	SKaWYlfsIGSNDY	GgRKFafinVpplGC1Pt	EYVFWdsiHltE
<i>Oryza sativa</i>	lFVFGDSiVDAG	aTGRFSNGKvpgDi	SeslYmWvtGtdDl	GARrvnVAGappIGCvP	kFLFDtYHltE
<i>Arabidopsis thaliana</i>	YFIFGDSLVDSG	PTGRFSNGKTTvDv	SKCIYSIGLGSNDY	GARKFaLvGIGaIGCsP	EYVFWdaFHPGE
<i>Nicotiana tabacum</i>	YFIFGDSLVDnG	PTGRFSNGKTTvDv	SKCIYSVGLGSNDY	GARKFvLiGVGqIGCsP	EYLFWdaFHPGE
<i>Vitis vinifera</i>	YFIFGDSLVDnG	PTGRFSNGKTTvDv	SKCIYSIGLGSNDY	GARKvVLiGVGqIGCsP	EYLFWdaFHPGE
<i>Alligator sinensis</i>	IaALGDSLTAGS	gGyStGsGpntPN	DWKlvTLFIGNDL	GAkAlnMstQArtLVEl	sFFavDCFFHae
<i>Mus musculus</i>	IGALGDSLTAGN	KGFSVGTGKEstrsr	DWKIITvFIGNDL	GARAqDMPAQaktLVkK	TFfSEDCFFHSD
<i>Homo sapiens</i>	IGALGDSLTAGN	KGFSVGTGKETSPN	DWKIITLFIGNDL	GARArDMPAQawDLVER	TFfSEDCFFHSD
<i>Macaca mulatta</i>	IGALGDSLTAGN	KGFSVGTGKETSSn	DWKIITLFIGNDL	GARArDMPAQawDLVER	TFfSEDCFFHSD

Figure 1.1: Conserved sequence blocks and conserved catalytic residues of GDSL hydrolases in prokaryotic and eukaryotic genomes. The red arrows and boxes indicate the catalytic residues Ser, Gly, Asn and His in conserved blocks I, II, III and V.

1.2 Large GDSL hydrolases family

Multigene families arise via gene duplications at the chromosomal or full-genome level (Volokita *et al.*, 2010). Evolutionarily, the retention of these duplicated genes reflects their having provided a selective advantage or divergent function, such as the acquisition of a new function or a sub-functionalization of an ancestral function. In plants, the genes encoding GDSL hydrolases belong to a large gene family and several, from different plant genomes, have been sequenced and functionally characterized, including *Oryza*

sativa, *Zea mays*, *Brassica sp.* and *Arabidopsis thaliana*. Some of the known plant GDSL hydrolases and their characterized functions are listed in Table 1.1.

In *Arabidopsis thaliana*, there are 100 putative genes containing specific GDSL motifs (Chepyshko *et al.*, 2012; Lai *et al.*, 2017; Ding *et al.*, 2019) (Fig.1.2). These genes are distributed across the five *Arabidopsis thaliana* chromosomes and several have been functionally characterized (Table 1.2) whereas the functions of many others are thus far unknown.

Table 1.1: Known GDSL hydrolases in plants

Gene	Plant genome	Biochemical function	Reference
Endo8	<i>Medicago sativa</i>	Acetyl and butyle	(Coque <i>et al.</i> , 2008)
	<i>Medicago truncatula</i>	esterase activity	(Dickstein <i>et al.</i> , 1993)
BnSCE3/ BnLIP2	<i>Brassica napus</i>	Sinapine esterase activity of long-chain aliphatic esters	(Clauß <i>et al.</i> , 2008)
CaGLIP1	<i>Capsicum annuum</i>	Hydrolytic activity for short and long-chain p-nitrophenyl esters	(Hong <i>et al.</i> , 2008)
	<i>Helianthus annuus</i>	Fatty acyl ester hydrolytic activity	(Beisson <i>et al.</i> , 1997)
	<i>Glycin max</i> <i>Solanum tuberosum</i> <i>Oryza sativa</i>	Non-specific acyl ester hydrolytic activity	(Beisson <i>et al.</i> , 1997)
BS1	<i>Oryza sativa</i>	Xylan deacetylation	(Zhang <i>et al.</i> , 2017)
MHZ11	<i>Oryza sativa</i>	Regulates ethylene signaling through sterol homeostasis	(Zhao <i>et al.</i> , 2020)

1.3 Phylogenetic analysis of GDSL hydrolases family

During the course of evolution, the *Arabidopsis thaliana* genome has undergone large segmental duplications of chromosomal regions along with small-scale duplications and

Table 1.2: Known GDSL hydrolases in *Arabidopsis thaliana*

Gene	Biological function	Reference
AtFXG1	Regulation of plant cell wall components	(de la Torre <i>et al.</i> , 2002)
AtLTL1	LiCl stress tolerance	(Naranjo <i>et al.</i> , 2006)
ESM1	Controls glucosinolate hydrolysis and/or insect herbivory resistance	(Zhang <i>et al.</i> , 2006)
Arab-1	Role in developmental processes	(Mikleušević <i>et al.</i> , 2009)
EXL4	Increases hydration in early pollination stage	(Updegraff <i>et al.</i> , 2009)
CDEF1	Cutinase activity	(Takahashi <i>et al.</i> , 2009)
GLIP1	Regulates systemic resistance associated with ethylene signalling	(Kwon <i>et al.</i> , 2009), (Kim <i>et al.</i> , 2013, 2014)
GLIP2	Important in plant immune response against <i>Erwinia carotovora</i> via negative regulation of auxin signalling	(Lee <i>et al.</i> , 2009)
SFARs	Associated with total seed fatty acid content and composition	(Chen <i>et al.</i> , 2012), (Huang <i>et al.</i> , 2015), (Karunarathna <i>et al.</i> , 2020)
RVMS	Restores fertility of thermo-sensitive male sterile plants	(Zhu <i>et al.</i> , 2020)

local re-arrangement events leading to the current complex genome and its inclusion of large gene families such as GDSL hydrolases (Cannon *et al.*, 2004; Lai *et al.*, 2017). Several gene families in *Arabidopsis thaliana* have evolved through occasional polyploidy or large segmental duplication events, resulting in identical gene sequences in multiple locations of the genome, both intrachromosomally and interchromosomally (Cannon *et al.*, 2004). Population genetics modeling has shown that the duplicated genes resulting from segmental duplication events can be retained in the genome, especially when they acquire novel functions or sub-functionalized the ancestral function (Levasseur and Pontarotti, 2011; Panchy *et al.*, 2016). A detailed phylogenetic analysis of the segmental duplication events in *Arabidopsis thaliana* revealed the retention of 11 pairs of GDSL genes during evolution, including AT5G45670 (CGM3) and AT4G18970

(CGM4) (Lai *et al.*, 2017). Although *in-silico* data showed the differential expression of these two GDSL genes in distinct tissues (imbibed seeds and young leaf tissue, respectively), they share 90% sequence similarity (Fig.1.2).

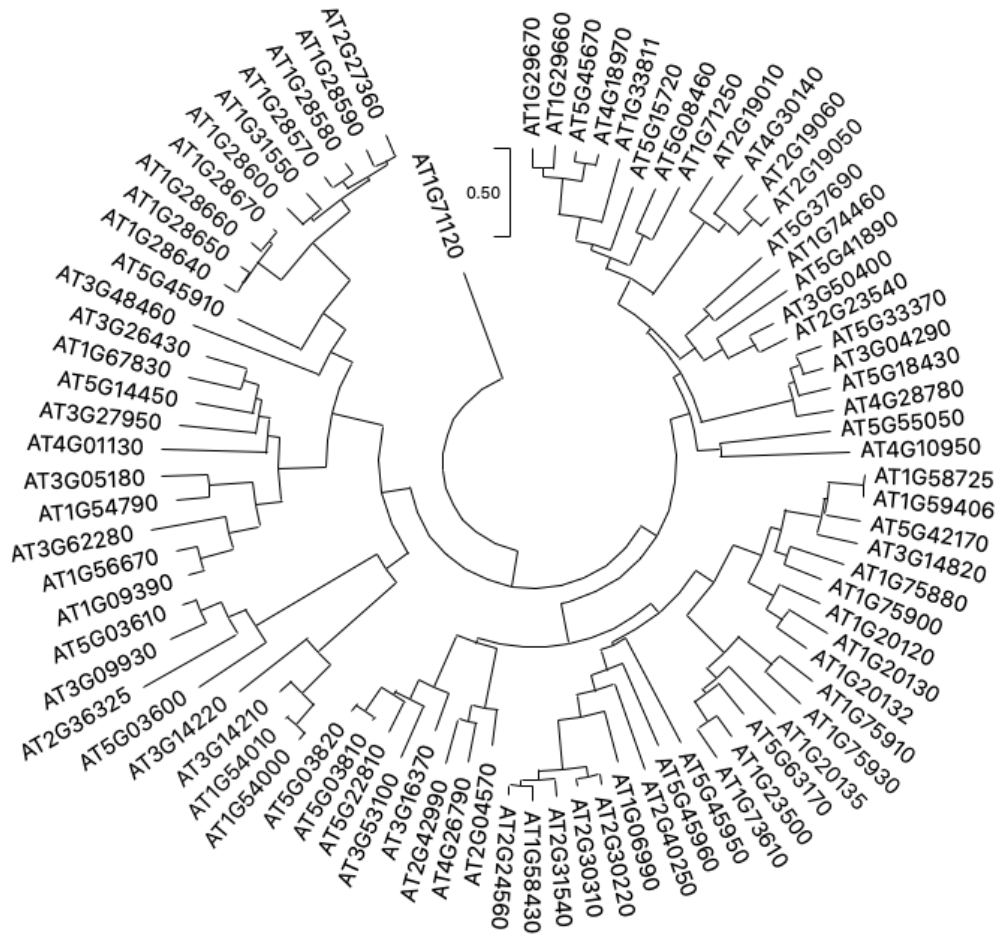


Figure 1.2: Phylogenetic tree of *Arabidopsis thaliana* GDSL hydrolases.

1.4 Localization of GDSL hydrolases family

Most of the GDSL hydrolases contain a signal peptide motif at the N-terminal end of their sequences (Oh *et al.*, 2005; Ling, 2008; Ding *et al.*, 2019). Signal peptides are

short stretches of amino acids present at the N-terminus of the secretory proteins. These proteins are transported to the extracellular space via conventional secretory pathways and perform various biological functions, including cell wall modification and defense (Chung and Zeng, 2017). In the conventional secretory pathway, proteins are transported from the endoplasmic reticulum (ER) to the Golgi apparatus and then to the trans-Golgi network (TGN), and from there to the plasma membrane, extra cellular space or other endosomal compartments (Cai *et al.*, 2014) (Fig.1.3). The signal peptide sequence is recognized by the signal recognition particle (SRP), a cytosolic protein that translocates the secretory protein to the ER. There, the proteins undergo maturation via endoproteolytic cleavage at specific cleavage sites as well as different modifications, such as glycosylation, phosphorylation, and disulfide bond formations. Afterwards, the proteins are transported into the Golgi apparatus, in a process mediated by the coat protein complexes, where they undergo additional modifications. The mature secretory proteins are then transported to the plasma membrane and secreted into the extracellular spaces (Barlowe and Miller, 2013).

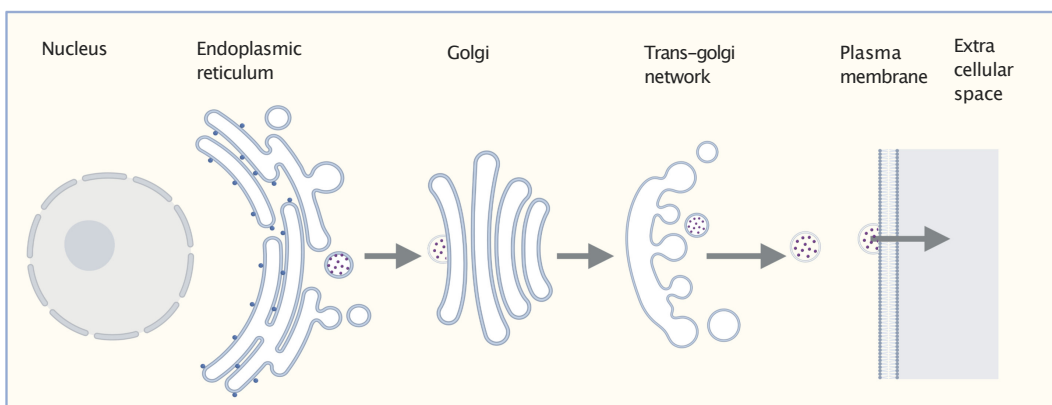


Figure 1.3: Schematic representation of conventional protein secretory pathway in plants. Graphical concept adapted from Rose and Lee (2010). Figure created with BioRender.com.

Most GDSL hydrolases are predicted to be apoplastic, but recent studies have characterized GDSL hydrolases that are functional in the Golgi apparatus (e.g., xylan deacetylation by rice GDSL hydrolase, BS1 (Zhang *et al.*, 2017)) and in the endoplasmic reticulum (e.g., pollen and anther development by maize GDSL hydrolase, ZmMs30 (An *et al.*, 2019)). ER and Golgi residing proteins generally contain specific retention motifs (KKXX and KXD/E, respectively) at the C-terminus of their sequences that enable retention of the proteins in specific compartments and the maintenance of their structural stability (Cosson and Letourneur, 1994; Gao *et al.*, 2012; Montesinos *et al.*, 2013; Gao *et al.*, 2014). However, neither motif has been detected in the sequences of GDSL hydrolase such that localization in the ER or Golgi has been questioned. While the localization of the BS1 protein in the Golgi apparatus has been demonstrated in the rice protoplast system, whether the protein is absent from the extracellular space was unclear (Zhang *et al.*, 2017). Therefore, it cannot be ruled out that BS1 is a secreted protein temporarily retained in the Golgi apparatus prior to its secretion.

1.5 Stomata

Plants migrated from water to land and underwent a series of key adaptations to the new environment (Hetherington and Woodward, 2003; Berry *et al.*, 2010; Chater *et al.*, 2017) (Fig.1.4). Land plants must maintain a balance between CO₂ uptake from the environment and water vapor transpiration from plant cells. To carry out both functions plants have evolved a specialized organ, the stoma, on the surface of their above-ground parts. The stoma consists of a pore connecting the inner space of the leaf with the atmosphere and a pair of guard cells surrounding the pore (Zeiger *et al.*, 1987; Jezek and Blatt, 2017; Chater *et al.*, 2017). Different plant and environmental factors, such as

light, CO₂ and phytohormones, influence stomatal opening and closing (Raschke, 1975; Vialet-Chabrand *et al.*, 2017). The stoma opens in response to certain solutes, including K⁺, Cl⁻, malate and sugars, whose accumulation in guard cells triggers an influx of water from neighboring cells and causes the guard cells to become turgid (Von Mohl, 1856). This increased turgor pressure induces the deformation of the guard cells that widens the stomatal pore. In the reverse process, metabolism of the solutes the release of the metabolites to the apoplast results in the closure of the stoma, albeit via different signaling and regulatory cascades (Jezek and Blatt, 2017). This stomal plasticity allows plants to modulate water loss as well as photosynthetic products. Thus, stomata have a significant impact on global water and carbon cycling (Beljaars *et al.*, 1996; Jezek and Blatt, 2017).

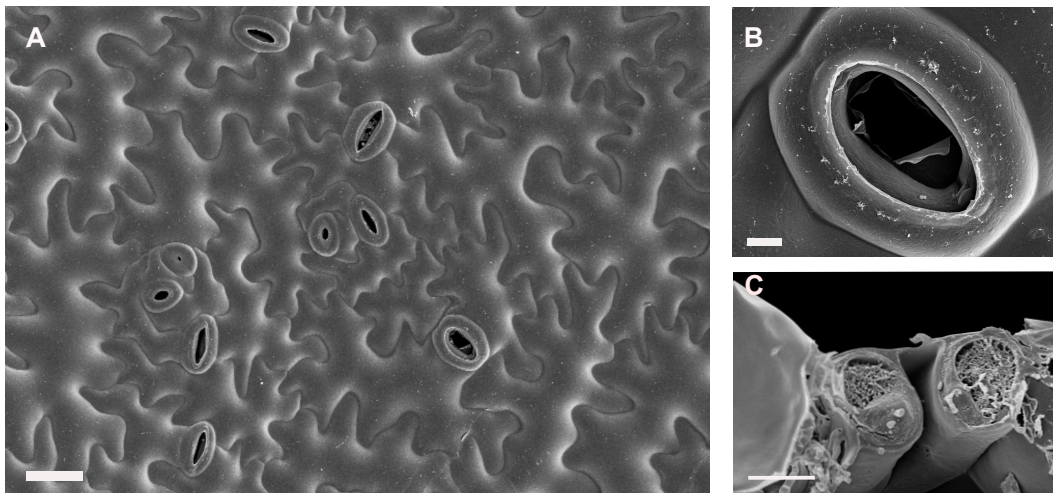


Figure 1.4: Distribution and structure of stomata. (A) The distribution of stomata in the abaxial side of the *A. thaliana* leaf. The scale bar, 30 μm . (B) An *A. thaliana* stoma (3Kx) under SEM. The scale bar, 4 μm . (C) A transverse section of *A. thaliana* stoma (3Kx) under SEM showing uneven thickening at the ventral wall. The scale bar, 4 μm .

1.6 Developmental pathway of Stomata

The developmental pathway of stomata has been extensively studied in *Arabidopsis thaliana*. The epidermis of the young leaves contains undifferentiated protodermal cells, some of which develop into mature stomata following specific routes of cell division and differentiation. A subset of the protodermal cells become meristemoid mother cells (MMC), which initially undergo asymmetric cell division to yield a smaller meristemoid and a larger stomatal lineage guard cell (SLGC) (Larkin *et al.*, 1997; Zoulias *et al.*, 2018). SLGCs further differentiate into epidermal cells, but they can also initiate a second asymmetric division to form another meristemoid, which undergoes further differentiation to yield a round guard mother cell (GMC). The GMC undergoes symmetric division that results in two immature guard cells, which expand to form mature guard cells and develop the stomatal pore. Alternatively, GMC that lack the proper regulatory signals instead differentiate into pavement cells (Zoulias *et al.*, 2018).

Each step in stomatal development is regulated by several transcription factors, most of which belong to the basic helix-loop-helix (bHLH) group (Ohashi-Ito and Bergmann, 2006; MacAlister *et al.*, 2007; Pillitteri *et al.*, 2007). The initial transformation of protodermal cells into the meristemoid mother cell and the fate of the first asymmetric division is regulated by the SPEECHLESS (SPCH) transcription factor. Broadly, SPCH RNA is expressed in developing leaves, but expression of the protein is restricted to the meristemoid stage (Simmons and Bergmann, 2016). During that stage in the GMC pathway, SPCH activity is reduced and the fate of the GMC is regulated by MUTE (Pillitteri *et al.*, 2007; Adrian *et al.*, 2015). In the loss-of-function mutant *mute* the GMC phenotype is highly altered such that the cells are stuck in a continuous stage of cell renewal. By contrast, MUTE overexpression induces the stomatal precursor fate in all

epidermal cells (Pillitteri *et al.*, 2007; Simmons and Bergmann, 2016). Finally, the symmetric division of GMC to yield guard cells (GC) is regulated by FAMA (Ohashi-Ito and Bergmann, 2006). At their respective expression stage, these three transcription factors (SPCH, MUTE and FAMA) form heterodimers with two additional bHLH transcription factors ICE1/SCREAM (SCRM) or SCRM2 (Kanaoka *et al.*, 2008). Loss of ICE1 or SCRM2 function completely abolishes the stomatal lineage (Fig.1.5).

A critical stage of the stomatal lineage is the establishment of stomatal fate in MMCs, which is regulated by SPCH (MacAlister *et al.*, 2007). In addition to its important role during stomatal lineage development, this transcription factor regulates the fate of pavement cells. Mutants lacking SPCH function are unable to establish the lineage such that pavement cells develop only in the epidermis. Therefore, the pattern and density of stomata on a leaf is regulated by differences in the expression pattern of SPCH. The activity of SPCH is regulated by a peptide signaling pathway in which SPCH is phosphorylated by the MAPKs cascade (Lampard *et al.*, 2008; Simmons and Bergmann, 2016). SPCH was shown to bind to 8327 regions in *Arabidopsis thaliana*, 70% of which are the promoter sites of genes involved in cell division, peptide signaling and meristemoid fate regulation (Lau *et al.*, 2014). Most of the binding sites are located 500 bp upstream of the transcription start site, with CDCGTG as the most commonly recognized motif. *In-silico* studies based on RNAseq/ChIPseq datasets predicted that several GDSL hydrolase genes are expressed in the stomatal lineage (Lau *et al.*, 2014), some of which are also targeted by SPCH and contain the SPCH-binding motif at their 5' UTR (untranslated region). In fact, the induction of SPCH is accompanied by the upregulation of these genes in the stomatal lineage. However, their exact function of these GDSL hydrolase gene family members in stomatal development or functionality remains unknown.

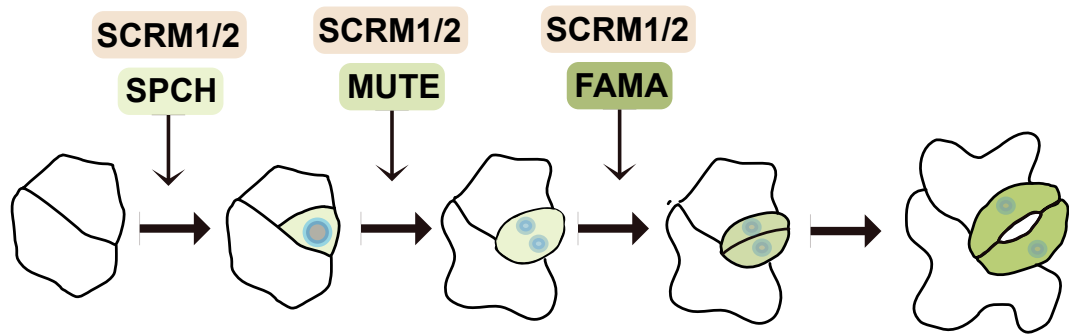


Figure 1.5: Schematic representation of developmental pathway of stomata and the key transcription factors involved in the pathway. Graphical concept adapted from Lau and Bergmann (2012).

1.7 Stomatal patterning and receptor like kinases

Stomatal patterning on the dicot leaves follows a “one-cell spacing” rule, in which two stomata are separated by at least one non-stomatal epidermal cell (Larkin *et al.*, 1997; Zoulias *et al.*, 2018). This spacing is very important for stomatal function as it ensures efficient gas exchange. The key regulators of the “one-cell spacing” arrangement of stomata are three cysteine-rich peptides, EPF1, EPF2 and EPFL9 (Hara *et al.*, 2007, 2009; Hunt and Gray, 2009; Sugano *et al.*, 2010; Hunt *et al.*, 2010). EPF1 and EPF2 negatively regulate stomatal development by acting on the neighbouring cells of stomatal precursors, while EPFL9 is a positive regulator (Zoulias *et al.*, 2018). The signaling cascade triggered by EPFs involves three Erecta family of leucine-rich repeat (LRR) receptor-like kinases (ER, ERL1 and ERL2) and the LRR receptor-like protein TMM (Too Many Mouth). The genes for these LRR-RKs and LRR-PRs are expressed at distinct stages of the stomatal lineage, suggesting their stage specific functions (Zoulias *et al.*, 2018) (Fig.1.6).

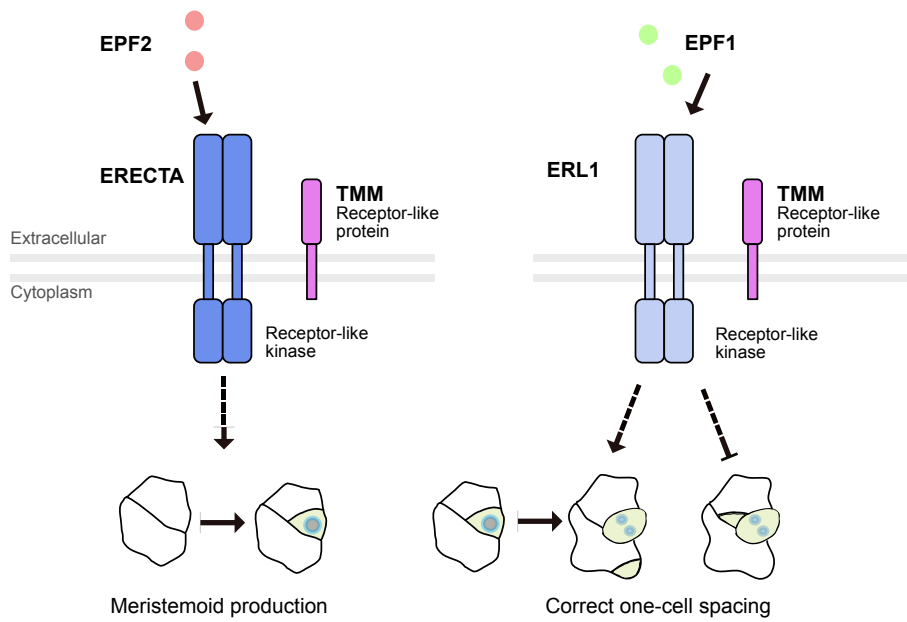


Figure 1.6: Different receptor-like kinases and proteins in distinct stages of stomatal development. Graphical concept adapted from Lau and Bergmann (2012).

1.8 Stomatal function

Stomata play a central role in the regulation of gas exchange between the internal and external leaf environment (Cowan and Troughton, 1971). Plants require sufficient CO_2 for photosynthesis, while conserving water to prevent tissue dehydration (Lawson and Morison, 2004). Therefore, stomata are constantly opening and closing to regulate the uptake of CO_2 and balance the release of water vapor (Hetherington and Woodward, 2003; Berry *et al.*, 2010; Chater *et al.*, 2017). Under limiting environmental conditions, such as a reduced water or high CO_2 concentration, the stomata close, which facilitates water retention and the avoidance of dehydration (Raschke, 1975; Vialet-Chabrand *et al.*, 2017; Jezek and Blatt, 2017). As discussed above, stomatal closing and opening mechanisms are driven by internal hydrostatic pressure, i.e., the turgor pressure

(Von Mohl, 1856; Jezek and Blatt, 2017). The influx/efflux of solutes creates changes in the water potential, which in turn changes both the cell volume and the turgor pressure, thus driving the opening/closing of the stomata (Jezek and Blatt, 2017). When the stomata are open, solutes actively accumulate in the guard cells via a number of transport pathways (Kearns and Assmann, 1993; Pandey *et al.*, 2007; Jezek and Blatt, 2017) and energy supplied by ATP, which powers H⁺-ATPases to pump out H⁺ and thus generate a membrane potential allowing K⁺ uptake via specific K⁺ channels in the membrane (Fig.1.7). Stomatal closure is triggered by environmental stimuli such as darkness, high CO₂ levels, plant pathogens, and the phytohormone ABA, all of which induce the release of solutes from guard cells (Fig.1.8) (Kearns and Assmann, 1993; Pandey *et al.*, 2007; Jezek and Blatt, 2017). Voltage clamp studies have shown that, in the presence of ABA, K⁺ channels are altered following plasma membrane depolarization, resulting in K⁺ efflux (Blatt, 1990; Linder and Raschke, 1992). Moreover, ABA suppresses H⁺-ATPase activity and the inward rectifying K⁺ channels, which prevents K⁺ uptake and induces the outward rectifying K⁺ channels to facilitate K⁺, Cl⁻ and malate efflux. Simultaneously, the binding of ABA to its receptors (PYR/PYL) triggers the phosphorylation cascade in the ABA signaling pathway (Munemasa *et al.*, 2015).

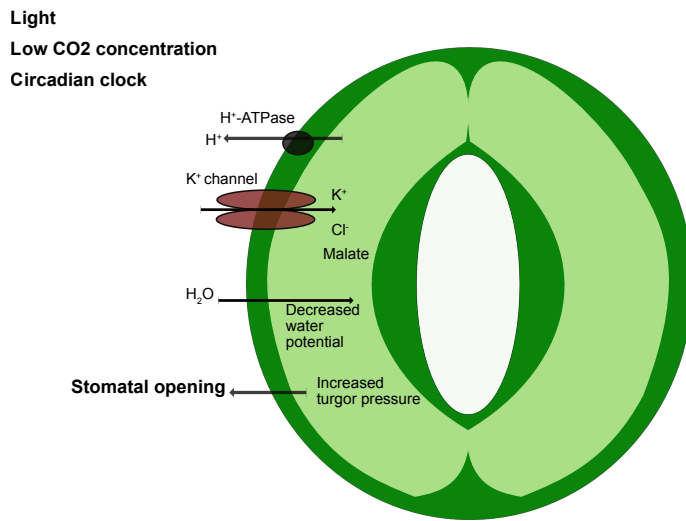


Figure 1.7: Basic mechanism of stomatal opening. Graphical concept was adapted from Daszkowska-Golec and Szarejko (2013).

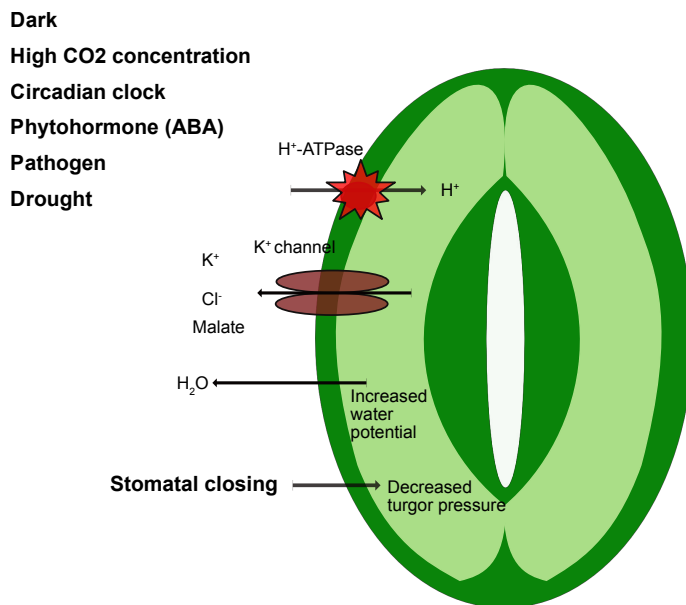


Figure 1.8: Basic mechanism of stomatal closing. Graphical concept was adapted from Daszkowska-Golec and Szarejko (2013).

1.9 Mechanical properties of stomata

Because turgor-driven stomatal dynamics are essentially mechanical, an understanding of the physical properties of guard cells is important to understand stomatal function (Aylor *et al.*, 1973; Woolfenden *et al.*, 2018). When the stomata are in an open state, the increased turgor pressure leads to the inflation of the guard cells by 25% of their volume and 15% of their total area. During their closure in response to a decrease in the turgor pressure, the guard cells shrink back to their original size (Meckel *et al.*, 2007; Woolfenden *et al.*, 2018). These dynamics of guard cells require their remarkable elasticity and exceptional physical strength (Woolfenden *et al.*, 2018; Yi *et al.*, 2019). However, little is known about the mechanical properties of stomata during the opening-closing dynamics.

The plant cell wall is mainly composed of polysaccharides along with structural proteins, glycoproteins and polyphenols (Knox, 2008; Burton *et al.*, 2010; Hocq *et al.*, 2017). The polysaccharides include cellulose, hemicellulose and pectin. Structural modeling of the cell wall has shown that cellulose microfibrils associated with hemicellulose and embedded in the pectin matrix are the primary component (Somerville *et al.*, 2004; Cosgrove, 2005; Schultink *et al.*, 2015; Hocq *et al.*, 2017). The cellulose microfibrils are made of β -1,4-glucan chains, while hemicellulose and pectin consist of various glycosyl units and linkages and are prone to modification, such as acetylation and methylation (Pauly *et al.*, 2013; Hocq *et al.*, 2017). Advanced imaging techniques used to explore the ultrastructure of stomatal guard cell walls have shown that the asymmetric distribution of cell wall materials (Zhao and Sack, 1999). The ventral walls facing the stomatal pore are thicker than the dorsal cell walls facing neighboring cells (Fig.1.4). This uneven thickening may be an adaptation to support the stom-

atal region, which is exposed to a higher stress during the stomatal opening process (Von Mohl, 1856; Carter *et al.*, 2017). Biochemical and computational modelling studies have provided a deeper understanding of stomatal mechanics, by showing that, along with the differential thickening of the guard cells, the stiffness of the polar region of the guard cells is an important factor in stomatal dynamics (Carter *et al.*, 2017; Woolfenden *et al.*, 2018; Yi *et al.*, 2019). The results of early stomatal modeling studies revealed that the cellular microfibrils are radially arranged around the guard cells (Aylor *et al.*, 1973; Cooke *et al.*, 1976). This specific arrangement limits the cross-sectional expansion of the guard cell during the increase in turgor pressure. Later studies using atomic force microscopy (AFM) showed that the polar region of the guard cell is stiffest during stomatal opening, presumably due to the increased deposition of crystalline cellulose and demethylesterified homogalacturonan (HG) pectin deposition at this region (Carter *et al.*, 2017; Woolfenden *et al.*, 2018; Yi *et al.*, 2019).

Pectin is the most abundant polysaccharide in plant cell walls, accounting for almost 30% of the plant's dry weight (Caffall and Mohnen, 2009; Hocq *et al.*, 2017). The pectin backbone consists of homogalacturonan (HG), polymers of α -1,4-GalA (galacturonic acids) and other modified HGs, such as xylo-galacturonans, apiogalacturonans and rhamnogalacturonans-I (RG-I) and RG-II. Galacturonic acid, the acidic sugar component, forms complexes with calcium ions via electrostatic interactions that play a crucial role in the rigidity of the plant cell wall (Caffall and Mohnen, 2009; Harholt *et al.*, 2010; Hocq *et al.*, 2017) (Fig.1.9). HGs are synthesized in the Golgi apparatus and transported to the apoplast in a highly methylated form. Upon reaching the apoplast, they are demethylesterified by pectin methylesterases (PMEs) (Caffall and Mohnen, 2009; Harholt *et al.*, 2010; Hocq *et al.*, 2017). Immunolabeling with pectin epitopes revealed that while highly methylesterified HG pectin is excluded demethylesterified HG

pectin is distributed throughout the guard cell wall (Amsbury *et al.*, 2016). The genes encoding the enzymes required for pectin biosynthesis, modification and degradation mostly belong to large gene families, consistent with the complexity of these pathways and their tight regulation (Caffall and Mohnen, 2009; Harholt *et al.*, 2010; Hocq *et al.*, 2017; Anderson, 2019). Although a few have been studied in detail (e.g., PME and polygalacturonases), the vast majority are as yet uncharacterized.

While cellulose and xyloglucans are crucial elements in the structural anisotropy of guard cells and influence stomatal kinetics, evidence suggests that pectins are key determinants of stomatal dynamics (Rui and Anderson, 2016; Rui *et al.*, 2017, 2018). A study showed that the treatment with arabinanase impairs stomatal opening (Jones *et al.*, 2003). In *pme6* mutant plants, the lack of PMEs results in guard cell walls that are highly methylesterified and in abnormal stomatal dynamics (Amsbury *et al.*, 2016). In *pme34* mutant plants, the stomatal response to heat stress is defective (Huang *et al.*, 2017). Pectin degradation, mediated by PGX3, is also important for stomatal development as well as guard cell dynamics (Rui *et al.*, 2017).

The cell wall backbone and their side chains also undergo different types of modifications that regulate functionality. Modifications such as methylation and acetylation alter the structure of pectin and hemicellulose (Caffall and Mohnen, 2009; Schultink *et al.*, 2015). The nature of the glycosyl linkages also plays a functional role. For example, xyloglucans contain xylosyl, galactosyl, fucosyl, arabinosyl and galacturonosyl substitutions on their β -1,4-glucan backbone and xylan is heavily O-acetylated (Schultink *et al.*, 2015; Pauly *et al.*, 2013; Bethke *et al.*, 2016). The altered xyloglucan 9 (AXY9) protein regulates polysaccharide acetylation along with the RWA and TBL proteins (Schultink *et al.*, 2015; Zhang *et al.*, 2017). *Arabidopsis thaliana axy9* loss-of-function mutants exhibit severe growth defects and a collapsed xylem. Although little is

known about the enzymatic pathway involved in polysaccharide O-acetylation in the cell wall, this modification influences the solubility, gelation and enzymatic accessibility of polysaccharides. Acetylation differs in its pattern and degree depending on the plant's developmental stage and is tissue-specific, which requires that acetyltransferases are tightly regulated. The same is true for deacetylation mediated by deacetylases (Zhang *et al.*, 2017) (Fig.1.9)

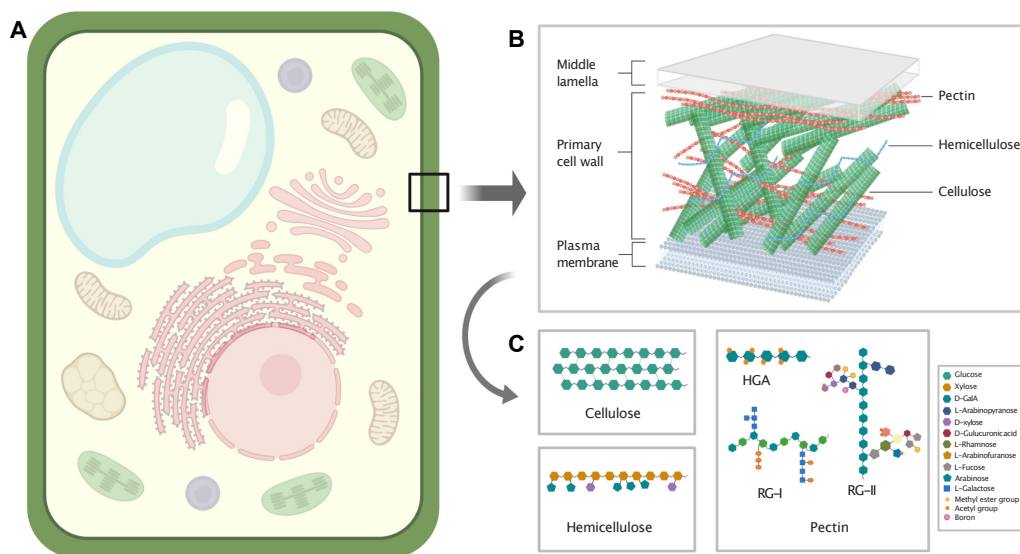


Figure 1.9: Plant cell wall composition. (A) Simple representation of a plant cell. (B) Basic structure and composition of primary cell wall of plants. Graphical concept was adapted from Sticklen (2008) (C) Schematic structure of different cell wall polysaccharides. HGA, homogalacturonan; RG-I, rhamnogalacturonan I; RG-II, rhamnogalacturonan-II. Graphical concept was adapted from Bhatia *et al.* (2017); Gawkowska *et al.* (2018). Figures created with BioRender.com.

1.10 Seed germination

Measurements of the resistance of different layers of seed tissues have shown that the endosperm is the major barrier for the radicle protrusion in the seeds. Conditions favorable for seed germination weaken this mechanical barrier via rupture of the testa/seed coat and endosperm, thus releasing the radicle (Groot and Karssen, 1987; Finch-Savage and Leubner-Metzger, 2006; Nonogaki, 2019). However, detailed biochemical and biophysical studies of endosperm weakening are lacking.

Seed germination involves the cell wall components xyloglucan and pectin (Nonogaki, 2019). Genetic studies with α -xylosidase as well as PME and its inhibitor (PMEI) have shown that both xyloglucan and pectin are essential for seed dormancy and germination (Ren and Kermode, 2000; Chen *et al.*, 2002; Cavalier *et al.*, 2008; Wolf *et al.*, 2009; Scheller and Ulvskov, 2010; Müller *et al.*, 2013; Scheler *et al.*, 2015; Sechet *et al.*, 2016). PME participates in weakening the micropolar megagametophyte, the seed-covering tissue similar to the endosperm, in gymnosperm species (Ren and Kermode, 2000) whereas PME15 overexpression in *Arabidopsis thaliana* was shown to stimulate endosperm and testa rupture, thus enhancing seed germination (Müller *et al.*, 2013).

Studies of a mutant α -xylosidase, *xy11*, showed the involvement of the enzyme in xyloglucan (XyG) biosynthesis. as the mutants contained a higher abundance of less substituted subunits of XyG (XXG, XXXL) and fewer more-substituted XyG subunits (XXFG, XLFG) than in the wild type (Sechet *et al.*, 2016). The xyloglucan backbone consists of β -(1,4)-glucopyranosyl residues (G) that undergo substitution reactions mediated by xylosyltransferases, galactosyltransferases and fucosyltransferases, resulting in α -(1,6) xylosyl (X), β -galactosyl (G) and α -(1,6) fucosyl (F) residues, respectively (Scheller and Ulvskov, 2010; Nonogaki, 2019). These substitution reactions contribute

to the heterogeneity of XyG and therefore to the physical properties of the cell wall in endosperm tissue (Scheller and Ulvskov, 2010). Mutant *xyl1* displays reduced seed dormancy and is resistant to paclobitrazol (PAC), an inhibitor of gibberellin during germination.

GDSL hydrolase genes also play a role in the seed germination process, via the metabolism of fatty acids (FAs) (Chen *et al.*, 2012). Both FA and FA-derived compounds are deposited in the radicle, endosperm and seed coat of *Arabidopsis thaliana* seeds and influence seed germination as well as successful seedling establishment (Li *et al.*, 2006; Graham, 2008). These GDSL hydrolases, encoded by SFAR (seed fatty acid reducer) genes, act downstream of the gibberellic acid (GA) pathway in *Arabidopsis thaliana* seeds. In *sfar* mutants, the FA content of the seed is higher than in the wild-type whereas SFAR over-expression results in a lower FA content and a higher rate of germination under stress conditions.

1.11 Known GDSL hydrolases in cell wall modification

GDSL lipases are involved in secondary cell wall biosynthesis and mechanics, and therefore in plant development and growth. For example, a plant GDSL lipase family protein, BS1, was recently identified as an acetyl-xylan esterase (Zhang *et al.*, 2017). The enzyme removes acetyl moieties from the O2 and O3 positions of xylopyranosyl residues in the xylan backbone. BS1 is localized in the vascular bundles and *bs1* mutant plants show an abnormal secondary wall architecture. In addition, *bs1* mutants are characterized by excess xylan acetylation, decreased plant growth, a brittle leaf sheath and a smaller panicle (Zhang *et al.*, 2017). Another GDSL lipase gene, AtFXG1, localized in the apoplast, exhibits α -L-fucosidase activity in *Arabidopsis thaliana*. AtFXG1

regulates XXFG ($\text{Glc}_4\text{Xyl}_3\text{Fuc}_1\text{Gal}_1$), a derivative of xyloglucan (Fry *et al.*, 1993), by removing t-fucosyl residues (de la Torre *et al.*, 2002; Günl *et al.*, 2011). However, the effect of AtFXG1 on plant architecture and function is unknown.

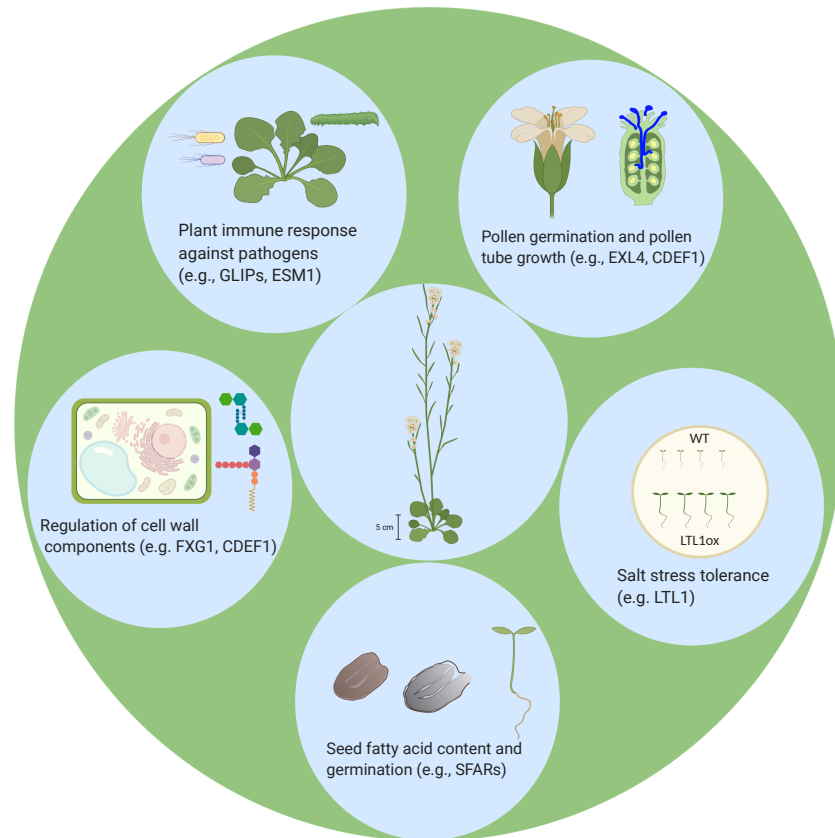


Figure 1.10: Known biological functions of GDSL hydrolases in *Arabidopsis thaliana*. Figure created with BioRender.com.

Chapter 2

Material and Methods

2.1 Molecular biology

2.1.1 Polymerase chain reaction (PCR)

The DNA fragments were PCR-amplified using a proof-reading polymerase, KOD Hot-start. The reaction was set up according to the manufacturer's instructions as follows:

10x buffer	5 μ l
MgSO ₄	3 μ l
dNTPs	5 μ l
Forward Primer	1.5 μ l
Reverse Primer	1.5 μ l
KOD polymerase	1 μ l
Template	0.2 μ l
H ₂ O	33 μ l

The PCR program followed the manufacturer's instructions and was typically run for 35 cycles:

95°C	3 min
95 °C	20 sec
Tm-5°C	20 sec
70°C	40 sec (15-20s/kbp)
70°C	1 min

2.1.2 Restriction digestion reaction

Restriction enzymes (NEB or ThermoFisher) were used for molecular cloning and to confirm positive transformants. The buffer solution was selected according to the enzyme requirements and the reaction was set up according to the manufacturer's protocol as follows:

Suitable buffer	4 μ l
Enzyme	2 μ l
Template	10 μ l
Water	34 μ l

The incubation temperature was 37°C and the reaction time was 3-5 hr depending on the enzyme's activity.

2.1.3 Plasmid extraction protocol

Bacterial cultures were inoculated into 5 ml of LB medium (Luria-Bertani medium) along with appropriate antibiotics and incubated at 37°C overnight with shaking. The cells were harvested by centrifugation of the cultures in benchtop microcentrifuge at maximum speed (12000 g) for 1 min at room temperature. The supernatant was discarded and the cell pellets were resuspended in 400 μ l of solution I (50 mM glucose, 25 mM Tris-Cl (pH 8.0), 10 mM EDTA (pH 8.0) in deionized water) in microcentrifuge

tubes followed by vortex mixing. After the addition of 400 μ l of solution II (0.2 N NaOH, 1% (w/v) SDS in deionized water) the samples were mixed gently by inverting the tubes for 5 min. Four hundred μ l of solution III (5 M potassium acetate, glacial acetic acid in deionized water) was then added, followed by gentle mixing of the tubes as before. The lysed cells were centrifuged at maximum speed for 15 min at 4°C and the supernatant, containing the plasmids, then transferred into new 2-ml tubes to which 1 ml of isopropanol was added. The samples were then mixed thoroughly and centrifuged at maximum speed for 30 min at 4°C. The supernatant was discarded and the pellet was washed with 70% ethanol (v/v) by centrifugation as above for 10 min at 4°C. The supernatant was discarded and the pellets, containing the plasmid DNA, were air dried, dissolved in 50–100 μ l of water and stored at 4°C until further use.

2.1.4 Gateway cloning techniques

Genes or promoter regions of interest were cloned using the Gateway™ cloning technique, in which a DNA fragment is incorporated into a pDONR vector backbone using a proprietary set of recombination sites (“Gateway att” sites). The PCR primers were designed for the gene of interest with “Gateway att” sites. The PCR-amplified products were initially incorporated into the pDONR vector using the BP clonase enzyme, and the desired gene fragment was transferred to the final vector backbone using the LR clonase enzyme.

2.1.5 BP clonase reaction

The BP Clonase reaction was set up according to the manufacturer’s protocol as follows:

PCR amplified fragment	1 μ l
Plasmid of Entry Vector	1 μ l
BP Clonase enzyme	0.5 μ l

The reaction was incubated at room temperature for 3 hr and the reaction products then transformed into *Escherichia coli* Top-10 competent cells (see below), followed by selection with the appropriate antibiotics. Positive transformants were selected either by colony PCR (see Sec. 2.1.9) or restriction digestion with the appropriate restriction enzyme.

2.1.6 LR clonase reaction

The LR clonase reaction followed the manufacturer's protocol:

Plasmid of BP Clonase reaction product	1 μ l
Plasmid of Destination Vector	1 μ l
LR Clonase enzyme	0.5 μ l

The reaction was incubated at room temperature for 3 hr and the reaction products were then transformed into *E. coli* Top-10 competent cells (see below) followed by selection with the appropriate antibiotics. Positive transformants were selected either by colony PCR (see Sec. 2.1.9) or restriction digestion with the appropriate restriction enzyme.

2.1.7 *Escherichia coli* mediated transformation

The plasmids were transformed into *Escherichia coli* (*E. coli*) competent Top-10 cells and *ccdB* survival cells depending on the construct. The frozen competent cells were thawed on ice for 15 min and 8–10 μ l of plasmid was then added. The tubes were incubated on ice for 15 min and then heat-shocked at 42°C for 45 sec. After a brief cooling of the tubes, 1 ml of liquid LB medium was added, followed by thorough mixing, incubation at 37°C for 1 hr with shaking at 400 rpm and centrifugation at 800 rpm for 1

min to pellet the plasmids. The supernatant was discarded and the pellet was dissolved in 100 μ l of LB liquid medium. The suspension was poured onto plates of LB solid medium containing antibiotics appropriate to the constructs and then evenly distributed using glass beads (2.85–3.45 mm). The plates were incubated overnight at 37°C and the colonies that had developed were selected. Positive transformants were confirmed by colony PCR (see Sec. 2.1.9) or restriction digestion.

2.1.8 *Agrobacterium tumefaciens* mediated transformation

The plasmids were transformed into competent *Agrobacterium tumefaciens* cells (GV3101) specific for transformation. The frozen competent cells were thawed on ice for 20–30 min, mixed with 8 μ l of plasmid solution and incubated on ice for 5 min. Freeze-thawing was conducted by subjecting the tubes to liquid nitrogen for 1 min followed by warming at 37°C for 5 min. *A. tumefaciens* was recovered by the addition of 1 ml of liquid LB to the tubes, following by incubation at 28°C for 2 hr and centrifugation at 800 rpm for 1 min to pellet the cells. The supernatant was discarded and the pellet was dissolved in 100 μ l of LB liquid. The suspension was poured onto plates of LB solid medium containing antibiotics appropriate to the constructs and then evenly distributed using glass beads (2.85–3.45 mm). The plates were incubated overnight at 28°C for and the positive transformants were confirmed by testing several colonies in a colony PCR or using the *A. tumefaciens* rescue protocol described below.

Single colonies were selected from the *A. tumefaciens* transformants on the LB plates and inoculated in 5 ml of LB containing the appropriate antibiotics. The inocula were incubated overnight at 30°C with shaking. Plasmid was extracted from the overnight culture (see sec. Plasmid isolation) and 5 μ l of the plasmid preparation was used to

transform *E. coli* competent cells as described above. After a 1 hr incubation at 37°C with shaking, 100 μ l of the *E. coli* transformant culture was directly inoculated into 5 ml of LB containing appropriate antibiotics. After an overnight incubation at 37°C, the cultures were screened for positive transformants by restriction digested with appropriate restriction enzyme or colony PCR (see Sec. 2.1.9) carried out with appropriate primer pairs. For the long-term storage of the positive *A. tumefaciens* transformants, 930 μ l of the *A. tumefaciens* culture was mixed with 70 μ l of DMSO in a screw capped tube, which was stored at 80°C.

2.1.9 Colony PCR for positive transformants

To screen the positive plasmid inserts directly from the *E. coli* cultures, colony PCR was performed using Taq polymerase (Ampliqon). Several colonies from the transformed LB plates were individually picked, with a portion used for streaking on a replica plate and the remainder dissolved into 50 μ l of water. From the latter, 2 μ l was used as a template for the colony PCR. The PCR mixture (25 μ l per reaction) was prepared as below:

10x Taq buffer	2.5 μ l
2.5mM dNTPs	2.5 μ l
Forward primer	1 μ l
Reverse primer	1 μ l
Taq polymerase	0.5 μ l
Template	2 μ l
Water	15.5 μ l

The PCR program followed the manufacturer's instructions and was typically run for 35 cycles:

95 °C	2 min
95°C	40 sec
Tm-5°C	40 sec
72 °C	40 sec (15-20s/kbp)
70°C	3 min

2.1.10 *Agrobacterium tumefaciens* mediated floral dipping

An aliquot of the *A. tumefaciens* stock containing the construct of interest was inoculated into 50 ml of LB medium containing appropriate antibiotics and incubated at 28°C with shaking overnight. The next day, a secondary culture was set up by adding 50 ml of the primary culture to 500 ml of fresh LB containing appropriate antibiotics. After an overnight incubation at 28°C with shaking, the culture was centrifuged at 5000 rpm for 20 min at room temperature. The pellet was then resuspended in dipping solution containing ½ Murashige and Skoog (MS) medium, 5% sucrose and 0.02% Silwet solution. *A. thaliana* plants were grown for 5 weeks until they developed floral buds. The bacterial culture was added to a glass beaker and the plants were inverted and dipped into the solution for 3-4 sec such that all of the above ground tissue was immersed. The dipped plants were then placed in a plastic tray, which was covered to generate sufficient humidity. The plants were left overnight and then cultivated until the seeds that formed had matured and dried. The harvested seeds were then selected on ½ MS plates containing antibiotics appropriate for the transformants.

2.1.11 *Nicotiana benthamiana* infiltration for transient expression assay

The *A. tumefaciens* stock containing the construct of interest was inoculated in 5 ml of LB along with appropriate antibiotics and incubated at 28°C with shaking overnight.

The next day, a secondary culture was prepared by adding 500 μ l of the primary culture to 4.5 ml of fresh LB containing the appropriate antibiotics. After the secondary culture had been incubated at 28°C with shaking for 4-6 hr, the OD₆₀₀ was measured using a spectrophotometer. The cells were then pelleted by centrifugation at 4000 rpm for 15 min at 4°C and resuspended in infiltration medium containing 10 mM MES (pH 5.6), 10 mM MgCl₂ and 200 μ M acetosyringone to reach an OD₆₀₀ of 1. The suspension was incubated on ice for at least 1 hr and then used to infiltrate well-watered *N. benthamiana* leaves were infiltrated with the inoculum, via a plastic 1-ml syringe. The plants were kept in the dark for over 48 hr and the leaves then observed for fluorescence under confocal microscopy and/or extracted for protein analysis.

2.1.12 Quantitative Real-Time PCR (qRT-PCR) analysis

RNA was extracted from 7-day-old seedlings or 4-5 week old short-day-grown rosette leaves using the Roboklon Universal RNA purification kit according to the manufacturer's protocol. Total RNA from 100 mg of tissue was extracted and transcribed into cDNA using a cDNA kit (Protoscript II) according to the manufacturer's protocol. The expression levels of the genes of interest were quantified by qRT PCR (Luna Universal qPCR mix) using a procedure adapted from the manufacturer's protocol (Luna Universal qPCR mix) and the following program:

95 °C	2 min
95°C	15 sec
64°C	30 sec
Plateread	
Go to 2, 39x	
68°C	31 sec
64°C	5 sec
+0.5°C/cyle	
Ramp 0.5°C/s	
Plateread	
Go to step7, 54x	

The qPCR primers used for this study are listed in (Table A.4).

2.1.13 Transcriptome analysis using RNAseq

The leaves of five wild-type Col-0 and *cgm3cgm4* plants were incubated in the light for 3 hr with 10 μ M ABA and, as the control, the leaves of five other plants were incubated under the same conditions but without ABA. Total RNA was extracted from the leaves using the Roboklon Universal RNA purification kit according to the manufacturer's protocol. The RNAseq analysis was conducted using 150 ng RNA/ μ l concentration and performed in collaboration with the CeGat (<https://www.cegat.de>), Tübingen. The paired-end sequencing (2x 100bp) was carried out on a NovaSeq6000 sequencing system.

The RNAseq outcome data were further analyzed with the help of Dr. Minou Nowrouzian, Department of Molecular and Cellular Botany, University of Bochum, Bochum, using DESeq2 and Lox. A p-value < 0.05 or < 0.1 was considered to indicate statistical significance. The list of ABA-induced genes was adopted from (Hoth *et al.*, 2002) and the comparative analysis of the gene expression ratios was done using the wild type Col-0 and *cgm3cgm4* leaves treated or not ABA.

2.2 Cloning of different expression vectors

2.2.1 Cloning of GW-nls-eGFP vector

The gateway cassette of R1-CmR-ccdB was excised from V358 (pUC::nls-eGFP-Dest) using NdeI and SalI restriction enzymes and then ligated into NdeI/SalI-digested V292 (pUC-35S::R3R2-eGFP), yielding the new vector (V392) containing the R1R2 gateway site and eGFP. After linearization of vector V392 (pUC-GW-eGFP) using the SpeI restriction enzyme, an nls sequence (without stop codon) was introduced in front of the eGFP sequence. The new vector V395 (pUC::nls-eGFP) thus contained the R1R2 gateway cassette and an nls-eGFP sequence at the C-terminal. To check the functionality of the construct, a CaMV 35S promoter sequence was recombined via an LR reaction with V395. The expression vector was transformed into tobacco (*N. benthamiana*) protoplasts and the localization of p35S:nls-eGFP was monitored using confocal microscopy. As expected, nls-eGFP was detected in the nucleus, confirming that the vector was functional. The whole R1R2 gateway site-nls-eGFP cassette was then introduced into a set of plant-specific binary vectors (V274 (pBBb), V388 (pBBk), V389 (pBBh)) harboring, respectively, basta, kanamycin and hygromycin resistance cassettes, for plant selection. The resulting vectors, V396 (pBBb-nls-eGFP), V397 (pBBk-nls-eGFP) and V398 (pBBh-nls-eGFP), were used for to analyze several promoter localizations. The promoter sequences were amplified with attB1 and attB2 extension sequence and introduced into the BP compatible entry vector V001 (pDONR207), via a BP clonase reaction. The entry clones were then used in LR clonase reactions with the respective nls-eGFP vector, depending on the plant's resistance marker.

2.2.2 Cloning of Promoter of interest(POI)/p35S-mScarlet-3xHA

The mScarlet sequence was amplified from V409 (pUC57::mScarlet-I) along with flanking restriction sites for 5' SpeI and 3' FspI. The backbone vector V387 (pUBQ10::GW-3xHA) was digested with SpeI and treated with CIP. The amplified product (SpeI-mScarlet-FspI) was then ligated into SpeI-digested V387. The new vector, with the mScarlet tag at the N-terminal, was named V470 (pUBQ10::GW-mScarlet-3HA). The 35S promoter-driven CGM4 or CGM4 full genomic sequence, including the CGM4 promoter, was amplified and ligated into V470 using SacI/BglII double restriction enzyme digestion.

2.2.3 Cloning of CGM3 and CGM4 promoter construct

A promoter fragment 1693 Kb and 1865 Kb upstream of the CGM4 and CGM3 start codon, respectively, was PCR-amplified and cloned into entry vector V001 (pDONR207). The promoter fragments were then recombined via LR clonase into destination vector V396 (pBBb-nls-eGFP), which contains nls and eGFP coding sequences at the 5' end of the insert location. These constructs were then transformed into wild-type Col-0 *A. thaliana* and into the *cgm3_2* and *cgm4_1* background, respectively, using the floral dipping method. For the construct inducing ubiquitous over-expression, the full genomic fragments of CGM4 and CGM3 were amplified and cloned into the pUBC-Dest series vector (Grefen *et al.*, 2010), which contains a GFP tag at the N-terminal and the UBQ10 promoter in the 3' end of the insert. These constructs were transformed into wild-type Col-0 plants using the floral dipping method. To create the full-length complemented lines, the full genomic fragment (including introns and 3' UTR) and the 1693-kb upstream promoter sequences from CGM4 were amplified and cloned into the destina-

tion vector V041 (pMDC123). This construct was used to transform *cgm3cgm4* double knockout mutants using the floral dipping method. All primers used in the cloning are listed in (Table A.4).

2.3 Plant growth

2.3.1 Plant growth condition

All mutant and transgenic *A. thaliana* lines had a Columbia-0 (Col-0) background. Seeds were imbibed on wet paper and kept for 2–4 days in the dark at 4°C. They were then induced to germinate by sowing them on soil or by surface sterilization with chlorine gas and plating on ½ strength solid MS medium (2.1 gm/L) and plant agar (pH 5.7). The plants were cultivated in an 8 hr light/16 hr dark cycle at 23/18°C, 51 $\mu\text{mol}/\text{m}^2/\text{s}$ photon light intensity and 55/75% relative humidity. Cultivation was carried out in a growth chamber for all physiological experiments or in a continuous light chamber with 40% relative humidity and a temperature of 23°C for seed regeneration.

2.3.2 T-DNA insertion lines

T-DNA insertion lines were obtained from NASC (Nottingham, UK) (Table 2.1). The insertions were confirmed by screening homozygous plants by PCR using the primers used listed in (Table A.4). PMElox lines were provided by Prof. Sebastian Wolf, Centre for Organismal Studies, Heidelberg (Wolf *et al.*, 2012).

Table 2.1: T-DNA insertion lines (seeds)

Name	AGI Code	T-DNA line
cgm3_2	AT5G45670	GK-609A07
cgm4_1	AT4G18970	SALK-029865
spch_3	AT5G53210	SAIL-36-B06
fama_1	AT3G24140	SALK-100073
cgm19_1	AT3G04290	SALK-012570C
cgm19_2		SALK-082848C
cgm7_1	AT5G08460	GK-552A03
cgm7_2		SALK-141771C
cgm54_1	AT2G04570	SALK-094557C
cgm54_2		SALK-106116C
cgm22_1	AT4G28780	SALK-129661C
cgm22_1		SALK-046877C
cgm21_1	AT5G18430	SALK-116756
cgm21_2		SALK-002060
cgm58_1	AT3G16370	SALK-150917
cgm58_2		SALK-091361C
cgm57_1	AT5G45950	SALK-062354
cgm57_2		SALK-095874
PMElox		AW517

2.3.3 Vapor phase seed sterilization

The seeds were surface-sterilized according to the vapor-phase seed sterilization method, using Chlorine gas. Microcentrifuge tubes containing the seeds were labeled and placed in a vacuum container under a fume hood. The lids of the tubes were kept open inside the container. A 250-ml bottle containing 100 ml of bleach solution (sodium hypochloride) was placed inside the vacuum container and 3 ml of concentrated HCl was added to the bleach solution. The lid of the vacuum container was then sealed and the tubes were incubated for 5-6 hr or overnight undisturbed. They were then taken out of the vacuum container and their lids closed immediately.

2.4 Plant physiology

2.4.1 Stomatal aperture analysis

The dynamics of the stomatal aperture were analyzed in plants grown under short-day conditions and using 4- to 5-week-old plant leaves. Epidermal peels collected from the abaxial side of the leaves were cut into two parts. In one part stomatal opening was induced by incubation in a buffer solution (20 mM KCl, 1 mM CaCl₂ and 5 mM MES-KOH, pH 6.15) for 3 hr under continuous light. In the other part stomatal closing was induced by incubation under the same conditions and in the same solution but containing 10 μ M ABA or 1 mM H₂O₂. Another sets of leaves was incubated in the same buffer for 3 hr in the dark to induce stomatal closure, with the duplicate set of leaves incubated under the same dark conditions in the same buffer solution but containing the fungal compound Fusicoccin (10 μ M) to induce stomatal opening. Snapshots of the epidermal peels were taken using a Zeiss AxioCam 512 color camera fitted on a Zeiss Axiophot microscope with a 40 \times objective. Stomatal pore dimensions (aperture length and width) and guard cell pair dimensions (length and width) were measured using ImageJ software (Schindelin *et al.*, 2012).

2.4.2 Gas exchange analysis

The gas exchange rate of 4- to 5-week-old plants was measured using a LI-6400XT portable photosynthesis system (Li-Cor Biosciences Inc.). Three to five individual plants, grown under short-day conditions, were used for each experiment, and each experiment was repeated five times. The conditions in the whole-plant chamber for light-dependent experiments were as follows: flow rate 200 μ mol/sec, block tempera-

ture 20°C, relative humidity 50–70%, [CO₂] 400 μmol/mol. For differential light conditions, the plants were dark-exposed (0 PAR) for 30 min and then light-exposed (400 PAR) for 30 min followed by another dark (0 PAR) phase for 30 min. The data were logged every 30 sec. For the differential CO₂ condition, constant 400 PAR light was applied as follows: 30 min in 100 μmol/mol [CO₂], increasing to 1000 μmol/mol for 30 min, and then another 30 min of 100 μmol/mol. The LI-6400XT portable photosynthesis system (Li-Cor Biosciences Inc.) generate the raw data for rate of transpiration over time with a default value for the area of the plants. The equation summary for the rate of transpiration can be found in the manual of LI-6400 portable photosynthesis system (<http://sites.middlebury.edu/biol323/files/2011/01/6400MAN.pdf>, p.1-7). After the measurement of gas exchange rate, the area of the plant is measured with ImageJ (Schindelin *et al.*, 2012). This value is then added to the raw data from LI-6400XT system which automatically update the rate of transpiration measurement according to the plant area. Furthermore, the time scale is adjusted according to the experiment. For example, the time point 0 is set at the time of 400 PAR light or 1000 μmol/mol [CO₂] and subsequently 30 min in negative scale and 60 min in positive scale can be adjusted in the x-axis of the graph.

2.4.3 Drought stress evaluation

The drought induction study was performed using 4- to 5-week-old plants grown under short-day, well-watered conditions. Drought stress was induced by depriving the plants of water for 14 days after which the plants were re-watered for 2 days and the number of surviving plants were then counted. Images were taken of the well-watered plants, of the plants deprived of water for 14 days, and of the plants 2 days after re-watering. Leaf

fresh weight loss was measured using three individuals from 5- to 6-week-old plants. Five leaves from each plant were detached and immediately placed on a balance for fresh weight measurements. These leaves were dried on the laboratory bench for 90 min, with their fresh weight measured every 30 min.

2.4.4 Growth assay under differential light regimes

Seeds from the wild-type Col-0 and from the *cgm3cgm4*, *cgm3cgm4CGM4* and *CGM4ox* mutants were stratified at 4°C in the dark for 48 hr, sowed on soil and then germinated under the short-day condition as described above. Ten-day-old seedlings were then transferred to single pots and two sets of 10 plants from each plant line were prepared. One of the sets was placed under 75% light ($\mu\text{mol}/\text{m}^2/\text{s}$ photon) and the other under 100% light ($\mu\text{mol}/\text{m}^2/\text{s}$ photon) conditions in a Percival growth chamber (AR66L3). The plants were grown under the short-day conditions described above. After 4 weeks, the fresh weight of each plant from both sets was measured. The experiment was repeated at least three times.

2.4.5 Reactive oxygen species (ROS) accumulation assay

Guard-cell accumulation of ROS was analyzed using the dye DCFDA (2',7' -dichlorofluorescein diacetate). Epidermal peels were incubated in water or in stomatal opening buffer (20 mM KCL, 1 mM CaCl₂ and 5 mM MES-KOH, pH 6.15) for 3 hr, after which 50 μM DCFDA was added and the incubation was continued at room temperature in the dark for 10 min. The peels were then washed with water and their fluorescence was observed using a confocal microscope (Leica SP8). ImageJ software was used to measure the fluorescence intensity (Schindelin *et al.*, 2012). Another set of epidermal peels was

incubated for 30 min with 25 μ M DPI (diphenyleneiodohium), an NAD(P)H oxidase inhibitor with ROS scavenging activity. The peels were then washed with water, stained with 50 μ M DCFDA and the fluorescence of the guard cells was imaged by confocal microscopy as described above.

2.4.6 Germination assay

Surface-sterilized seeds (n=100/plant line) were sown on $\frac{1}{2}$ MS plates with sufficient space between each seed. The plates were stratified at 4°C in the dark for 48 hr to ensure uniform germination. The plates were then incubated under continuous light with 40% relative humidity and at a temperature of 23°C. The germination rate was determined every 24 hr for 3–4 days after light induction. The experiment was repeated at least 4 times.

For GA3 treatment, a 1 mM stock solution of GA3 was prepared in methanol and added to $\frac{1}{2}$ MS plates to achieve final concentrations of 5 μ M and 10 μ M. The surface-sterilized seeds were sown on the plates and processed as described above.

For ABA treatment, a working solution of 1 mM ABA was prepared in ethanol and added to the $\frac{1}{2}$ MS plates to achieve final concentrations 1 μ M and 2 μ M. The surface sterilized 100 seeds of each lines were sown on the plates and processed as described above.

2.5 Microscopy

2.5.1 Confocal microscopy

Confocal microscopy in this study was performed using the confocal Leica TCS SP8 (upright) and confocal Leica TCS SP8 AOBS-FLIM-FCS (inverted) microscopes of the central facility of ZMBP, Tübingen. The fluorophores used in the experiments and their excitation/emission spectra were as follows:

Fluorophore	Excitation	Emission spectra
eGFP	488 nm	488 nm-507 nm
mScarlet	552 nm	569 nm-593 nm
SR200	405 nm	415 nm-476 nm
Propidium iodide	488 nm	535 nm-617 nm

For propidium iodide staining, 10 μ l of stock stain solution (1 mg/ml) was diluted in 1 ml of water. SR2200, staining was performed using 10 μ l of stock stain solution diluted in 100 μ l of water. The subcellular localization experiment was performed by vacuum infiltrating 0.8 M mannitol (pH 9.0) was into the samples to induce plasmolysis. Virtual transverse sectioning was achieved by transforming the z-stacked images of individual stoma into 3D images using Leica software. Virtual sections were obtained at the center of the stoma.

2.5.2 Scanning electron microscopy (SEM)

The Zeiss Sigma VP FE-SEM microscope used in this study was from the lab of Prof. Dominik Begerow, Ruhr-University, Bochum. Leaf or seedling samples were glued onto the sample stub using Tissue-Tek O.C.T compound mixed with a small amount of

colloidal graphite. The samples were then fixed by cryo-immobilization, sublimated in a vacuum chamber at -90°C for 12 min, and sputter-coated with platinum particles in a sputtering system at 30 mA for 90 sec. SEM images were captured using at 10 kV voltage and 200 \times and 300K \times magnifications. To observe the transverse side of the leaf, the samples were freeze-fractured after cryo-fixation in the vacuum chamber.

2.5.3 Atomic force microscopy (AFM)

The stiffness of the stomatal pore areas of wild-type Col-0 and the *cgm3cgm4* mutant was measured using AFM, with the help of Prof Tilman Schäffer and his team from Institute of Applied Physics, University Tübingen.

Small pieces (2 mm \times 2 mm) of leaves from 4-week-old plants were cut and mounted on glass slides using double-sided adhesive tape. AFM was performed using Macro AFM and a single cantilever (PPP-NC hr, Nanosensors, spring constant 18.47 N/m) for all measurements. The stomata were not localized optically due to the inverse microscopy set-up. The position of the stoma was determined from the AFM topography overview images using scan ranges of several hundred square millimeters and a spatial resolution of 3–5 μm . The individual images of the stomata were acquired at high resolution (0.5 $\mu\text{m}/\text{px}$).

2.6 Biochemical assay of cell wall

2.6.1 Cell wall extraction

Wild-type Col-0 and mutant *cgm3cgm4* and CGM4ox plants were grown under short-day conditions for 4–5 weeks. The fully expanded leaves were used for cell wall extraction as follows: 60–70 mg of leaves were frozen in liquid nitrogen, ground into fine powder, and then mixed thoroughly with 1.5 ml of 70% aqueous ethanol. The samples were then centrifuged for 10 min at 10000 rpm to pellet the alcohol insoluble residues (AIR) of the cell wall. The supernatant was discarded and the pellets were suspended in 1.5 ml of chloroform/methanol (1:1 v/v) solution, After centrifugation at 10000 rpm for 10 min, the supernatant was discarded and the pellet was washed with 500 μ l of acetone. The solvent was evaporated and the completely dry AIR pellet was stored at room temperature until further analysis.

2.6.2 Metabolomics analysis

Assays of cell wall metabolomics and total sugar composition were done with the help of Dr. Mark Stahl and Dr. Joachim Kilian, respectively, at the Analytics Facility of the ZMBP, University of Tübingen.

Leaf tissue (100–110 mg) was harvested and immediately frozen in liquid nitrogen. After lyophilization, the samples were homogenized with a ball mill (twice for 30 sec) and extracted first with 400 μ l of 80% methanol containing 0.1% formic acid and then with 400 μ l of 20% methanol also containing 0.1% formic acid. The two extracts were combined, brought to dryness and resuspended in 120 μ l of 20% methanol containing

0.1% formic acid. Five ml of each sample was injected for analysis and 10 μ l was used to create pooled samples.

The analysis was done using a Waters UPLC-SynaptG2 LC/MS system operated in ESI positive and negative modes. The mass spectrometer was operated in MS and MSE mode from 50 to 2000 m/z at a scan rate of 0.2 sec. Separation was achieved using a flow rate of 200 μ l/min and a 10 min gradient from 99% water to 99% methanol (both with 0.1% formic acid) on a Waters Acquity C18 HSST3 column (100 mm x 2.1 mm, 1.8 μ m). The data were evaluated using the ProgenesisQI software from Nonlinear Dynamics.

2.6.3 Immunostaining with the pectin epitopes

Immunostaining with the pectin epitopes was performed with the help of Dr. Arun Sampathkumar and his team from MPIMP Golm (Avci *et al.*, 2012).

Leaves from 3-week-old wild-type Col-0 and mutant *cgm3cgm4*, *cgm3cgm4CGM4* and *CGM4ox* plants were fixed for 2–3 hr in a solution containing 1.6% (v/v) paraformaldehyde/0.2% (v/v) glutaraldehyde in 25 mM sodium phosphate buffer (pH 7.1), using the vacuum infiltration technique. The samples were washed first with washing buffer for 15 min and then twice with water. The samples were then dehydrated in an ethanol series (30%, 50%, 70% and 100%) for at least 30 min/step and then infiltrated with a LR White resin series diluted 1:1 in ethanol for 12–24 hr followed by undiluted LR White for 12–24 hr. The samples were then inserted in gelatin capsules subsequently filled with LR white resin and then induced to polymerize under UV light for 48 hr at 4°C. Thin

sections were cut with a histodiamond knife on an ultramicrotome and then incubated first for 30 min with 3% (w/v) milk protein in 10 mM potassium phosphate-buffered saline solution (KPBS, pH 7.1) and then for 1 hr at room temperature in 10-fold diluted primary pectin antibodies (LM19, LM20 and 2F4). After three washes in 10 mM KPBS the samples were incubated for 1 hr with the appropriate Alexa fluor 488 secondary antibody (anti-rat or anti-mouse, depending on the animal source of the primary antibody). The samples were counterstained with 0.25% (v/v) Calcofluor White solution and imaged using a confocal microscope.

2.6.4 Apoplastic sap extraction

The full-grown leaves of *A. thaliana* and *N. benthamiana* were selected for apoplastic fluid extraction. *N. benthamiana* leaves were infiltrated with *Agrobacterium* inoculum containing the construct of interest. Stable transformants of *A. thaliana* leaves were used for apoplastic fluid extraction. The leaves were detached from the plants at the base, washed thoroughly in cold water to remove the dirt and then dried. After the initial fresh weight was measured, the leaves were placed in a 60-ml plastic syringe filled with 40 ml of infiltration solution containing sodium-phosphate buffer (pH 6.5) mixed with protease inhibitor cocktail. The whole leaf area was infiltrated properly by creating a vacuum in the syringe. The infiltrated leaves were then carefully removed to avoid damage and their fresh weight was measured. The amount of apoplastic fluid was estimated by subtracting the initial from the final fresh weight. The infiltrated leaves were rolled in a single layer with a piece of Parafilm and placed in a 20-ml syringe head, which was then placed in a 50-ml Falcon tube to collect the apoplastic fluid. After centrifugation of the set-up at 1000 rpm for 10 min at 4°C, the apoplastic fluid was

collected in a fresh Eppendorf tube and stored at -80°C until further use.

2.6.5 Pectate lyase assay with commercial kit

A commercial pectin identification kit (K-PECID 08/18; Megazyme) was used for the pectate lyase assay, performed using cell wall extracts of leaves from wild-type Col-0 and the mutants *cgm3cgm4*, CGM4ox and PME15ox. The solutions and buffers (50 mM Tris-HCl buffer with 1 mM CaCl_2 , 0.5 M NaOH and 0.5 M HCl) were prepared according to the manufacturer's protocol. The pectate lyase enzyme (0.5 ml) was diluted in 50 ml of Tris-HCl buffer (pH 8.0). The kit contains five standards: (1) low-ester pectin extracted from citrus peel, (2) high-ester pectin extracted from citrus peel, (3) partly amidated low-ester pectin extracted from citrus peel, (4) pectin from sugar beet pulp, (5) lota carrageenan. The experiment was first conducted using the standards, prepared according to the manufacturer's protocol. Fifty mg of cell wall extract was moistened with two drops of propan-2-ol and then dissolved in 50 ml deionized water with stirring for 20–30 min using a magnetic stirrer. The pH of the solution was carefully adjusted to 12.0 with 0.5 M NaOH and incubated at room temperature for 15 min. Thereafter, pH was lowered to 8.0 by the addition of 0.5 M HCl and the final volume was adjusted to 100 ml with deionized water. The pectate enzyme treatment was set up as following:

Condition	Tris-HCl buffer (pH 8.0)	Sample	Deionised water	Diluted enzyme
Enzyme blank	0.5 ml	1.0 ml	1.0 ml	-
Sample blank	0.5 ml	-	1.5 ml	0.5 ml
Reaction	0.5 ml	1.0 ml	0.5 ml	0.5 ml

The enzyme treatments were set up in quartz cuvettes. After the contents had been

mixed, the cuvettes were incubated for 30 min at room temperature and their absorbance at 235 nm was then recorded. The final value was calculated as follows:

Blank absorbance = Enzyme blank + Sample blank

Delta Absorbance (dA) = Reaction Absorbance – Blank absorbance

Unsaturated product = $dA/L \times \epsilon$

(where, L= path-length of the reaction cuvettes(=1cm) and ϵ = the molar extinction coefficient of the reaction product ($4600M^{-1}cm^{-1}$))

Chapter 3

Results

3.1 Subcellular localization of CGM3 and CGM4

The *in-silico* tool SignalP-5.0 Server predicted the presence of an N-terminal signal peptide sequence in CGM3 and CGM4 and their putative cleavage sites, similar to the secretory proteins. The latter are transported to the extracellular space via the conventional secretory pathway, which includes the ER, Golgi, trans-Golgi network (TGN) and plasma membrane (see the *Introduction* for details). The presence of both an N-terminal signal peptide and a peptide cleave site suggested that CGM3, CGM4 and other GDSL hydrolases were driven to the secretory pathway (Fig.3.1).

The subcellular localization of CGM4 was determined by generating mScarlet-tagged CGM4 constructs under the 35S promoter and transiently expressed in tobacco (*N. benthamiana*) leaves. An analysis of the plants' epidermal cells showed the extracellular localization of CGM4. This result was verified by subjecting the epidermal cells to plasmolysis using 0.8 M mannitol (pH 9.0), in which case the mScarlet signal re-

mained in the apoplastic space. Furthermore, an additional construct was made in which CGM4 contained a mutated N-terminal signal peptide (dSP) under the 35S promoter (p35S:CGM4^{dSP}-mScarlet). This dSP construct did not localize in the extracellular space but remained in the cytoplasm as a punctate structure even after plasmolysis (Fig.3.2).

Full genomic sequence and signal-peptide-mutated constructs under the ubiquitin 10 promoter and tagged with GFP were generated and used to transform *A. thaliana* wild-type Col-0. The stable T2 lines were screened for higher expression of CGM3 and CGM4 transcripts using qRT-PCR. These plants were then used as CGM3 and CGM4 over-expression lines in subsequent experiments. In the mature root epidermal cells of these plants (pUBQ10:CGM4-GFP), the GFP signal was localized in the apoplast, whereas in the signal peptide mutants (pUBQ10:CGM4^{dSP}-GFP) localization was confined to the cytoplasm (Fig.3.3).

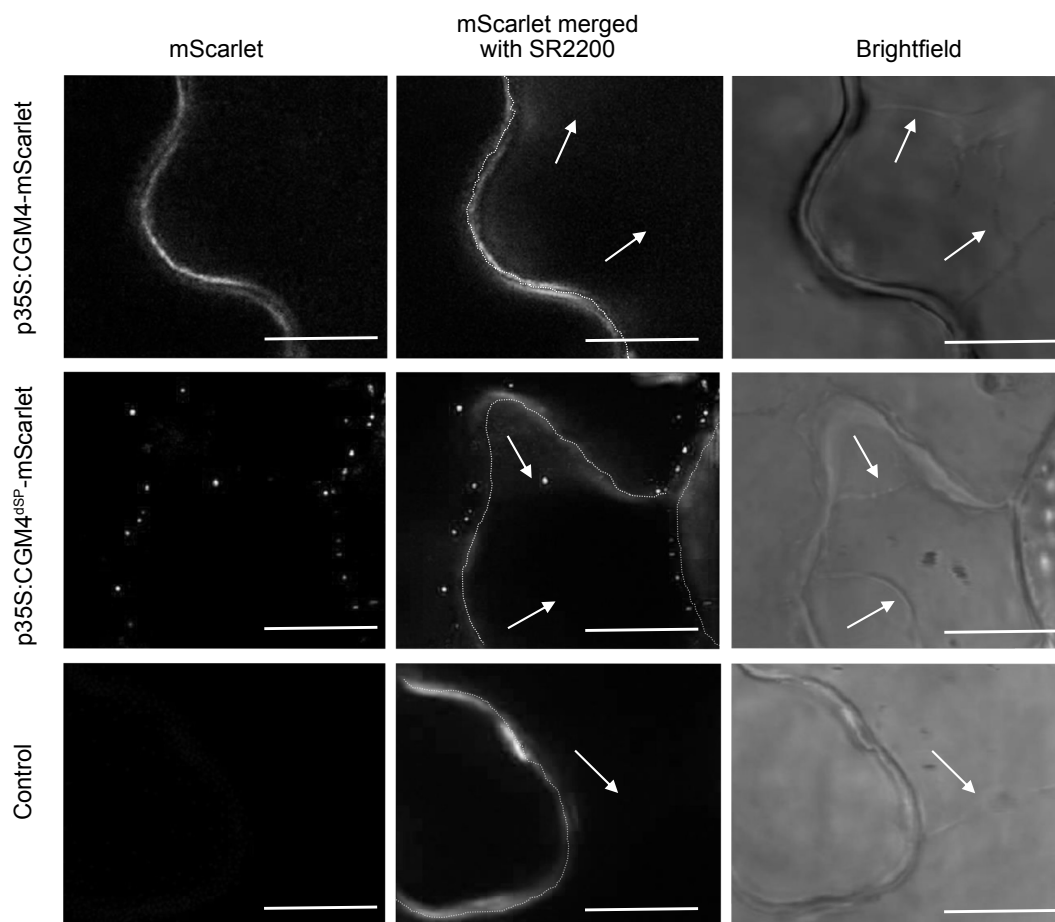


Figure 3.2: The p35S:CGM4-mScarlet localized in the extracellular space, p35S:CGM4^{ΔSP}-mScarlet localized in the cytoplasm as punctate structure. Un-infiltrated leaves were used as a negative control. The SR2200 dye was used to stain the cell wall. Plasmolysis was induced by 0.8 M mannitol (pH 9.0). White arrows indicate the location of plasma membrane after plasmolysis. The scale bar, 20 μm.

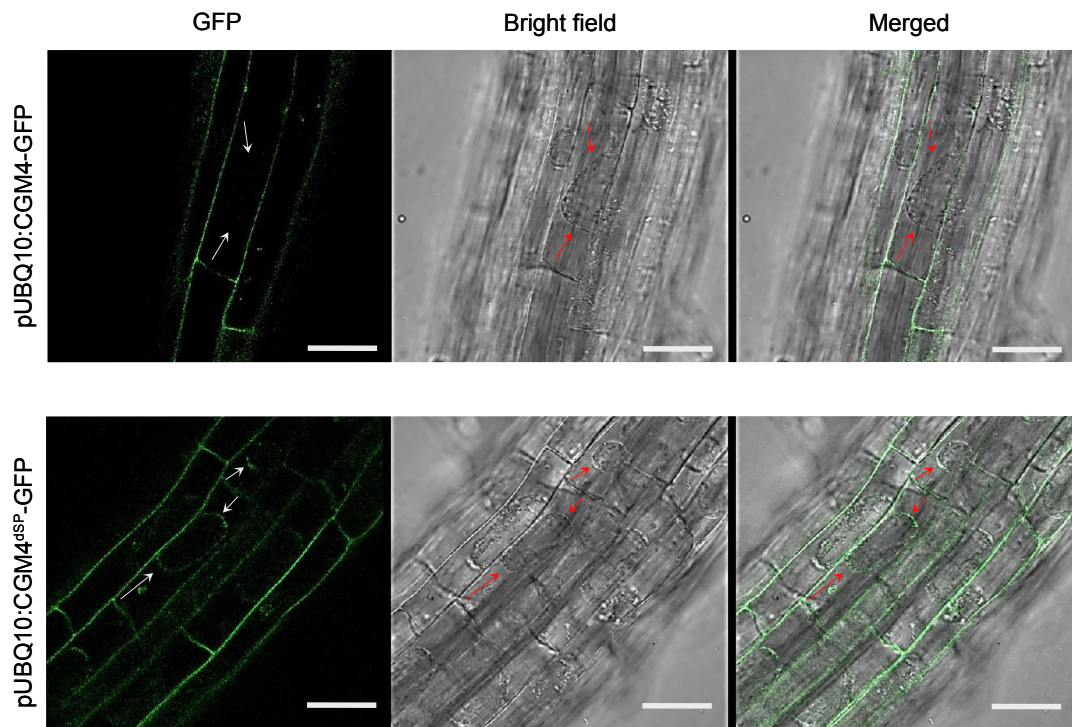


Figure 3.3: The pUBQ10:CGM4-eGFP localized in the extracellular space of root epidermis, pUBQ10:CGM4^{dSP}-eGFP localized in the cytoplasm as punctate structure. Plasmolysis was induced by 0.8 M mannitol (pH 9.0). The white and red arrows indicate the location of plasma membrane after plasmolysis. The scale bar, 30 μ m.

3.2 Tissue-specific expression of CGM4

The *in-silico* analysis with the eFP browser database (<https://bar.utoronto.ca/efp/cgi-bin/efpWeb.cgi>) predicted that, although homologous to each other, CGM3 and CGM4 were expressed in different tissues. While CGM3 was expressed in the imbibed seeds, CGM4 was expressed in the vegetative rosette. The CGM4 promoter, fused with GUS, drove expression in leaves, and specifically in the early developmental stages of stomata, but not in mature stomata (Grefen, 2008). To corroborate these findings, a CGM4 promoter fusion construct tagged with nls-GFP was used to transform *A. thaliana* wild-type Col-0 and tissue specific localization in the T2 lines were screened using confocal microscopy. The GFP signal was localized in the nucleus during the different stages of stomatal development: meristemoids, guard mother cells, early guard cells and mature guard cells (Fig.1.5). To quantify the signal intensity in the different stages, 100 screenshots of the different stages were captured and analyzed with ImageJ software. The fluorescence intensity (arbitrary units) was calculated and then standardized against the background signal. The results showed a higher tendency of signal intensity in the early developmental stages, specifically in the guard mother cells and early guard cells (Fig.3.4).

A previous study using ChIP-seq analysis identified genes that were upregulated by the induction of SPCH, a key transcription factor in stomatal development pathway. CGM4 was upregulated after SPCH induction. To investigate the regulation of CGM4 under SPCH induction, the CGM4 promoter fusion was expressed in the *spch* mutant background. The epidermis of the homozygous mutant seedlings was devoid of any stomata or stomatal lineage and a CGM4 promoter fusion signal was not detected (Fig.3.5).

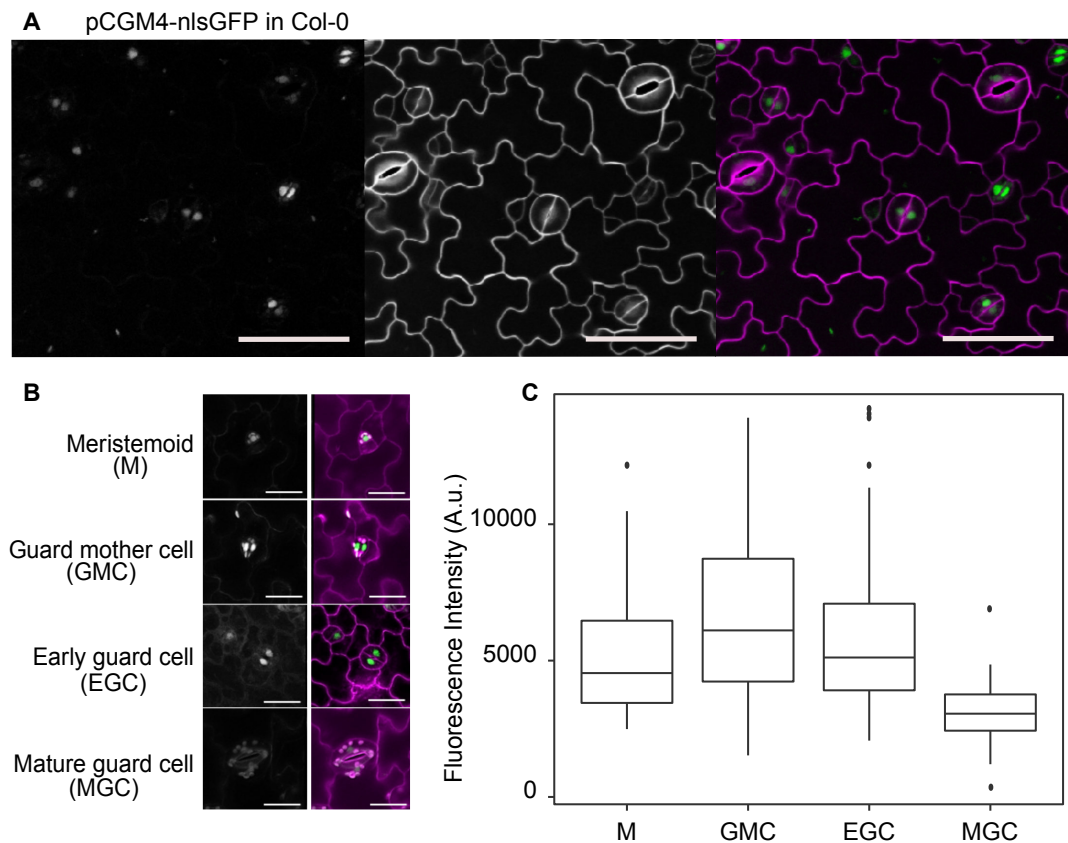


Figure 3.4: (A) Promoter GFP expression patterns of pCGM4:nlsGFP in different developmental stages of stomata in the cotyledons of 5 day old wild type Col-0 seedlings. Scale bar, 50 μ m. (B) Exemplary microscopic picture of different stages of stomatal lineages categorized as meristemoid, guard mother cell, early guard cell and mature guard cell, used for quantification of nlsGFP fluorescence intensity. Scale bar, 20 μ m. (C) Quantification of the fluorescence intensity (A.u.= Arbitrary unit) of GFP in different developmental stages categorized as meristemoid, guard mother cell, early guard cell and mature guard cell. Boxplots indicate the median (horizontal line) and interquartile range (box); whiskers show three times the interquartile range; points indicate values outside this range. n=100 cotyledons.

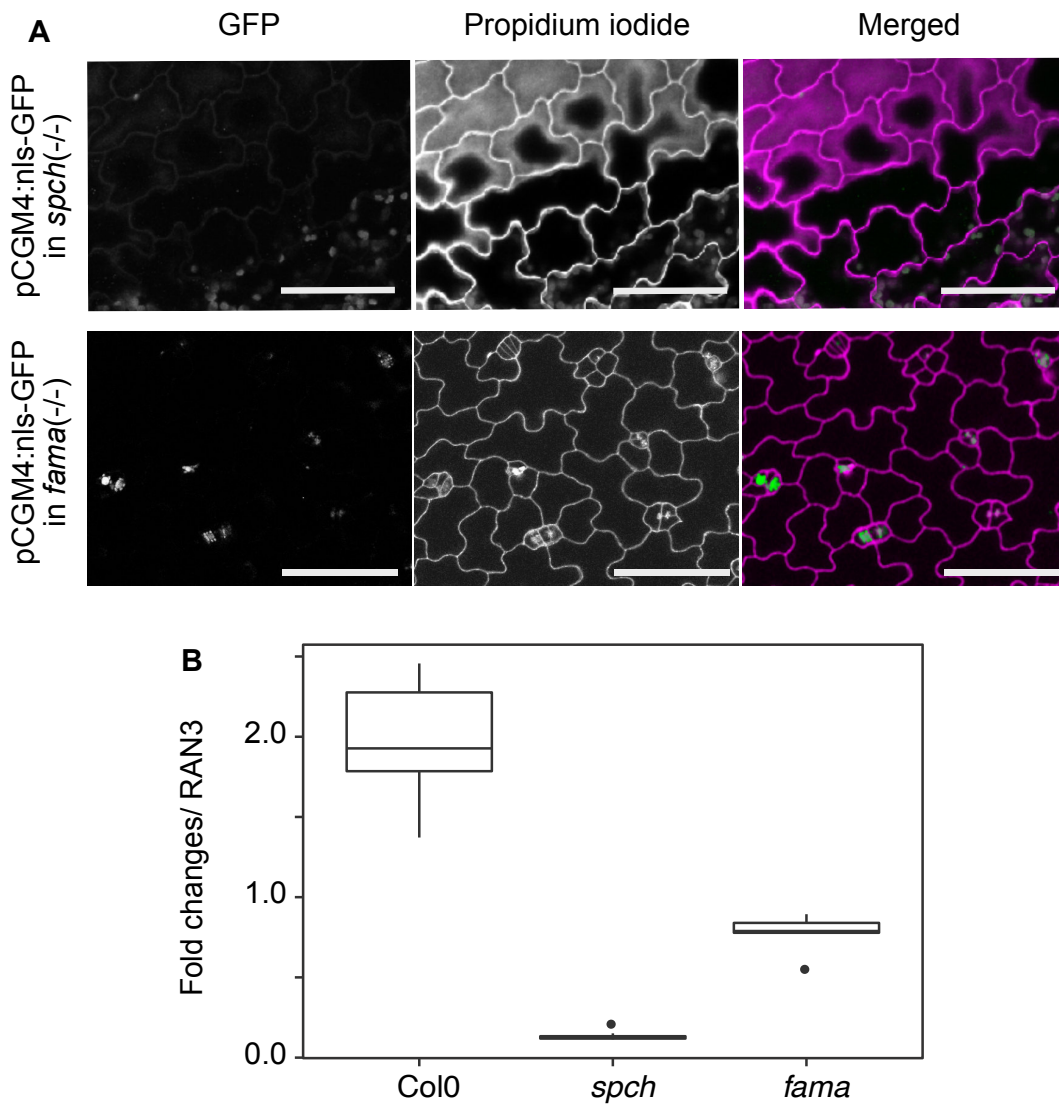


Figure 3.5: (A) Promoter GFP expression patterns of pCGM4:nlsGFP in the leaf epidermis of *spch* and *fama* mutant backgrounds. The scale bar, 50 μ m. (B) Quantification of CGM4 transcript compared to house-keeping gene RAN3 in wild type Col-0, *spch* and *fama* seedlings. Boxplots indicate the median (horizontal line) and interquartile range (box); whiskers show three times the interquartile range; points indicate values outside this range. n=6 biological replicates.

3.3 Tissue-specific expression of CGM3

Phylogenetic studies have suggested that CGM3 is a paralogous gene to CGM4. Although they share 90% sequence similarity, *in-silico* data suggest that the two genes are expressed in different tissues. A search of the *in-silico* database AtGenExpress using the eFP browser showed that CGM3 is expressed in imbibed seeds. In the expression analysis of ubiquitously over-expressed CGM3 (CGM3ox) and signal peptide-mutated CGM3 (CGM3^{dSP}ox) tagged with GFP a weak signal in the imbibed seeds was detected (Fig.3.6). An analysis of the CGM3 transcript level in wild-type Col-0, *cgm3* and CGM3ox seeds showed upregulation in the CGM3ox seeds compared to wild-type Col-0 but no obvious CGM3 transcripts in *cgm3* seeds (Fig.3.7).

Although CGM3 is the homolog of CGM4, it was not expressed in the stomatal lineages. However, in the absence of CGM4, in the *cgm4* mutant background, the CGM3 promoter fusion construct was weakly expressed in the early developmental stages of stomata (Fig.3.8). In an additional qRT-PCR analysis, the level of CGM3 transcripts in *cgm4* mutants was much higher than in wild-type Col-0 leaves, supporting the microscopy results (Fig.3.9).

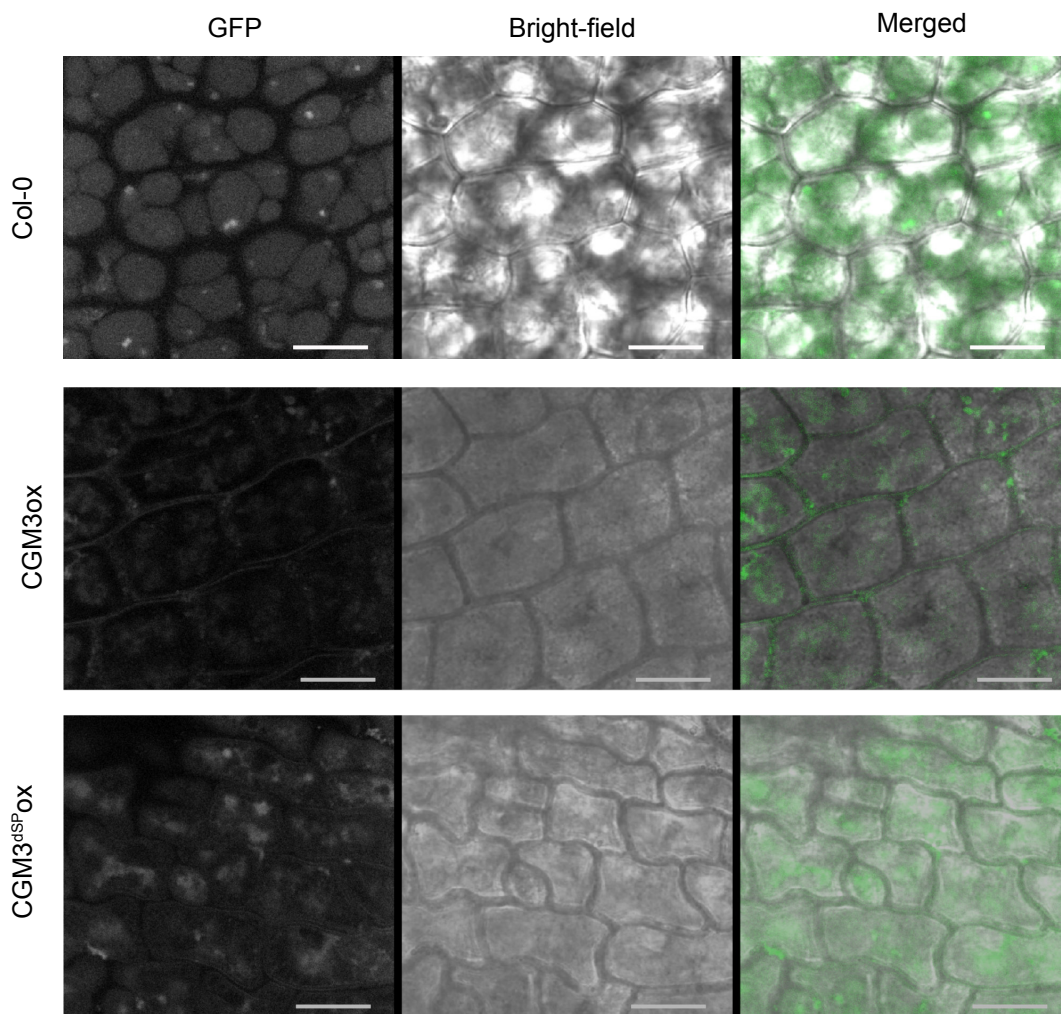


Figure 3.6: The pUBQ10:CGM3-eGFP localized in the extracellular space of imbibed seeds and pUBQ10:CGM3^{dSP}-eGFP localized in the cytoplasm of imbibed seeds. As negative control, imbibed seeds of wild type Col-0 was used. The scale bar, 10 μ m.

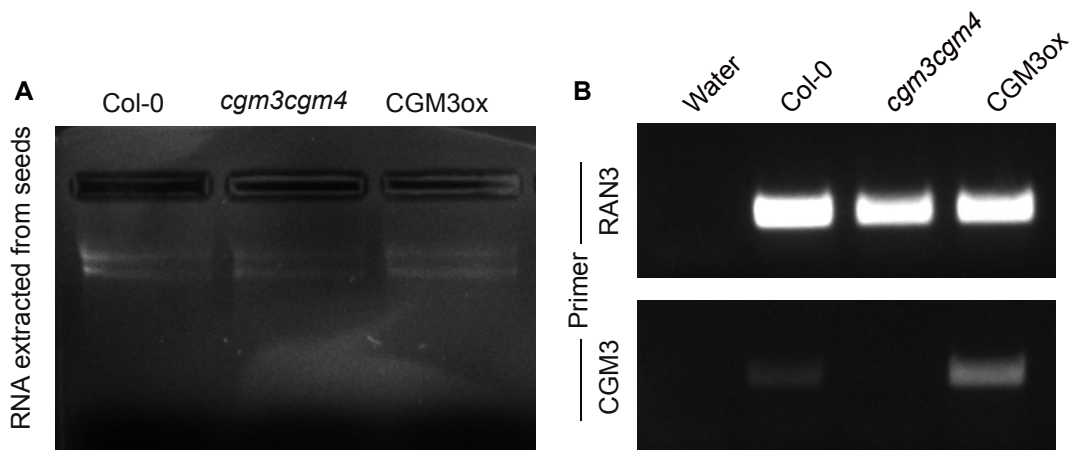


Figure 3.7: (A) Agarose gel image of RNA extracted from 24hr imbibed seeds of wild type Col-0, *cgm3cgm4* and CGM3ox. (B) Quantification of CGM3 transcript in 24hr imbibed seeds of wild type Col-0, *cgm3cgm4* and CGM3ox using semi-quantitative RT-PCR. Transcript level of house-keeping gene, RAN3, was used to verify equal amounts of inserted cDNA.

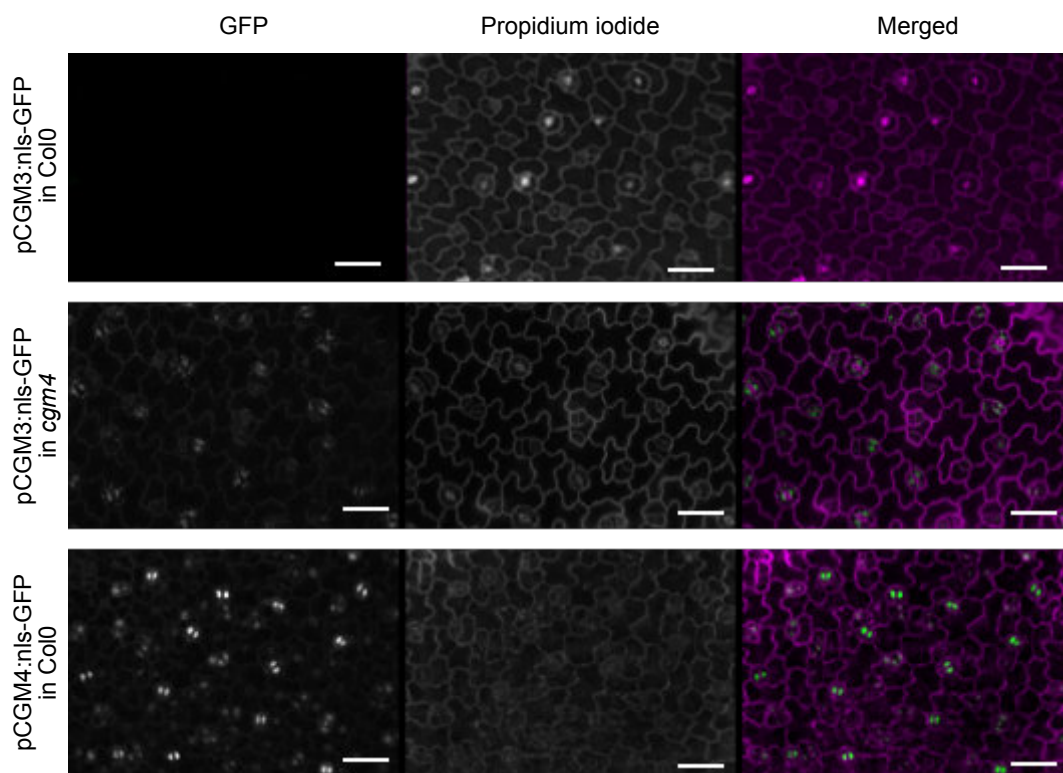


Figure 3.8: Promoter GFP expression patterns of pCGM3:nlsGFP in the leaf epidermis of wild type Col-0 and *cgm4*. Promoter GFP expression patterns of pCGM4:nlsGFP in the leaf epidermis of wild type Col-0. The scale bar, 50 μ m.

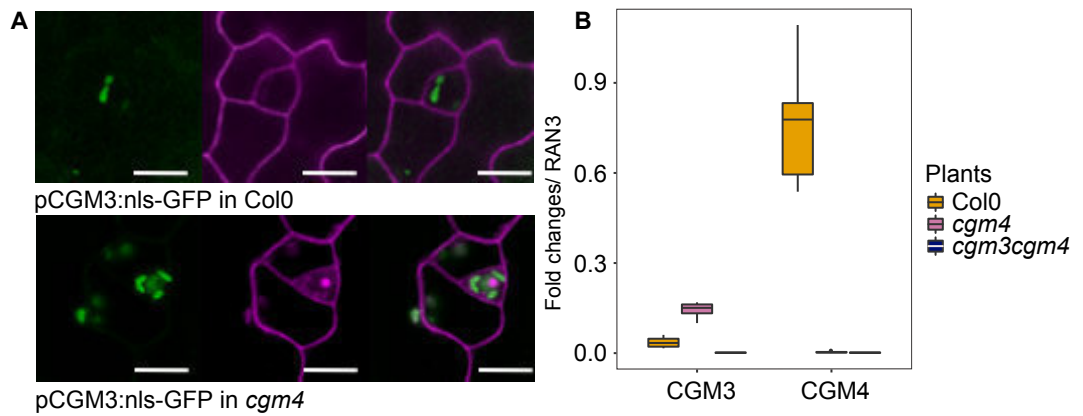


Figure 3.9: (A) Promoter GFP expression of pCGM3:nlsGFP in the meristmoid stage of stomatal lineage in wild type Col-0 and *cgm4*. Scale bar, 20 μ m. (B) Quantification of CGM3 and CGM4 transcript compared to house-keeping gene, RAN3, in wild type Col-0, *cgm4* and *cgm3cgm4* leaves using qRT-PCR. Boxplots indicate the median (horizontal line) and interquartile range (box); whiskers show three times the interquartile range; points indicate values outside this range. n=6 biological replicates.

3.4 Overall phenotype of *cgm3cgm4* plants

The function of the CGM3 and CGM4 genes was further investigated using single and double *cgm3* and *cgm4* mutant plants. No overall growth or phenotypic difference was seen in the mutant plants compared to wild-type Col-0 under ambient growth conditions. The flowering time and floral structure, mature silique structure and seeds, as well as root architecture and root hairs did not differ between the (single and double) *cgm3cgm4* mutants and wild-type Col-0 (Fig.3.10).

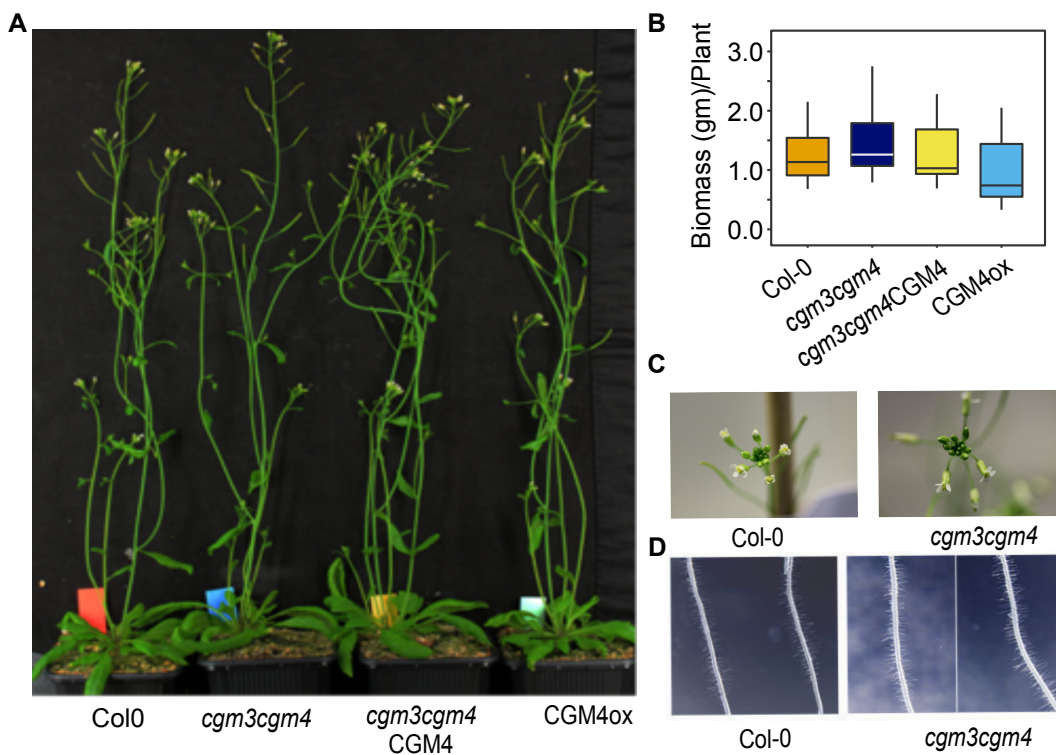


Figure 3.10: (A) 6 weeks old plants of wild type Col-0, *cgm3cgm4*, *cgm3cgm4CGM4* and CGM4ox grown under long day condition (B). Quantification of biomass production. Boxplots indicate the median (horizontal line) and interquartile range (colored box); whiskers show three times the interquartile range; points indicate values outside this range. n=40 plants. (C) The inflorescence tip of wild type Col-0 and *cgm3cgm4*. (D) The secondary root hair of wild type Col-0 and *cgm3cgm4*.

3.5 Stomatal index and patterning in *cgm3cgm4*

Following the detection of CGM4 expression in the stomatal lineage, stomatal number and patterning were studied in greater detail in the *cgm3cgm4* mutant seedlings. In the leaf epidermis of the wild-type, the stomata were distributed among the puzzle-shaped pavement cells following a 'one-cell spacing rule'. This pattern was seen in the epidermis of the mutant seedlings and there were no apparent differences in the structure of mature stomata. The number of stomata and pavement cells were determined and the stomatal index was calculated as the number of total stomata divided by the total number of cells. There was no apparent difference between the *cgm3cgm4* mutants and the wild-type Col-0 (Fig.3.11).

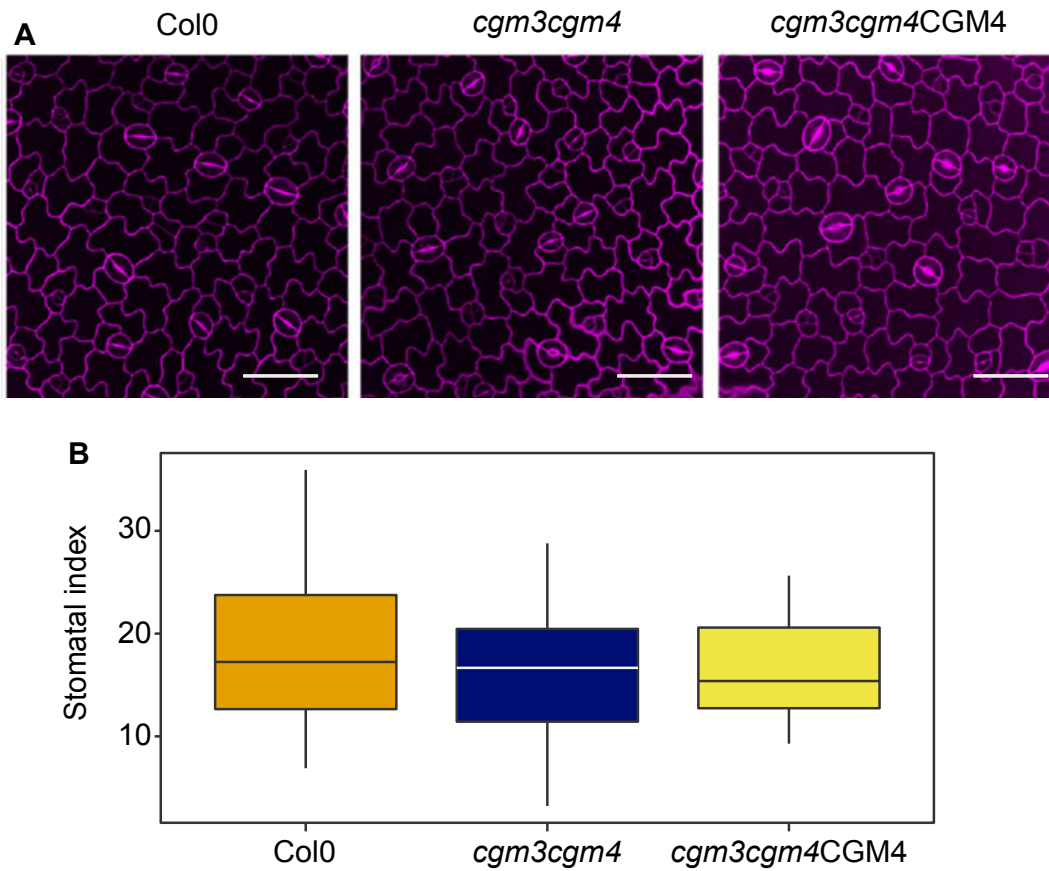


Figure 3.11: (A) The pattern and distribution of stomata in leaf epidermis of wild type Col-0, *cgm3cgm4* and *cgm3cgm4CGM4*. (B) The stomatal index (number of stomata/numbers of total cell) of wild type Col-0, *cgm3cgm4* and *cgm3cgm4CGM4*. Boxplots indicate the median (horizontal line) and interquartile range (colored box); whiskers show three times the interquartile range; points indicate values outside this range. n=50 cotyledons.

3.6 Stomatal aperture index in *cgm3cgm4* and *CGM4ox* under different abiotic stimuli

Stomata respond rapidly to different environmental stimuli, with their closure induced by phytohormone ABA, dark, H₂O₂ and a high CO₂ level, and stomatal opening by light, a low CO₂ level and the fungal compound fusicoccin. This study showed that *CGM4* was expressed in the stomatal lineage but did not influence the stomatal structure or patterning (see above). Thus, stomatal function was further investigated in wild-type Col-0 by and the mutants in *cgm3cgm4* and *CGM4ox* by measuring the width and length of the stomatal aperture and then determining their ratio to obtain the stomatal aperture index. The dynamics of stomatal opening and closing were followed by treating the epidermal peels of the leaves with several abiotic stimuli, including 10 μM ABA, 1 mM H₂O₂, 10 μM fusicoccin, and light and dark exposure. In wild-type Col-0 the ratio increased in response to light and fusicoccin treatment and decreased in response to ABA, H₂O₂ and dark treatment. By contrast, in the *cgm3cgm4* the ratio decreased in response to light exposure, ABA, H₂O₂, fusicoccin and darkness. However, complementation of the *cgm3cgm4* mutant with *CGM4* (*cgm3cgm4CGM4*) resulted in an increase in the ratio in response to light and fusicoccin and a decrease in response to ABA, H₂O₂ and darkness, similar to wild-type Col-0. The width to length ratio of the stomatal pore was higher in *CGM4ox* than in wild-type Col-0 following their exposure to light, dark, ABA, H₂O₂ and fusicoccin (Fig.3.12).

Three independent T1 lines of *CGM4ox* were studied for their response to light and ABA treatment. In two out of the three lines, the stomatal aperture index was clearly higher than that of the wild-type Col-0 following light and ABA treatment. Stomatal

opening-closing dynamics were also studied in the signal-peptide-mutated CGM4 construct CGM4^{dSP}ox in response to light and ABA. As the signal peptide was mutated in this construct, the mature enzyme was predicted to be mis-localized compared to the CGM4ox plants. In three independent T1 lines of CGM4^{dSP}ox, stomatal opening-closing dynamics, assessed as the width to length ratios of the stomatal pores, were similar to those of the wild-type Col-0 under light and ABA treatment (Fig.3.13).

3.6 Stomatal aperture index in *cgm3cgm4* and *CGM4ox* under different abiotic stimuli

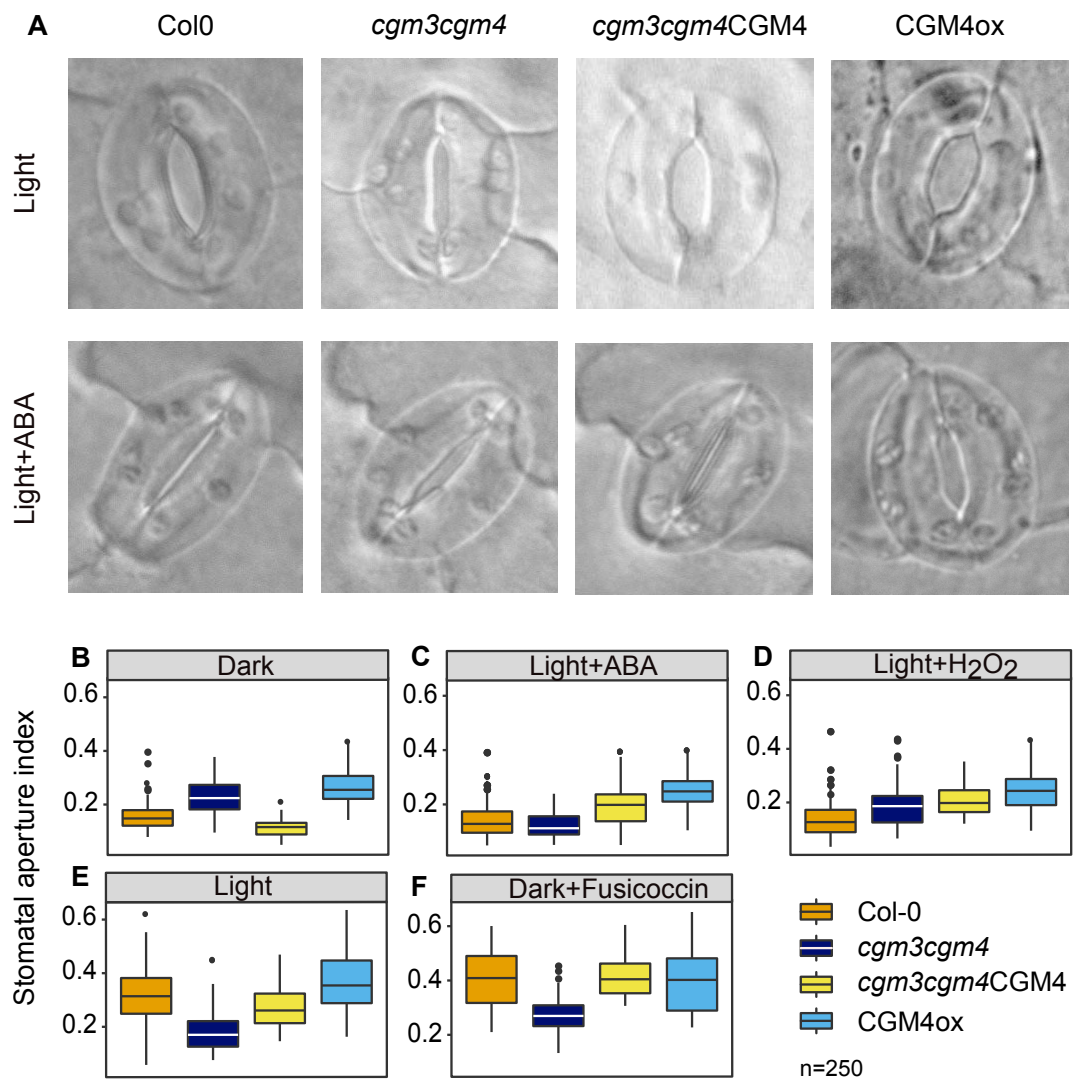


Figure 3.12: (A) Exemplary images of individual stomata of wild type Col-0, *cgm3cgm4*, *cgm3cgm4CGM4* and CGM4ox under the treatment of light to induce stomatal opening and ABA to induce stomatal closure. (B-F) Quantification of stomatal aperture index (width/length of stoma) in wild type Col-0, *cgm3cgm4*, *cgm3cgm4CGM4* and CGM4ox leaf epidermis upon treatment with dark (B), 10 μ M ABA (C), 1 mM H₂O₂ (D) to induce stomatal closure and light (E) and 10 μ M Fusicoccin (F) to induce stomatal opening. Boxplots indicate the median (horizontal line) and interquartile range (colored box); whiskers show three times the interquartile range; points indicate values outside this range. n=250 stomata.

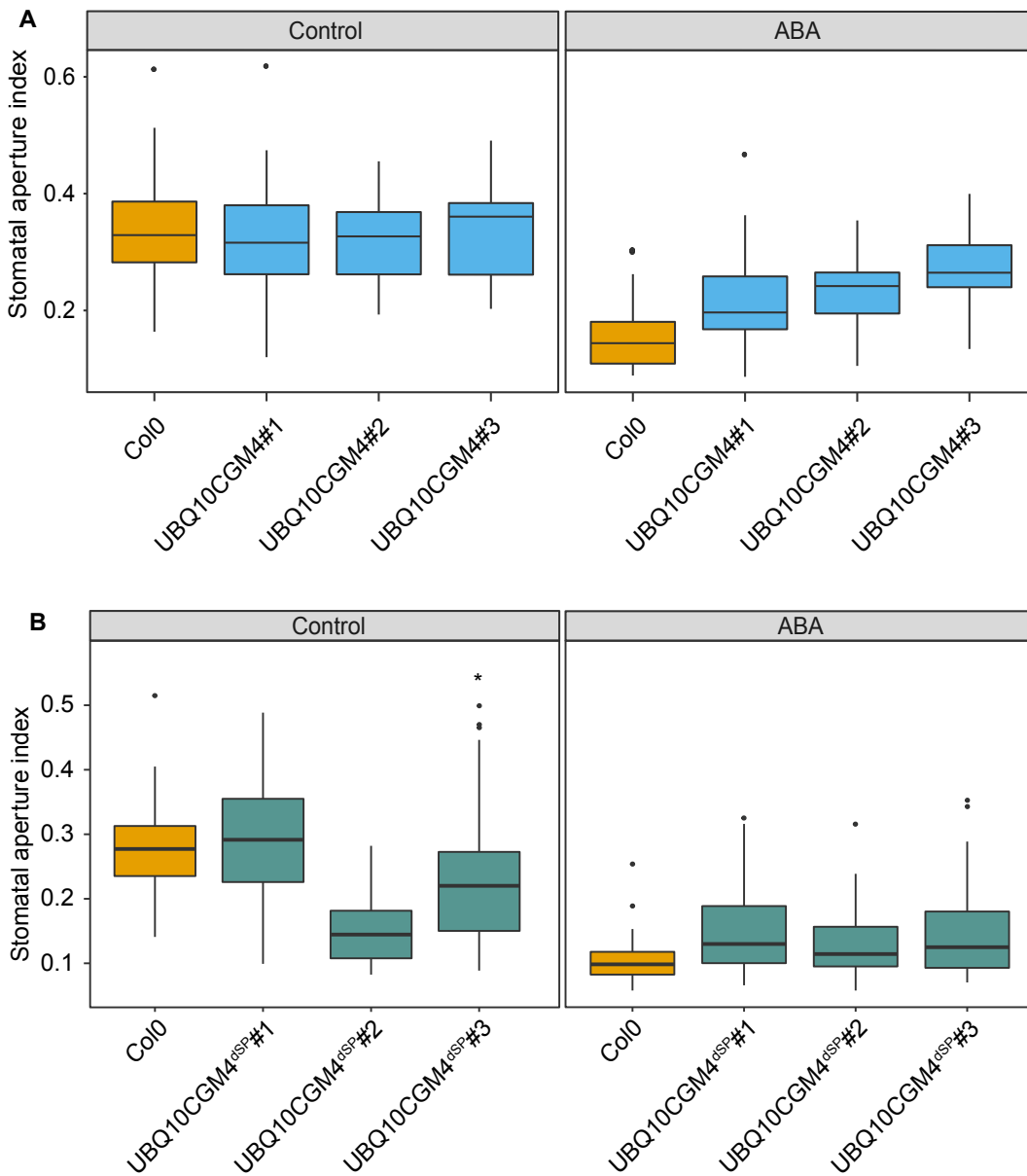


Figure 3.13: Quantification of the stomatal aperture index (width/length of stoma) in three independent CGM4ox (A) and CGM4^{dSP}ox (B) lines compared to wild type Col-0 under control conditions to induce stomatal opening and 10 μ M ABA treatment to induce stomatal closure. Boxplots indicate the median (horizontal line) and interquartile range (colored box); whiskers show three times the interquartile range; points indicate values outside this range. n=40 stomata.

3.7 Reactive oxygen species (ROS) accumulation assay in *cgm3cgm4* and wild-type Col-0

Reactive oxygen species (ROS) accumulation in guard cells is an early indicator of stomatal closure. ROS are found in the apoplast and chloroplast, where they regulate the activity of several ROS-producing enzymes, proteins and ion channels that in turn influence guard cell signaling. In this study, ROS accumulation in the stomata of *cgm3cgm4* and wild-type Col-0 was investigated using a fluorogenic dye DCFDA (2',7'-dichlorofluorescein diacetate) used to estimate hydroxyl, peroxy and other ROS activity in living cells. Epidermal peels were treated with stomatal opening solution or ABA to induce stomatal opening and closing, respectively, and then incubated in 50 μ M DCFDA for 10 min. The fluorescence intensity was measured using confocal microscopy. In stomatal opening buffer, there was no obvious fluorescence intensity in wild-type stomata whereas intense fluorescence was seen in *cgm3cgm4* stomata (Fig.3.14). The epidermal peels were then treated with 10 μ M ABA to induce stomatal closure and stained with DCFDA. The fluorescence of both *cgm3cgm4* and wild-type stomata was higher than in the respective stomata treated with stomatal opening solution. The effect of ROS scavenging activity was then analyzed using the NADPH oxidase inhibitor agent DPI (25 μ M) DPI followed by DCFDA staining. Fluorescence was seen in the stomata of *cgm3cgm4* plants but not in wild-type Col-0 stomata (Fig.3.15).

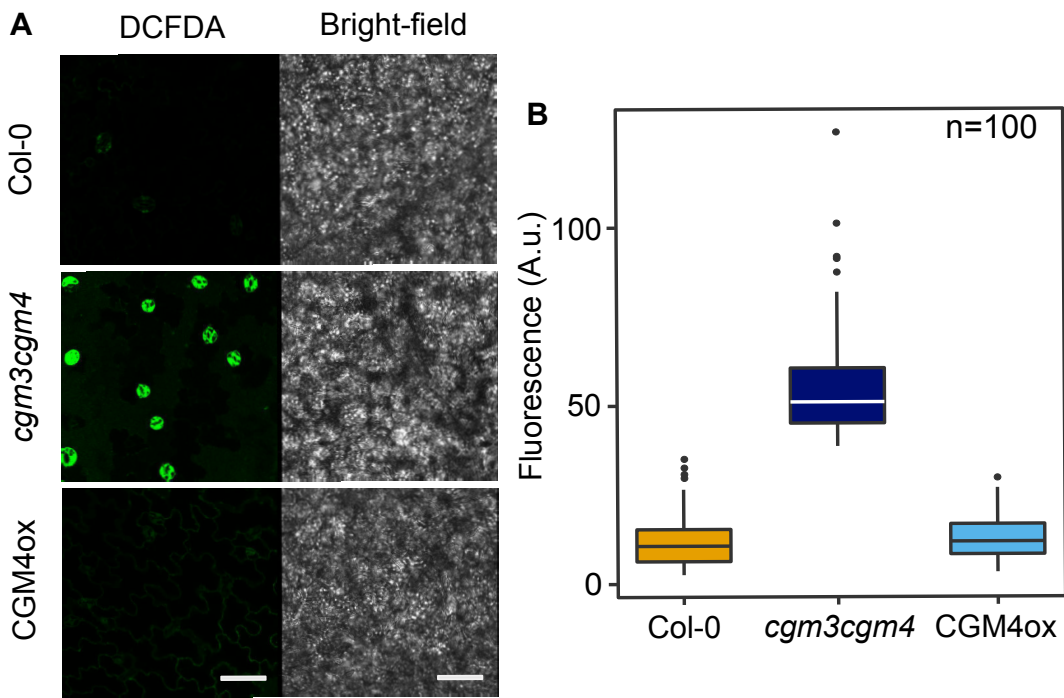


Figure 3.14: (A) Visualization of ROS (reactive oxygen species) accumulation in the epidermal peels of wild type Col-0, *cgm3cgm4* and CGM4ox stained with DCFDA (2',7'-Dichlorofluorescein diacetate). Scale bar, 50 μ m. (B) Quantification of DCFDA fluorescence intensity (A.u. = Arbitrary unit) in guard cells of wild type Col-0, *cgm3cgm4* and CGM4ox. Boxplots indicate the median (horizontal line) and interquartile range (colored box); whiskers show three times the interquartile range; points indicate values outside this range. n=100 stomata.

3.7 Reactive oxygen species (ROS) accumulation assay in *cgm3cgm4* and wild-type *Col-0*

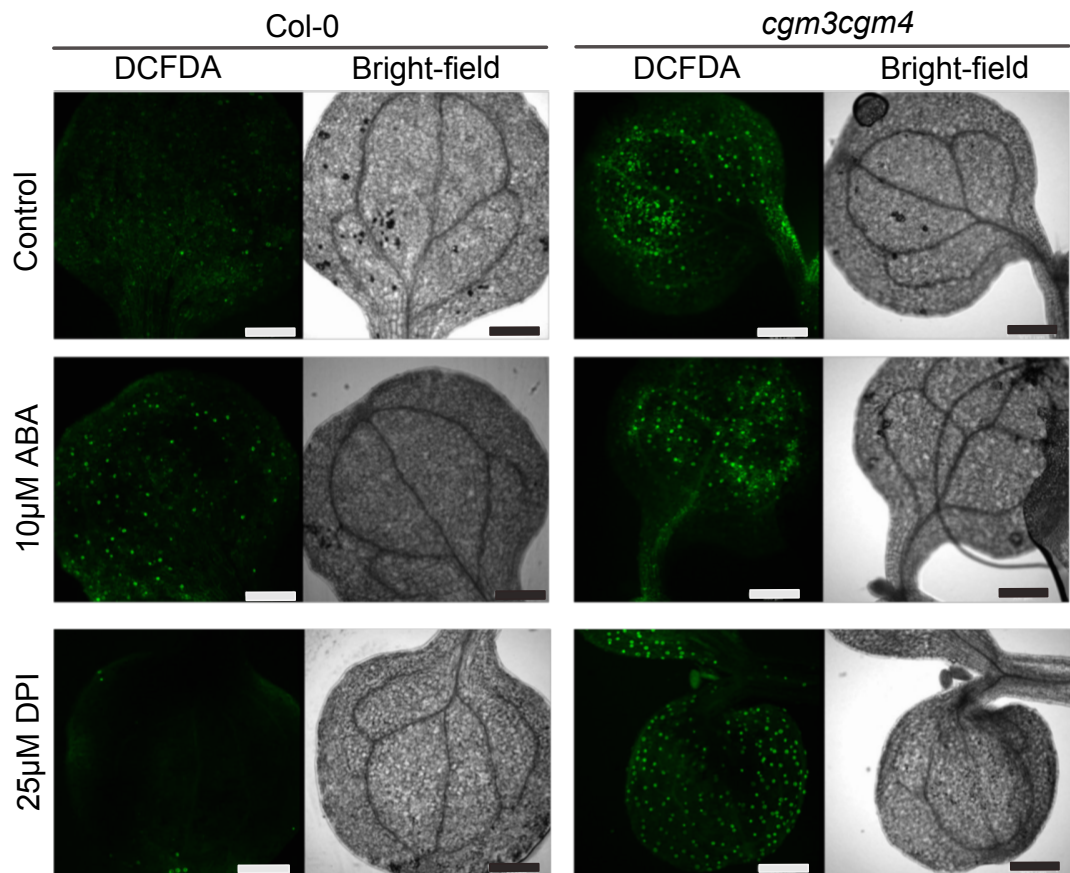


Figure 3.15: The ROS accumulation visualization of 5 days old seedling of wild type *Col-0* (left) and *cgm3cgm4* (right) under control condition (MES/KOH buffer) (upper), 10 μ M ABA treatment to induce ROS accumulation (middle) and 25 μ M DPI (Diphenyleneiodonium) to induce inhibit ROS production (lower).

3.8 Gas exchange in *cgm3cgm4* and CGM4ox in response to different abiotic stimuli

The opening-closing dynamics of the stomata influence gas exchange and therefore the physiological functions of the plant. A reduction in stomatal opening may thus affect the ability of the stomata to react to environmental stimuli and accordingly their transpiration rate. The transpiration rate in *cgm3cgm4* and CGM4ox leaves compared to wild-type Col-0 leaves was measured using an Infra-red gas analyzer (IRGA). In wild-type plants, the stomata rapidly responded to dark-light regimens and increased CO₂ levels. During the dark period, the transpiration rate of wild-type plants was low and upon light induction it increased, reaching a plateau in 60 min. During second period of dark induction, the transpiration rate again decreased. In *cgm3cgm4* plants, the transpiration rate induced by light induction tended to be lower than in wild-type plants, whereas in CGM4ox plants there was a tendency of a higher transpiration rate in response to both light and dark exposure. In the *cgm3cgm4CGM4* complemented lines, the values were similar to those of the wild-type Col-0 (Fig.3.16).

The CO₂ concentration surrounding the leaves also influences stomatal opening-closing dynamics and therefore the rate of gas exchange. In wild-type Col-0, the transpiration rate increased in response to 100 mmol CO₂ but at progressively higher CO₂ concentrations it gradually decreased. At a lower CO₂ concentration, the transpiration rate increased again. In the *cgm3cgm4* line, the transpiration rate in response to different CO₂ concentrations tended to be lower than in wild-type Col-0. By contrast, in the CGM4ox line there was a tendency towards a higher transpiration rate both at lower and higher CO₂ concentrations. In the *cgm3cgm4CGM4* complemented plants the response

3.8 Gas exchange in *cgm3cgm4* and *CGM4ox* in response to different abiotic stimuli

was similar to that of the wild-type Col-0 both at lower and higher CO₂ concentrations (Fig.3.17).

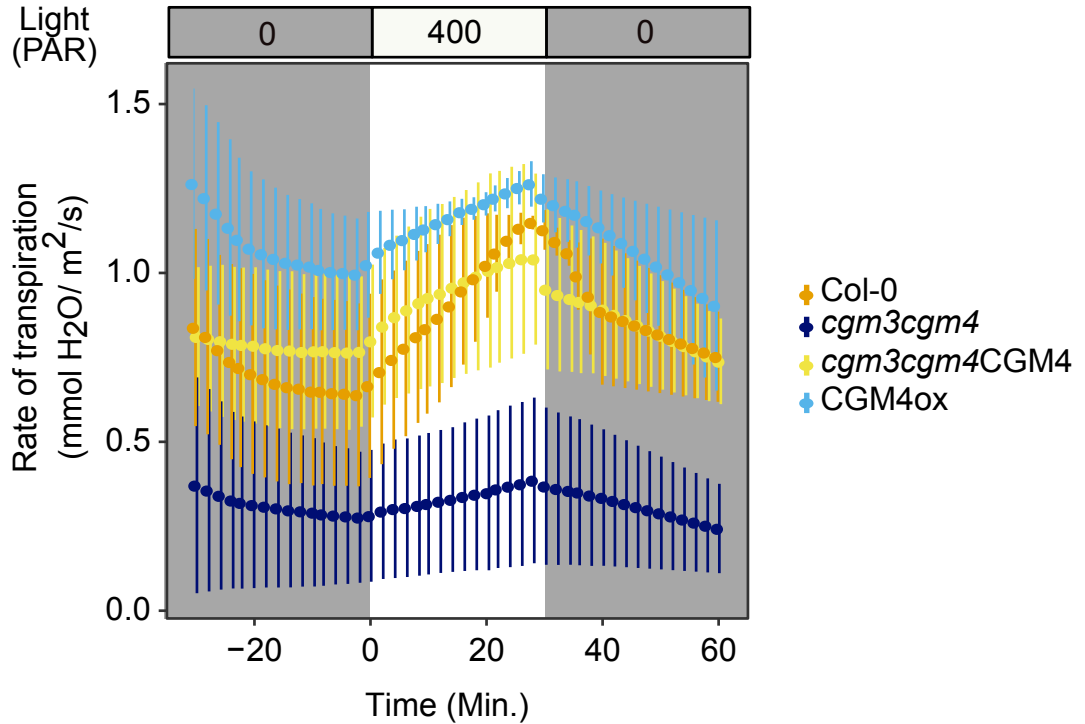


Figure 3.16: Response of stomata and rate of transpiration measurements with 4 weeks old wild type Col-0, *cgm3cgm4*, *cgm3cgm4CGM4* and *CGM4ox* plants under 0 PAR (photosynthetic active radiation) and 400 PAR light over time using IRGA (infra-red gas analyzer). The error bars indicate the standard error. n=3 independent plants.

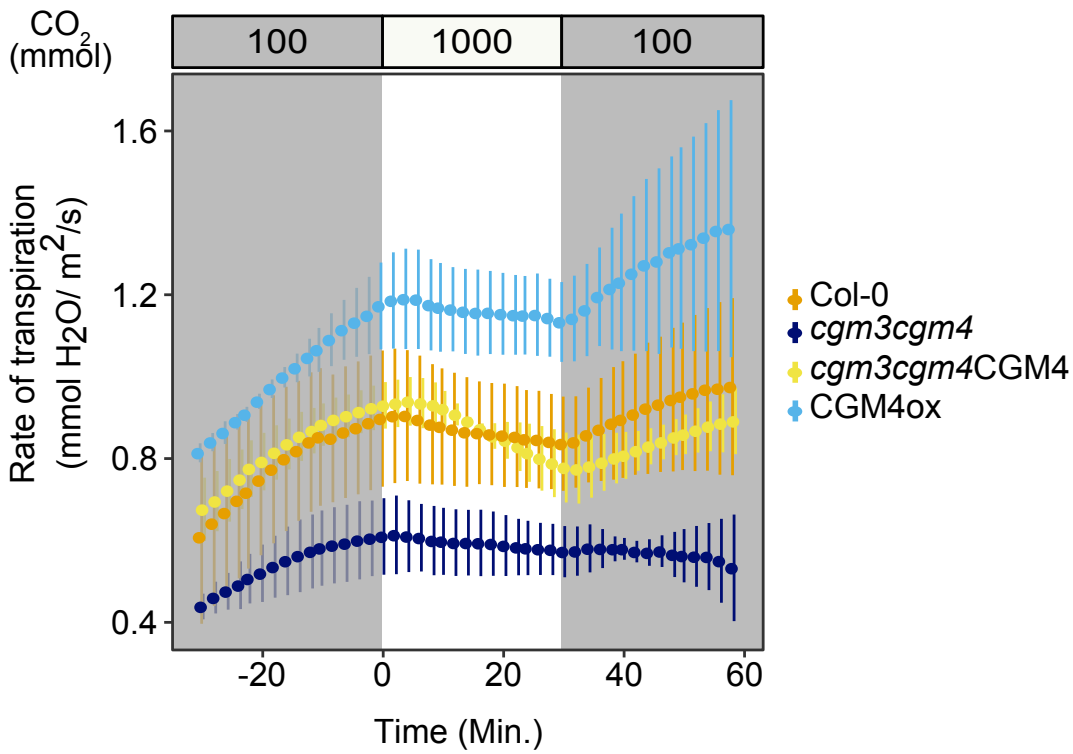


Figure 3.17: Response of stomata and rate of transpiration measurements with 4 weeks old wild type Col-0, *cgm3cgm4*, *cgm3cgm4CGM4* and CGM4ox plants under 100 mmol CO₂ and 1000 mmol CO₂ concentration over time using IRGA (infra-red gas analyzer). The error bars indicate the standard error. n=3 independent plants.

3.9 Response of *cgm3cgm4* and *CGM4ox* to pathogens

In addition to their central role in the regulation of gas exchange, stomata, as the natural pores on the plant surface, provide an entry for plant pathogens. Thus, stomatal opening-closing dynamics also influence the susceptibility to pathogens. To observe the reaction of the studied plants to pathogens, wild-type Col-0, *cgm3cgm4* and *CGM4ox* plants were infected with the bacterial pathogen *Pseudomonas syringae* pv. tomato DC3000 and observed for symptoms of infection. After infection of the plant surface with the bacterial inoculum and after 3 days the plants were examined for symptom development. Infection symptoms on the leaves, including yellow patches and necrotic brown spots, were more prominent in *CGM4ox* than in wild-type Col-0 whereas fewer infection symptoms were seen in *cgm3cgm4* (Fig.3.18).

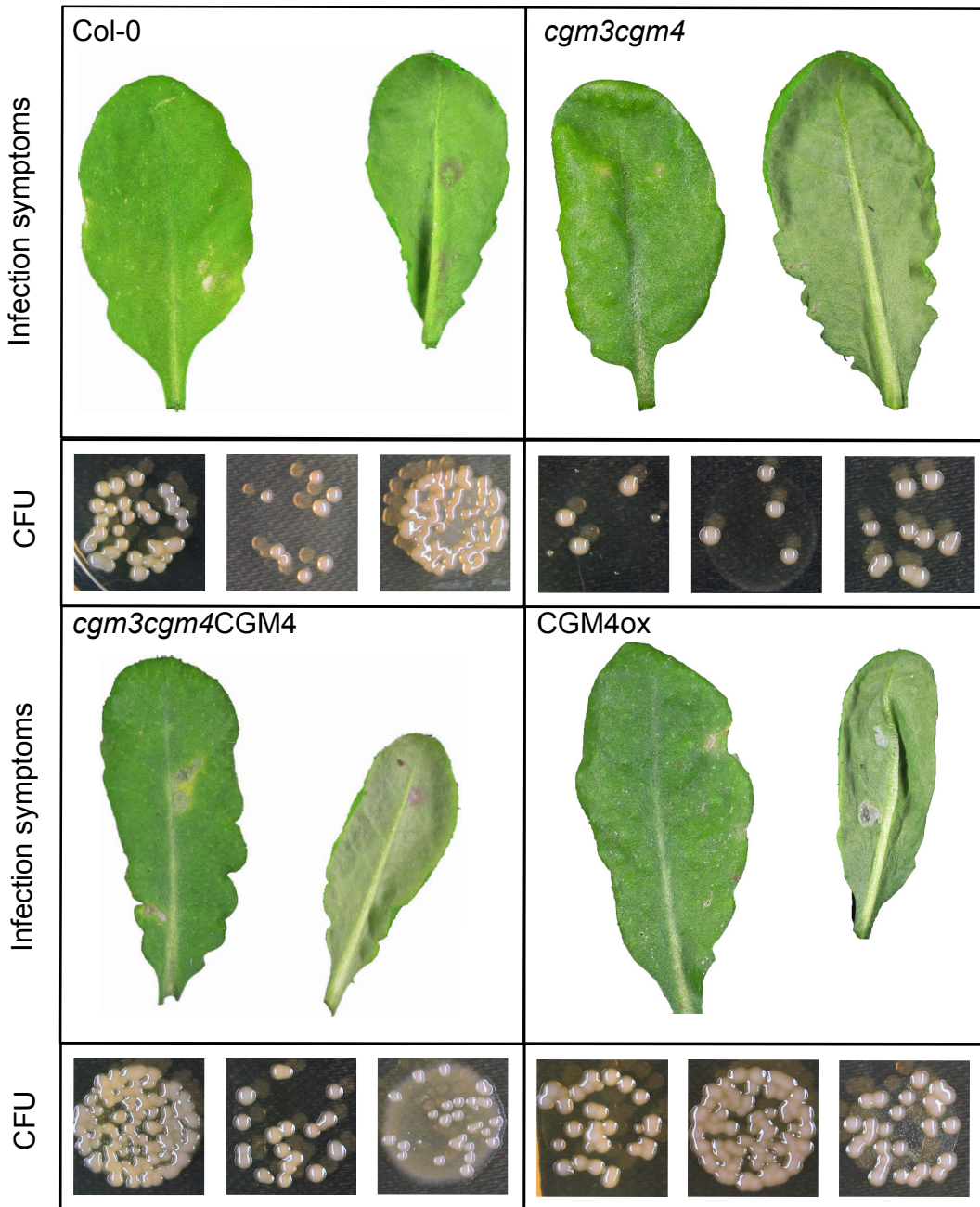


Figure 3.18: Infection symptoms on 4 week old leaves of wild type Col-0, *cgm3cgm4*, *cgm3cgm4CGM4* and CGM4ox 72 hr after treatment with *Pseudomonas syringae* pv. Tomato DC3000. Images of fungal colony on KB media from infected leaf extracts of wild type Col-0, *cgm3cgm4*, *cgm3cgm4CGM4* and CGM4ox.

3.10 Effects of drought stress in *cgm3cgm4* and *CGM4ox*

Previous studies have shown that by influencing gas exchange in plants stomatal opening-closing dynamics impact plant physiological responses to abiotic stresses such as drought. In this study, the number of plants that recovered from drought after re-watering was higher among *cgm3cgm4* plants and lower among *CGM4ox* plants than among wild-type Col-0 plants. Recovery from drought by complemented *cgm3cgm4CGM4* plants was the same as by wild-type Col-0 (Fig.3.19).

Water loss among the different plant was assessed by removing five leaves from each of three to five wild-type Col-0, *cgm3cgm4*, *CGM4ox* and *cgm3cgm4CGM4* plants and allowing them to dry on the laboratory bench. The fresh weights were measured at 0 min and then every 30 min and the percent water loss over time was calculated. The results showed that water loss tended to be slower in *cgm3cgm4* and faster in *CGM4ox* than in wild-type Col-0. In the complemented plants, the rate of water loss similar to that of wild-type Col-0 (Fig.3.20).

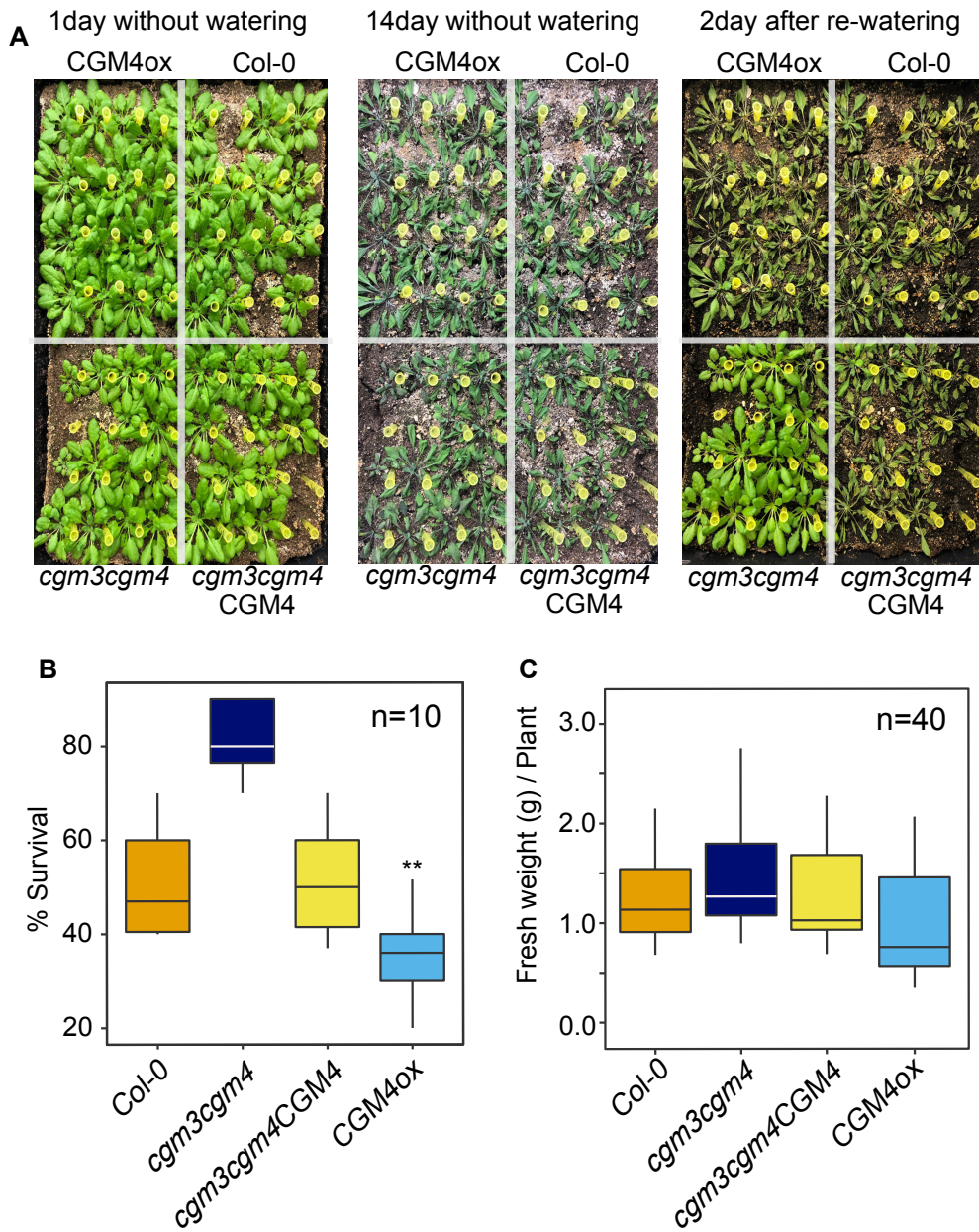


Figure 3.19: (A) The wild type Col-0, *cgm3cgm4*, *cgm3cgm4*CGM4 and CGM4ox plants were grown for 4-5 weeks under short day condition (left) and then they were exposed to drought by withholding water for 14 days (middle). The plants were then re-watered for 2 days (right) and the number of surviving plants were counted (B). Boxplots indicate the median (horizontal line) and interquartile range (colored box); whiskers show three times the interquartile range; points indicate values outside this range. n=10 (The experiment was repeated 10 times and each time 40 plants of each genotype were counted). (C) Quantification of the fresh weight of 5 weeks old short day grown plants of wild type Col-0, *cgm3cgm4*, *cgm3cgm4*CGM4 and CGM4ox. Boxplots indicate the median (horizontal line) and interquartile range (colored box); whiskers show three times the interquartile range; points indicate values outside this range. n=40 plants.

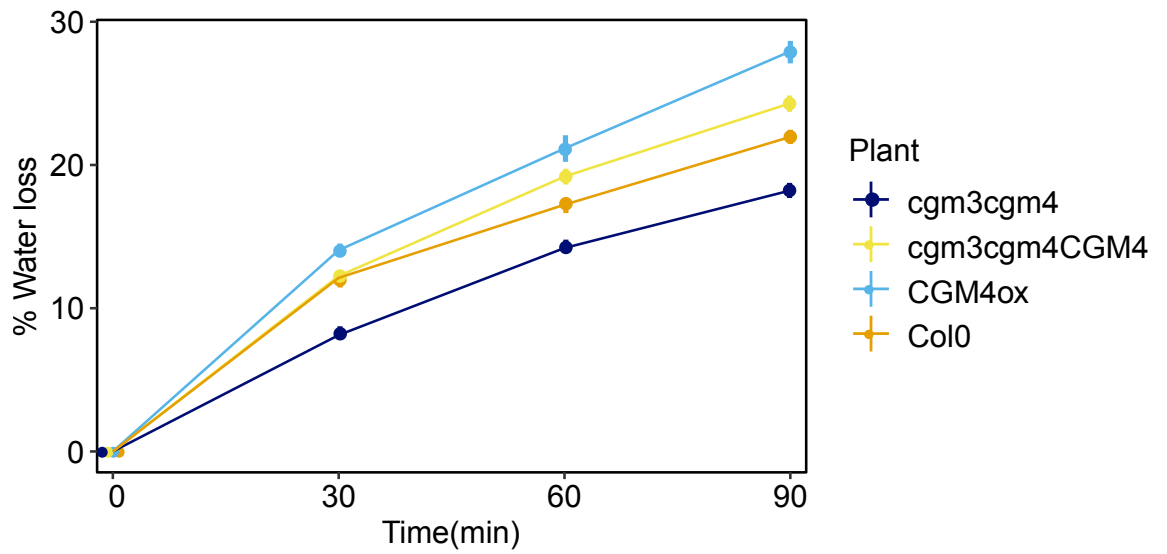


Figure 3.20: Quantification of water loss as difference between initial fresh weight and final fresh weight from the detached leaves of wild type Col-0, *cgm3cgm4*, *cgm3cgm4CGM4* and *CGM4ox* over time. The error bars indicate the standard error. n=5 individual leaves from independent plants.

3.11 ABA-induced gene transcription in *cgm3cgm4* and wild-type Col-0

The phytohormone abscisic acid (ABA) regulates several developmental processes in plants, including growth, seed germination and stomatal movement. ABA responds to biotic and abiotic stimuli, including drought and pathogen attack, and induces multiple signaling cascades leading to stomatal closure (Munemasa *et al.*, 2015). At the molecular level, ABA regulates physiological responses by altering the transcription level of its target genes (Hoth *et al.*, 2002), including in *A. thaliana* (Hoth *et al.*, 2002). In this study, in *cgm3cgm4* exposed to abiotic stimuli that induce stomatal opening and closing the stomatal aperture index and transpiration rate were clearly reduced compared to wild-type (Figs.3.12, 3.16, 3.17). To determine whether this change in stomatal opening-closing dynamics in *cgm3cgm4* was mechanical or ABA-induced, a transcriptome analysis was performed. The leaves of *cgm3cgm4* and wild-type were treated or not (control) with 10 μ M ABA for 3 hr under light conditions. The RNAseq results showed that in wild-type and *cgm3cgm4* plants a higher number of genes was upregulated in ABA-treated than in non-treated (control) leaves but there was no obvious differences between the two lines of treated plants (Fig.3.21). An analysis of the transcript level of 21 ABA-induced genes in *cgm3cgm4* vs. wild-type plants treated with ABA showed no obvious difference between them but that the transcript level was clearly upregulated in both compared to untreated plants (Fig.3.22, Tables3.1, 3.2, 3.3).

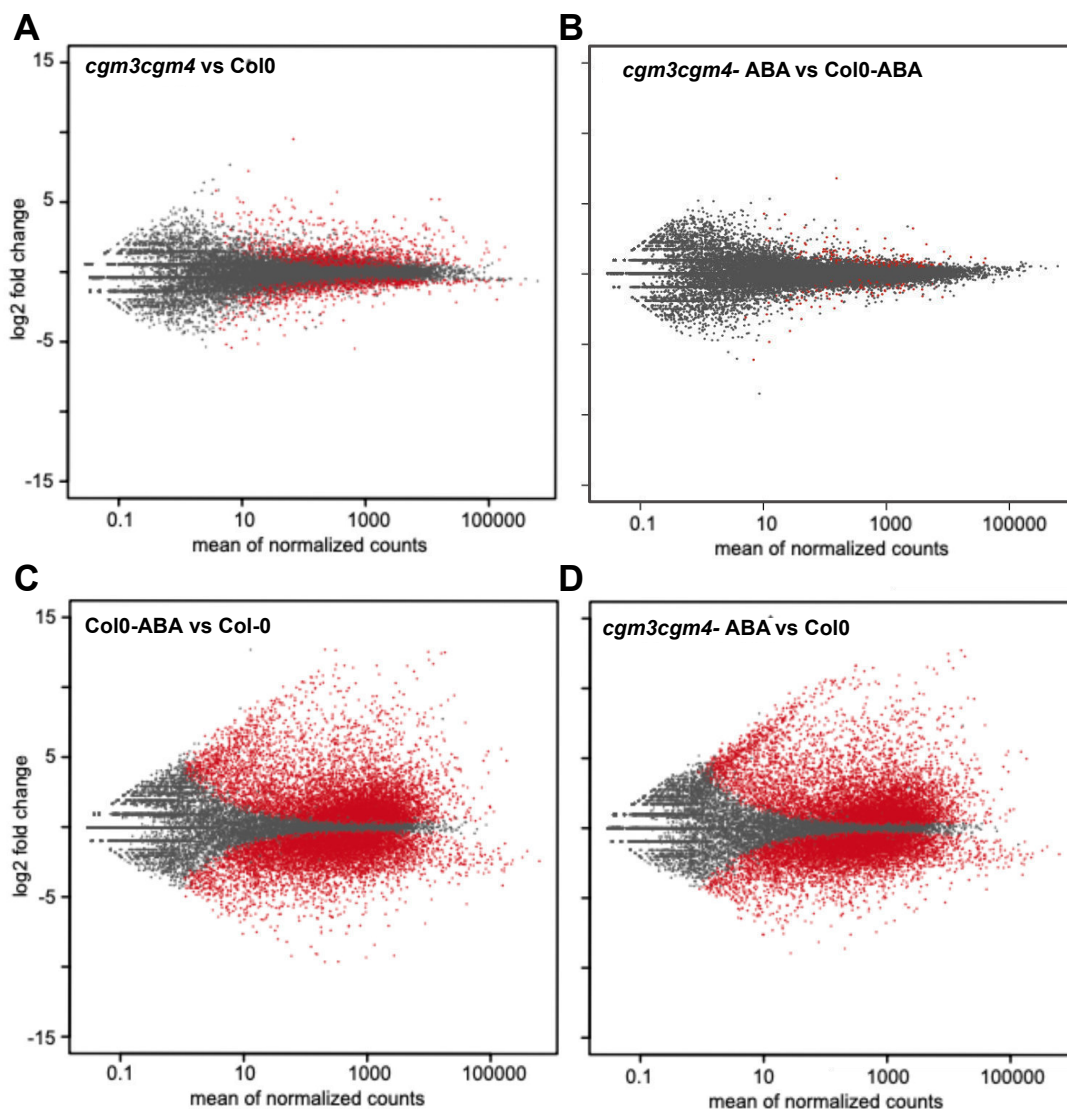


Figure 3.21: MA plots of expression ratios for ABA treated leaves of *cgm3cgm4* and wild type compared to untreated leaves of *cgm3cgm4* and wild type Col-0 vs. mean expression (x-axis) for all analyzed genes. Ratios and mean expression were calculated with DEseq2. Significantly differentially expressed genes (at $padj < 0.1$) were shown in red. $n=3$. The data were analyzed with the help of Dr. Minou Nowrousian, Department of Molecular and Cellular Botany, University of Bochum, Bochum.

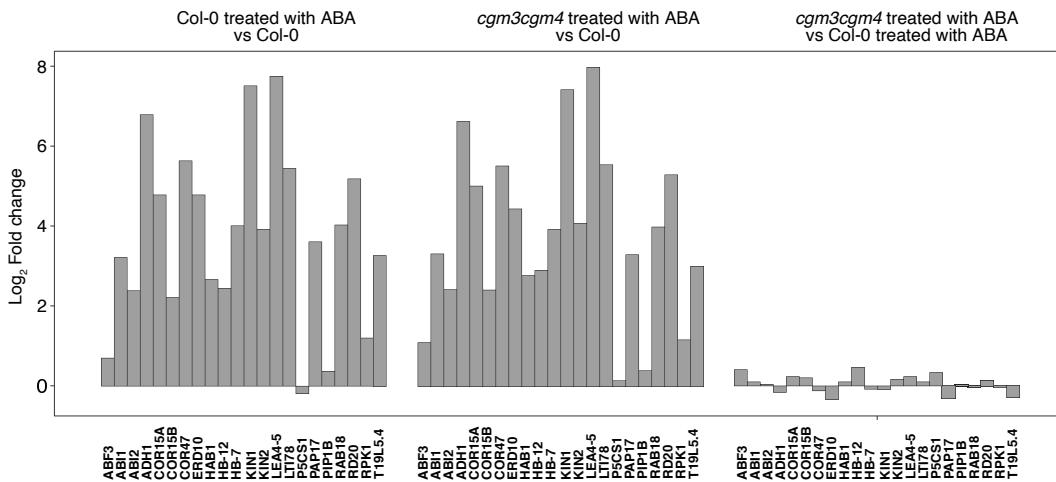


Figure 3.22: Transcriptome analysis of ABA-induced genes (Hoth *et al.*, 2002) in ABA-treated Col-0 leaves compared to control Col-0, ABA-treated *cgm3cgm4* leaves compared to control Col-0 and ABA-treated *cgm3cgm4* leaves compared to ABA-treated Col-0. Ratios and mean expression were calculated with DEseq2. n=3. The data were analyzed with the help of Dr. Minou Nowrousian, Department of Molecular and Cellular Botany, University of Bochum, Bochum.

Table 3.1: Transcriptome analysis of ABA-induced genes in ABA-treated Col-0 leaves compared to control Col-0. The data were analyzed with the help of Dr. Minou Nowrousian, Department of Molecular and Cellular Botany, University of Bochum, Bochum.

Gene	Common Name	LOX log2FoldChange	DESeq2 log2FoldChange	DESeq2 padj	LOX P(Col.ABA>Col0)	LOX P(Col.ABA<Col0)
AT1G20440	COR47	5,64	5,62	<0,01	1	0
AT1G20450	ERD10	4,82	4,77	<0,01	1	0
AT1G69270	RPK1	1,19	1,20	<0,01	1	0
AT1G72770	HAB1	2,67	2,66	<0,01	1	0
AT1G77120	ADH1	6,75	6,77	<0,01	1	0
AT2G33380	RD20	5,16	5,17	<0,01	1	0
AT2G39800	P5CS1	-0,13	-0,19	0,59	0	1
AT2G42530	COR15B	2,3	2,21	<0,01	1	0
AT2G42540	COR15A	4,87	4,77	<0,01	1	0
AT2G45960	PIP1B	0,43	0,37	0,12	1	0
AT2G46680	HB-7	3,96	4,00	<0,01	1	0
AT3G17790	PAP17	3,52	3,60	<0,01	1	0
AT3G61890	HB-12	2,44	2,44	<0,01	1	0
AT4G26080	ABI1	3,21	3,21	<0,01	1	0
AT4G34000	ABF3	0,71	0,70	0,01	1	0
AT5G06760	LEA4-5	7,72	7,73	<0,01	1	0
AT5G13200	T19L5.4	3,29	3,27	<0,01	1	0
AT5G15960	KIN1	7,48	7,49	<0,01	1	0
AT5G15970	KIN2	3,93	3,91	<0,01	1	0
AT5G52310	LTI78	5,52	5,43	<0,01	1	0
AT5G57050	ABI2	2,41	2,38	<0,01	1	0
AT5G66400	RAB18	4,07	4,02	<0,01	1	0

3.11 ABA-induced gene transcription in *cgm3cgm4* and wild-type Col-0

Table 3.2: Transcriptome analysis of ABA-induced genes in ABA-treated *cgm3cgm4* leaves compared to control Col-0. The data were analyzed with the help of Dr. Minou Nowrousian, Department of Molecular and Cellular Botany, University of Bochum, Bochum.

LOX Gene	DESeq2 Common Name	DESeq2 log2FoldChange	LOX log2FoldChange	LOX padj	P(<i>cgm3cgm4</i> _ABA>Col0)	P(<i>cgm3cgm4</i> _ABA<Col0)
AT1G20440	COR47	5,5	5,50	<0,01	1	0
AT1G20450	ERD10	4,45	4,43	<0,01	1	0
AT1G69270	RPK1	1,11	1,16	<0,01	1	0
AT1G72770	HAB1	2,73	2,77	<0,01	1	0
AT1G77120	ADH1	6,58	6,61	<0,01	1	0
AT2G33380	RD20	5,23	5,28	<0,01	1	0
AT2G39800	P5CS1	0,15	0,15	0,67	1	0
AT2G42530	COR15B	2,45	2,41	<0,01	1	0
AT2G42540	COR15A	5,06	5,00	<0,01	1	0
AT2G45960	PIP1B	0,44	0,40	0,10	1	0
AT2G46680	HB-7	3,85	3,92	<0,01	1	0
AT3G17790	PAP17	3,24	3,29	<0,01	1	0
AT3G61890	HB-12	2,83	2,90	<0,01	1	0
AT4G26080	ABI1	3,27	3,31	<0,01	1	0
AT4G34000	ABF3	1,01	1,10	<0,01	1	0
AT5G06760	LEA4-5	7,86	7,96	<0,01	1	0
AT5G13200	T19L5.4	2,98	2,98	<0,01	1	0
AT5G15960	KIN1	7,33	7,40	<0,01	1	0
AT5G15970	KIN2	4,01	4,07	<0,01	1	0
AT5G52310	LTI78	5,57	5,53	<0,01	1	0
AT5G57050	ABI2	2,39	2,42	<0,01	1	0
AT5G66400	RAB18	3,99	3,98	<0,01	1	0

Table 3.3: Transcriptome analysis of ABA-induced genes in ABA-treated *cgm3cgm4* leaves compared to ABA-treated Col-0. The data were analyzed with the help of Dr. Minou Nowrousian, Department of Molecular and Cellular Botany, University of Bochum, Bochum.

LOX Gene	DESeq2 Common Name	DESeq2 log2FoldChange	LOX log2FoldChange	LOX padj	P(<i>cgm3cgm4</i> _ABA>Col0_ABA)	P(<i>cgm3cgm4</i> _ABA<Col0_ABA)
AT1G20440	COR47	-0,14	-0,12	0,91	0	1
AT1G20450	ERD10	-0,37	-0,34	0,52	0	1
AT1G69270	RPK1	-0,08	-0,05	0,97	0,029	0,971
AT1G72770	HAB1	0,07	0,10	0,87	1	0
AT1G77120	ADH1	-0,17	-0,16	0,90	0	1
AT2G33380	RD20	0,07	0,12	0,90	1	0
AT2G39800	P5CS1	0,28	0,33	0,73	1	0
AT2G42530	COR15B	0,15	0,20	0,79	1	0
AT2G42540	COR15A	0,19	0,23	0,86	1	0
AT2G45960	PIP1B	0,02	0,03	0,98	0,994	0,006
AT2G46680	HB-7	-0,1	-0,08	0,95	0	1
AT3G17790	PAP17	-0,28	-0,31	0,78	0	1
AT3G61890	HB-12	0,39	0,46	0,32	1	0
AT4G26080	ABI1	0,06	0,10	0,91	1	0
AT4G34000	ABF3	0,3	0,40	0,59	1	0
AT5G06760	LEA4-5	0,14	0,23	0,91	1	0
AT5G13200	T19L5.4	-0,31	-0,28	0,55	0	1
AT5G15960	KIN1	-0,15	-0,09	0,96	0	1
AT5G15970	KIN2	0,08	0,16	0,90	1	0
AT5G52310	LTI78	0,06	0,10	0,94	1	0
AT5G57050	ABI2	-0,02	0,04	0,97	0,146	0,854
AT5G66400	RAB18	-0,08	-0,04	0,98	0	1

3.12 Growth of *cgm3cgm4* and CGM4ox under different light regimes

Light intensity plays an important role in plant growth and development and also affects the opening and closing of the stomata. Under optimal light conditions the stomata are open but very high or very low light conditions induces their closure, thus affecting gas exchange and the metabolism of the plants. In this study, wild-type Col-0, *cgm3cgm4*, CGM4ox and complemented *cgm3cgm4*CGM4 were grown under two different light intensities, 51 $\mu\text{mol photon/m}^2/\text{s}$ and 190 $\mu\text{mol photon/m}^2/\text{s}$, respectively, and the fresh weight of the plants was quantified after 4–5 weeks. All plant lines differed in their growth response to the tested light conditions and were larger under high light (190 $\mu\text{mol photon/m}^2/\text{s}$) than the low light condition (51 $\mu\text{mol photon/m}^2/\text{s}$). How-

3.12 Growth of *cgm3cgm4* and *CGM4ox* under different light regimes

ever, while the fresh weight of *cgm3cgm4* and wild-type Col-0 plants grown under low light intensity did not obviously differ, under high light intensity the fresh weight of the *cgm3cgm4* plants was less than that of wild-type plants. The fresh weight of the complemented *cgm3cgm4CGM4* was similar to that of wild-type Col-0 grown under both low and high light conditions (Fig.3.23).

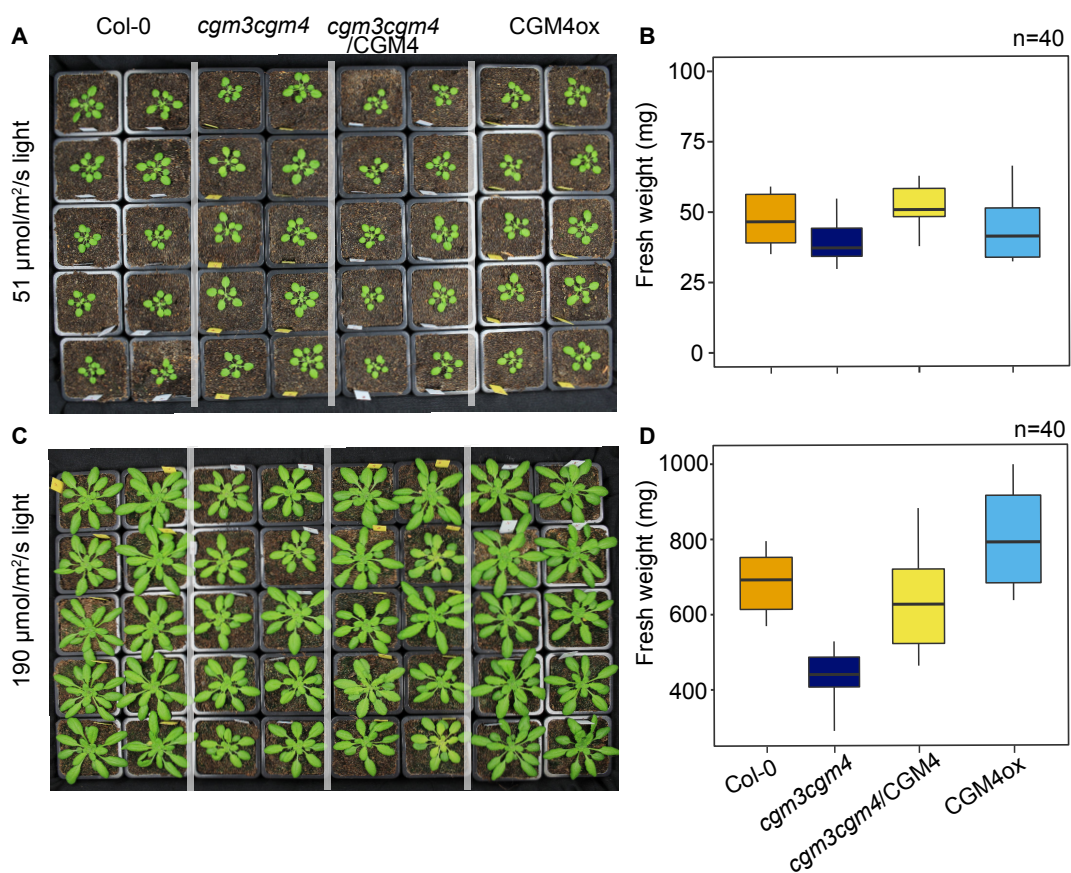


Figure 3.23: Images and quantification of fresh weight of 3week old plants of wild type Col-0, *cgm3cgm4*, *cgm3cgm4/CGM4* and CGM4ox grown under short day condition with 51 $\mu\text{mol/m}^2/\text{s}$ (70%) light intensity (A,B) and 190 $\mu\text{mol/m}^2/\text{s}$ (100%) light intensity (C,D). Boxplots indicate the median (horizontal line) and interquartile range (colored box); whiskers show three times the interquartile range; points indicate values outside this range. n=40 individual plants.

3.13 Biochemical assay of cell wall composition of *cgm3cgm4* and CGM4ox leaves

The internal turgor pressure that drives the opening-closing dynamics of stomata is mediated by the mechanical properties of the guard cell wall, which possesses unique physical strength and significant elasticity. As the plant cell wall consists of polysaccharides and structural proteins, glycoproteins and polyphenolics components, stomatal function was explored by examining the polysaccharide composition and metabolome of the guard cells of *cgm3cgm4*, CGM4ox and wild-type Col-0 plants.

The sugar composition of the cell wall in the three plant lines was analyzed by measuring the abundances of different monosaccharides using gas chromatography-mass spectrometry (GC-MS) techniques. The cell wall fraction was extracted from 4- to 5-week-old leaves using a methanol-acetone extraction protocol (see *Material and methods* for details). The different monosaccharides were identified according to their peak elution time on GC-MS and the total abundances were measured from those peaks. Among the 22 different monosaccharide peaks identified in the GC-MS, six major monosaccharides were compared among wild-type Col-0, *cgm3cgm4* and CGM4ox. The abundances of arabinose, fructose, galactose, glucose and raffinose were lower in *cgm3cgm4* plants and higher in CGM4ox plants than in wild-type Col-0 plants (Fig.3.24).

The total metabolome of the cell wall fractions of wild-type Col-0, *cgm3cgm4* and CGM4ox was analyzed using a UPLC-SynaptG2 LC/MS system. The MS metabolomic assay was done in a non-targeted workflow procedure. The metabolites detected in the

cell wall extractions were annotated based on a comparison of their mass spectra and retention times with the corresponding standards. The majority of the metabolites consisted of cell wall compounds, with polyphenolic group compounds having the highest abundances. Several polyphenolic compounds, including *p*-coumaric acid, sinapic acid, and a 3,2-hydroxybenzoic acid derivative tended to be of lower abundance in *cgm3cgm4* and of higher abundance in CGM4ox than in wild-type Col-0 (Fig.3.25).

The role of tannin compounds, including methyl caffeate, chlorogenic acid, neochlorogenic acid, malic acid and citric acid, was examined by analyzing the apoplastic fluid extracted from tobacco leaves infiltrated with pUBQ10:CGM4 and pCGM4:CGM4 constructs. Non-infiltrated leaves served as the controls. The levels of methyl caffeate, chlorogenic acid, malic acid and neo-chlorogenic acid were lower in the apoplasts of CGM4-overexpressing leaves than in non-infiltrated leaves, whereas the level of citric acid was higher than in the control leaves (Fig.3.26). The results could not be reproduced due to the use of non-comparable extraction strategies.

3.13 Biochemical assay of cell wall composition of *cgm3cgm4* and *CGM4ox* leaves

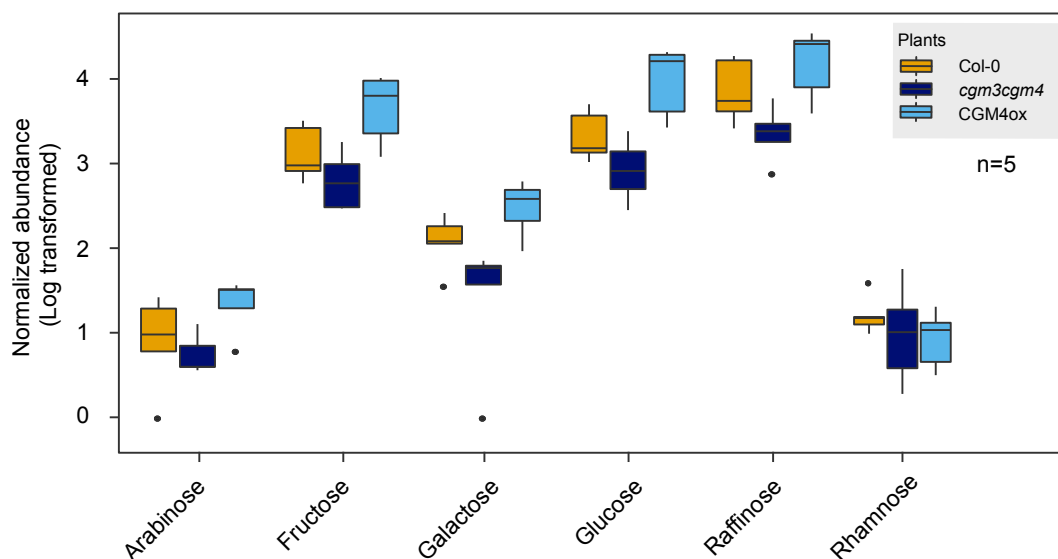


Figure 3.24: Normalized abundance of six monosaccharides from the cell wall extract of wild type Col-0, *cgm3cgm4* and CGM4ox leaves. Boxplots indicate the median (horizontal line) and interquartile range (colored box); whiskers show three times the interquartile range; points indicate values outside this range. n= 5 individual plants. The experiment was done with the help of Dr. Mark Stahl and Dr. Joachim Kilian at the analytical facility in ZMBP, University of Tübingen.

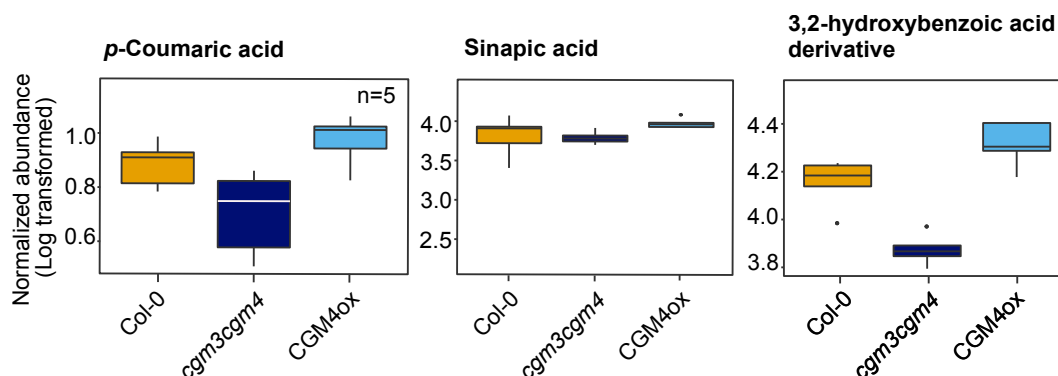


Figure 3.25: Normalized abundance of three polyphenolic compounds derivatives, *p*-Coumaric acid, Sinapic acid and 3,2-Hydroxybenzoic acid from the cell wall extract of wild type Col-0, *cgm3cgm4* and CGM4ox leaves. Boxplots indicate the median (horizontal line) and interquartile range (colored box); whiskers show three times the interquartile range; points indicate values outside this range. n=5 individual plants. The experiment was done with the help of Dr. Mark Stahl and Dr. Joachim Kilian at the analytical facility in ZMBP, University of Tübingen.

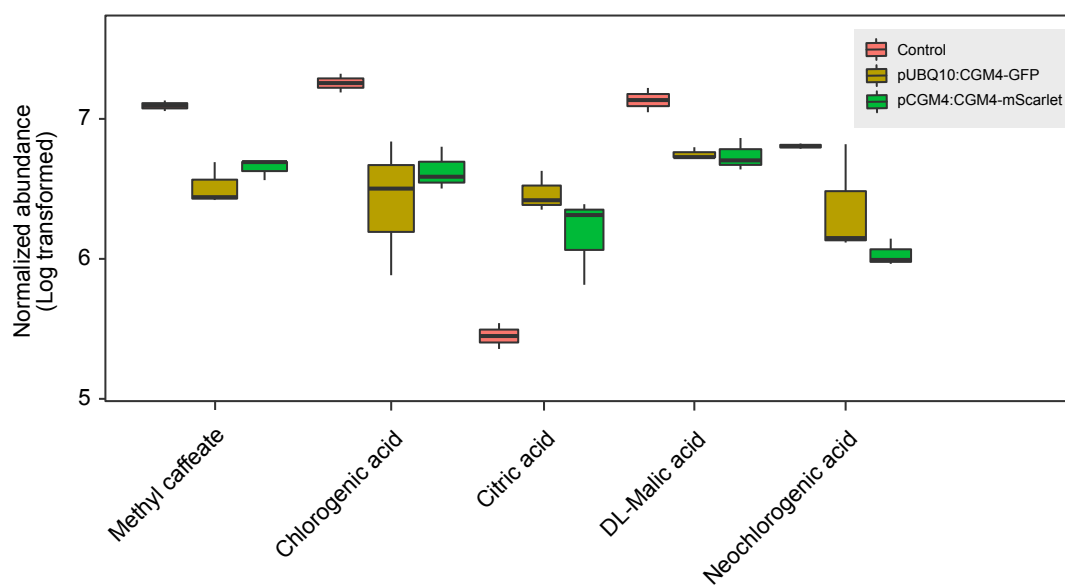


Figure 3.26: Normalized abundance of several polyphenolic derivatives identified from metabolome analysis of apoplastic fluid of *Nicotiana benthamiana* leaves transiently expressed with pUBQ10:CGM4-GFP and pCGM4:CGM4-mScarlet. The un-infiltrated leaves were used as control. Boxplots indicate the median (horizontal line) and interquartile range (colored box); whiskers show three times the interquartile range; points indicate values outside this range. $n=5$ individual leaves. The experiment was done with the help of Dr. Mark Stahl and Dr. Joachim Kilian at the analytical facility in ZMBP, University of Tübingen.

3.14 Immunolabelling of stomatal cell wall with pectin epitopes

The major polysaccharides that make up the plant cell wall are cellulose, hemicellulose and pectin. In guard cells, pectin has a very specific distribution pattern. The development of new epitopes for detecting pectin in different methylation states has allowed visualization of the pectin distribution in the cell wall in Immunolabeling studies.

In this study, cross-sections of leaves from wild-type Col-0, *cgm3cgm4*, CGM4ox and *cgm3cgm4* complemented with CGM4 (*cgm3cgm4CGM4*) were immunolabeled with different pectin epitopes. LM19 epitopes recognize and bind to the un-esterified homogalacturonan domain of pectic polysaccharides; the LM20 epitope recognizes and binds to highly methyl-esterified homogalacturonans. Epitope 2F4 binds to the calcium cross-links in homogalacturonans following the de-esterification of stretches of their galacturonic acids in a block-wise pattern. Previous studies of *A. thaliana* leaf cells showed strong LM19 immunolabeling signals in the cell walls of guard cells and epidermal cells, whereas LM20 is abundant in the junction that forms between the guard cell and neighboring epidermal cell wall, but not on the cell walls of the guard cells themselves. The labeling of calcium cross-links by 2F4 yields signal only in the junctions of guard cells and epidermal cells. To investigate the esterification state of the pectin polysaccharides in guard cell walls of the studied plant lines, leaf cross-sections were immunolabeled with different pectin epitopes in leaf cross-sections of wild-type Col-0, *cgm3cgm4*, CGM4ox and *cgm3cgm4CGM4*. The distribution pattern of epitopes LM19, LM20 and 2F4 in the guard cells of *cgm3cgm4* and CGM4ox was the same as that in the cells of the wild type. LM19 was strongly expressed in the guard cell walls

of all four tested plant lines whereas LM20 was excluded from the guard cell wall but expressed in the cell walls of neighboring epidermal cells. Epitope 2F4 was expressed in the junction of the two cell types (Fig.3.27).

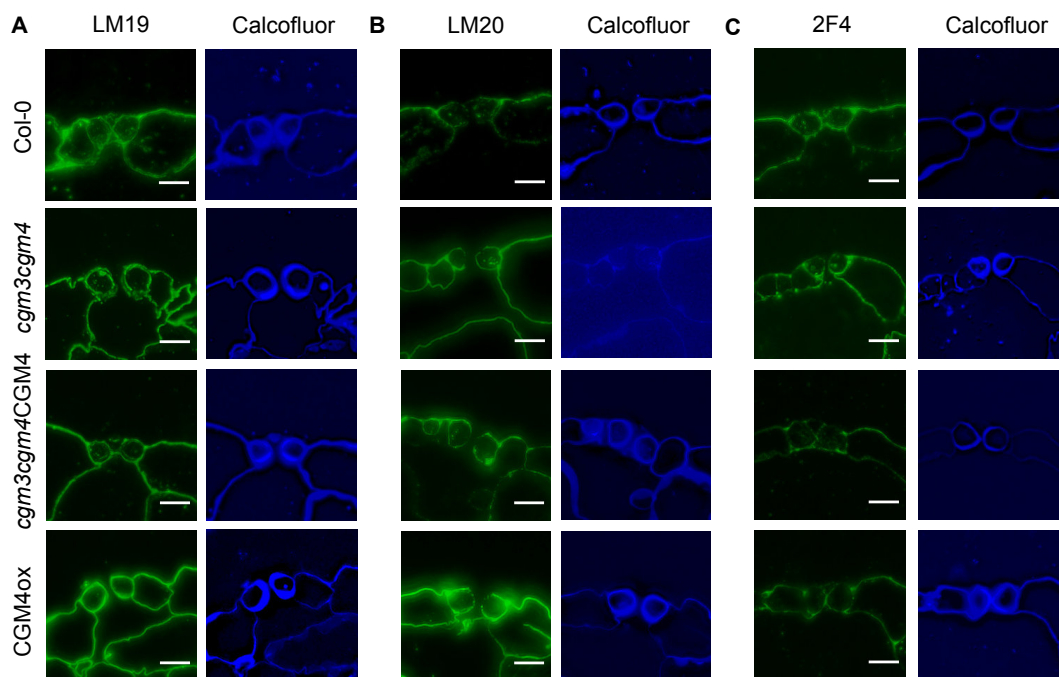


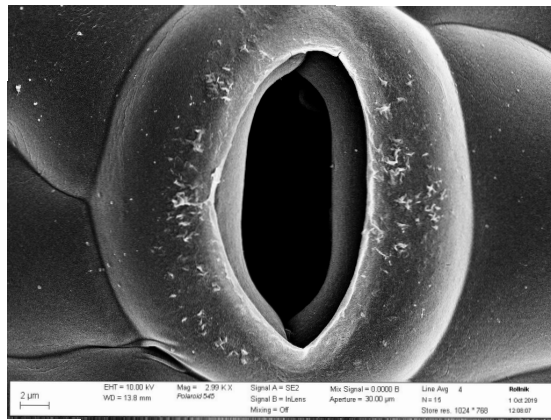
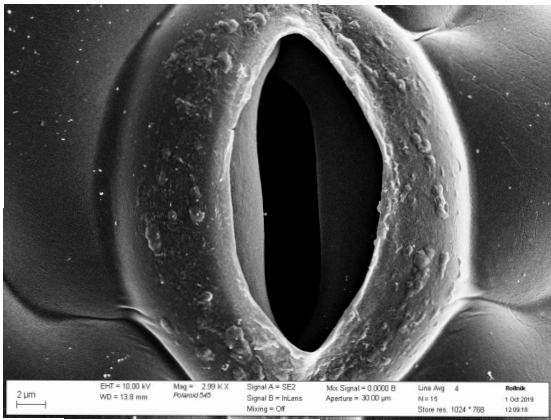
Figure 3.27: Immunolocalization of pectin epitopes LM19 (A), LM20 (B) and 2F4 (C) in leaf cross sections of wild type Col-0, *cgm3cgm4*, *cgm3cgm4CGM4* and CGM4ox. Scale bar, 10 μ m. The experiment was done with the help of Dr. Arun Sampathkumar and his team from MPIMP, Golm.

3.15 Scanning electron microscopy of the stomata of wild type Col-0 and *cgm3cgm4*

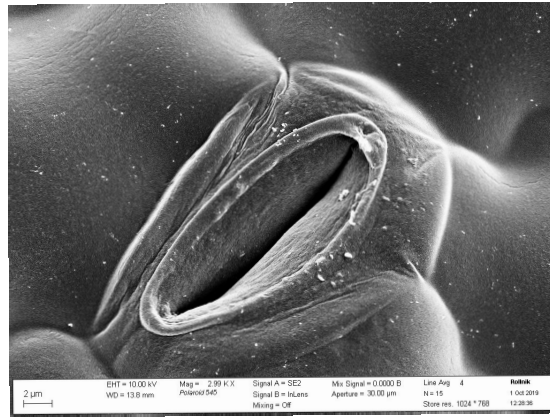
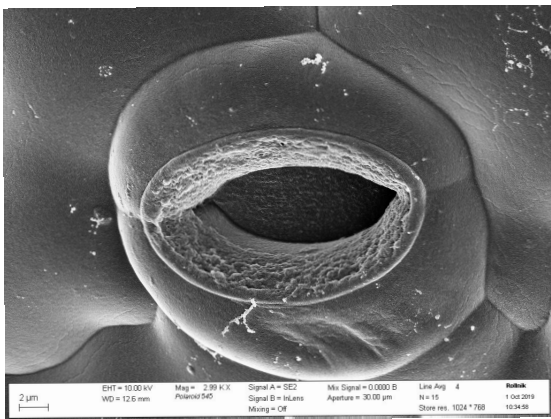
Although light microscopy is commonly used to examine cell morphology, it provides limited information on the surface morphology and topology of a tissue or organ, which can instead be obtained with SEM.

In this study, because light microscopy failed to reveal clear differences in the stomatal distribution or patterning between of *cgm3cgm4* and wild-type, a more detailed investigation of stomatal topology and morphology was conducted with SEM. The adaxial surface of wild-type Col-0, *cgm3cgm4* and *cgm3cgm4CGM4* leaf samples, prepared by cryo-fixation, sublimation, and platinum sputter coating, were scanned to reveal the distribution and structure of the stomata and of the epidermal pavement cells. In young immature stomata of wild-type Col-0, two turgid guard cells were seen attached to the polar region and a thin cuticular membrane-like structure covered the stomatal pore. In the mature stomata, the cuticular membrane had ruptured due to the pressure-driven inflation of the guard cells. By contrast, the stomata of *cgm3cgm4* were characterized by unusual cuticular ledges, the majority of the stomata were closed and very deformed/shrunken/wrinkled stomata were frequently seen. However, the stomatal structure of *cgm3cgm4CGM4* leaves was similar to that of the leaves of wild-type Col-0 (Figs.3.28, A.1).

Col-0



cgm3cgm4



cgm3cgm4/CGM4

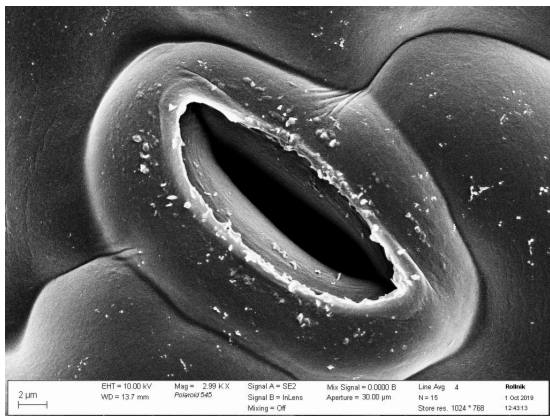
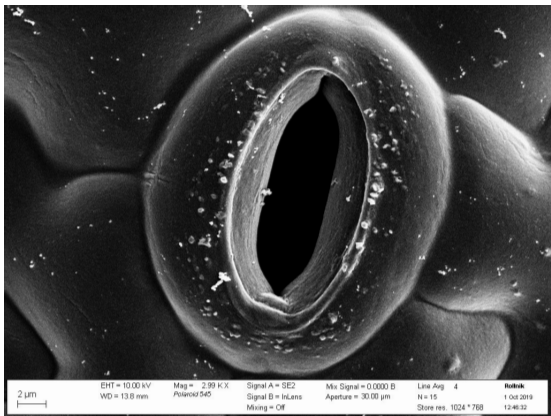


Figure 3.28: Scanning electron microscopy of individual stomate of wild type Col-0, *cgm3cgm4* and *cgm3cgm4/CGM4*. For more number of individual stomata of the different plant lines, see Fig.A.1.

3.16 Transverse views of stomatal structure as revealed using confocal microscopy

Guard cell walls are uneven in their thickness, with the ventral wall, facing the stomatal pore, being thicker than the dorsal wall (Zhao and Sack, 1999; Merced and Renzaglia, 2018). This difference in wall thickness contributes to the structural stability of the stomata and to their opening-closing dynamics (Von Mohl, 1856; Schwendener, 1881; Pautov *et al.*, 2016). The uneven thickening is best seen in transverse confocal and scanning electron microscopy studies of the stomata (Zhao and Sack, 1999; Merced and Renzaglia, 2018).

Confocal microscopy investigations of transverse section of the stomata were conducted using propidium iodide-stained leaves of wild type Col-0 and *cgm3cgm4* and by obtaining Z-stacked images that were subsequently reconstructed the Leica SP8 software. The outer ledge thickness of the stomatal pore was quantified. The results revealed the greater thickness of the ventral wall of *cgm3cgm4* than of wild type Col-0 stomata. The fluorescence intensity at the stomatal pore/ledge area was calculated from virtual transverse sections of the stomata. The CTCF value (arbitrary units) at the stomata ledge was higher in *cgm3cgm4* than in wild type Col-0 (Fig.3.29).

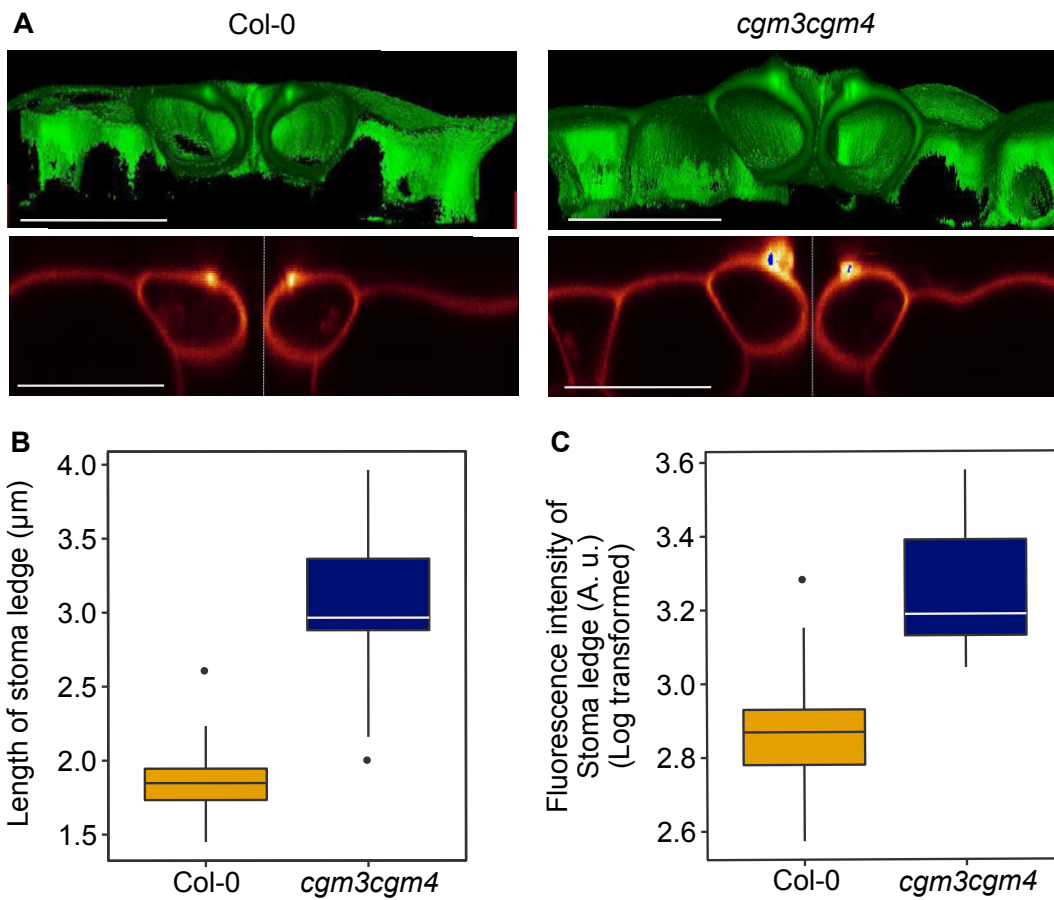


Figure 3.29: (A) Virtual transverse section of stomata of wild type Col-0 and *cgm3cgm4* and the heatmap from z-stacked confocal. Scale bar, 10 μm . (B) Quantification of length of stoma ledges from the virtual transverse section of wild type Col-0 and *cgm3cgm4* stomata. Boxplots indicate the median (horizontal line) and interquartile range (colored box); whiskers show three times the interquartile range; points indicate values outside this range. $n=16$ stomata (C) Quantification of fluorescence intensity from the heatmap of virtual transverse section of wild type Col-0 and *cgm3cgm4* stomata. $n=16$ stomata.

3.17 The abundance of unsaturated pectin products in cell wall extracts of *cgm3cgm4* and CGM4ox

One of the most abundant compound in the plant cell wall is pectin, whose backbone mainly consists of polygalacturonic acid. Among the several methods available to identify pectin is simple spectrophotometry using a highly purified enzyme from *Aspergillus niger*. Pectin is demethylated at pH 12.0 and upon treatment with pectate lyase the demethylated pectin undergoes beta-elimination, which leads to the formation of double bonds in the galacturonic acid located between C-4 and C-5. Cleavage of polygalacturonic acid by pectate lyase produces unsaturated oligosaccharides, which have a strong absorbance at 235 nm. The standards used in the assay consisted of different forms of esterified pectins from different origins, including low-ester pectin from citrus peel, high-ester pectin from citrus peel and partly amidated low-ester pectin from citrus peel. The absorbance of the low-ester pectin substrate was the highest, followed by the high-ester pectin and the partly amidated low-ester pectin (Fig.3.30).

The abundance of unsaturated products in the cell walls of *cgm3cgm4*, CGM4ox, wild type Col-0 and PME15ox was compared using whole-leaf extracts treated with pectate lyase. The pectin methylesterase inhibitor, AtPME15 influences plant morphology by affecting the biochemical properties of the cell wall. Plants constitutively over-expressing PME15 had a twisted growth pattern and curled leaves. Cell wall extracts from the leaves of these plants contained lower levels of unsaturated oligosaccharide products than measured in the wild-type. Similar reductions were determined in CGM4ox extracts, whereas in those of *cgm3cgm4* the levels of unsaturated oligosaccharide products was higher than in the other three plant lines (Fig.3.30).

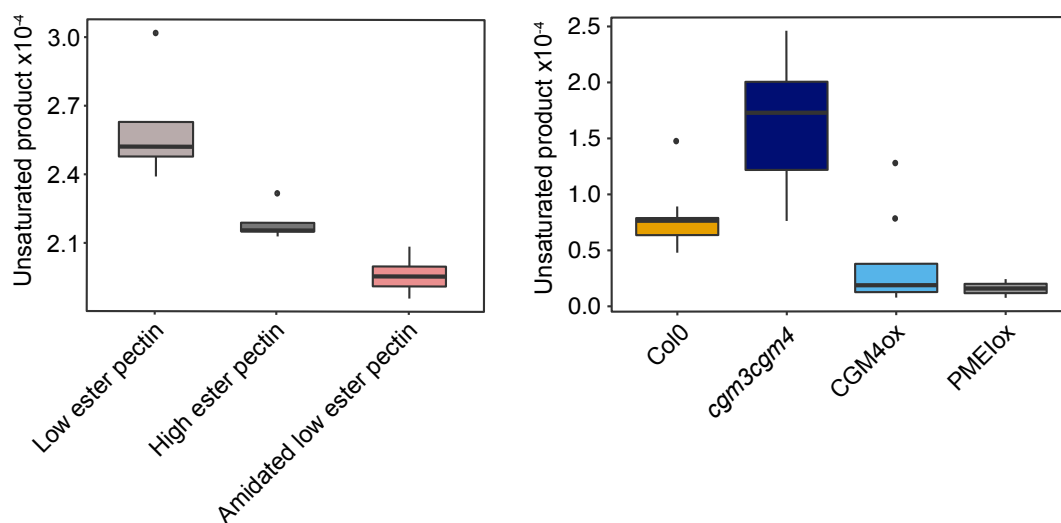


Figure 3.30: (A) Quantification of the abundance of unsaturated product from different forms of esterified pectin extracted from citrus peel under treatment of Pectate lyase used as standard for the analysis. Boxplots indicate the median (horizontal line) and interquartile range (colored box); whiskers show three times the interquartile range; points indicate values outside this range. n=5. (B) Abundance of unsaturated product from the cell wall extract of wild type Col-0, *cgm3cgm4*, CGM4ox and PME1ox leaves upon treatment with Pectate lyase enzyme. n=5.

3.18 Quantification of stomatal pore area stiffness using atomic force microscopy (AFM)

Stomatal opening-closing dynamics, whether in response to abiotic or biotic stimuli, are essentially turgor driven, as discussed above. To accommodate the changing turgor pressure, the plant cell wall undergoes biochemical changes that result in different mechanical stresses and changes in the stiffness of the stomata. AFM together with finite element modeling has been used to quantify the mechanical stress and stiffness of stomata (Sampathkumar *et al.*, 2014; Carter *et al.*, 2017; Rui *et al.*, 2018). The AFM is a type of Scanning Probe Microscopy (SPM) where the probe scans through a sample surface and measures the interaction between the sample and the probe (Binnig *et al.*, 1986; Carter, 2015). In case of AFM, it uses a sharp tip at the end of a cantilever which interacts with the sample surface and creates a topographic image of the sample surface.

In this study, topography and stiffness were measured in the stomatal pore area and the area surrounding the stomata (Fig.3.31). The measured median stiffness ratio (stomata/surrounding area) was found to be higher in *cgm3cgm4* than in wild-type stomata (Figs.3.32, 3.33).

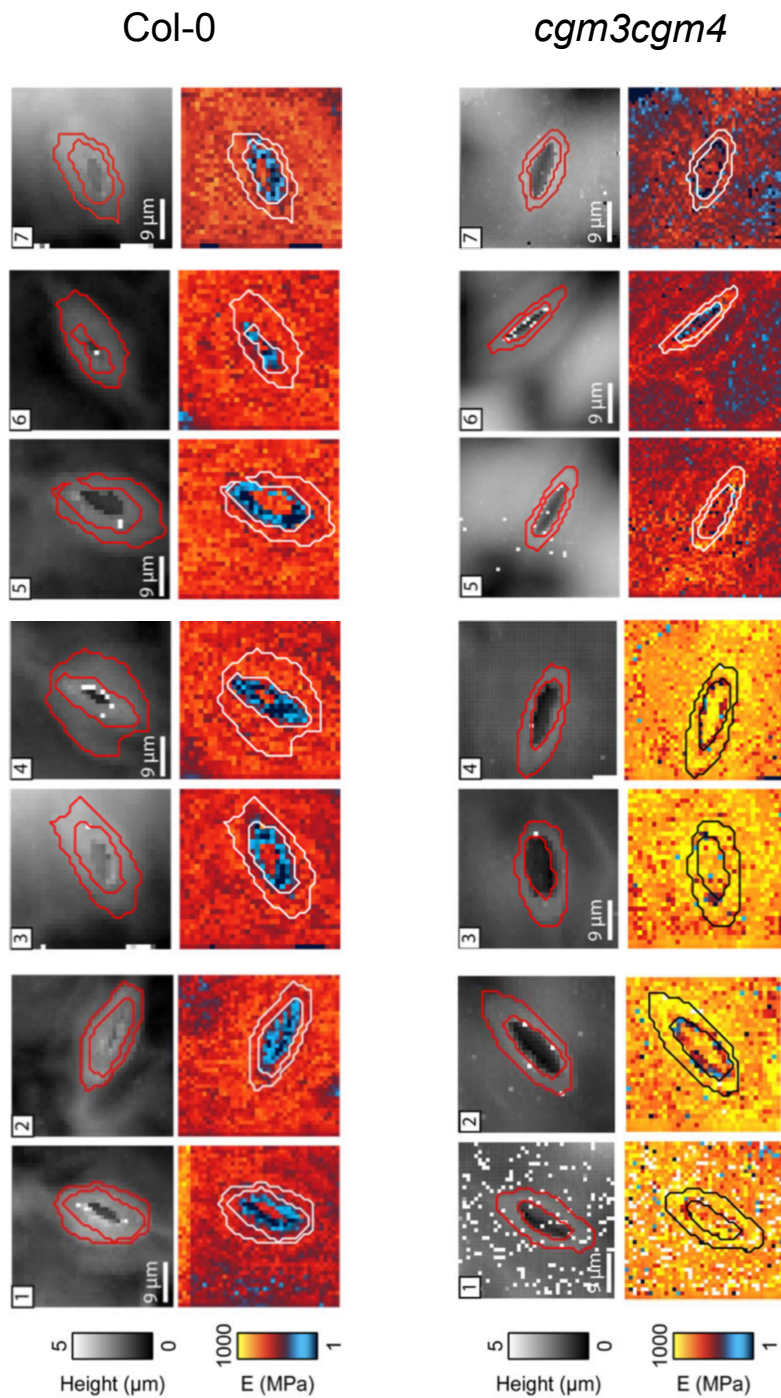


Figure 3.31: Stomatal topography (top row) and stiffness (bottom row) of wild type Col-0 and *cgm3cgm4*. Two different regions of interest were selected from the topography images. The inner contour encloses a region that was excluded from further analysis. The outer contour defines the boundary of the stoma. $n=7$. The experiment was done with the help of Prof. Tilman Schäffer and his PhD student Todor Krastev from Institute of Applied Physics, University of Tübingen.

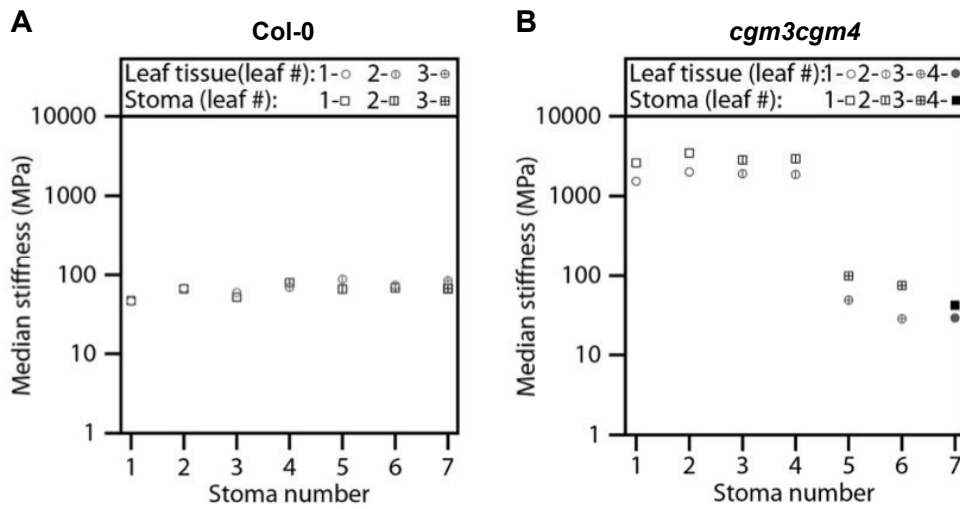


Figure 3.32: Median stiffness of stoma and surrounding leaf tissues of wild type Col-0 (A) and *cgm3cgm4* (B). $n=7$ stomata. The experiment was done with the help of Prof. Tilman Schäffer and his PhD student Todor Krastev from Institute of Applied Physics, University of Tübingen.

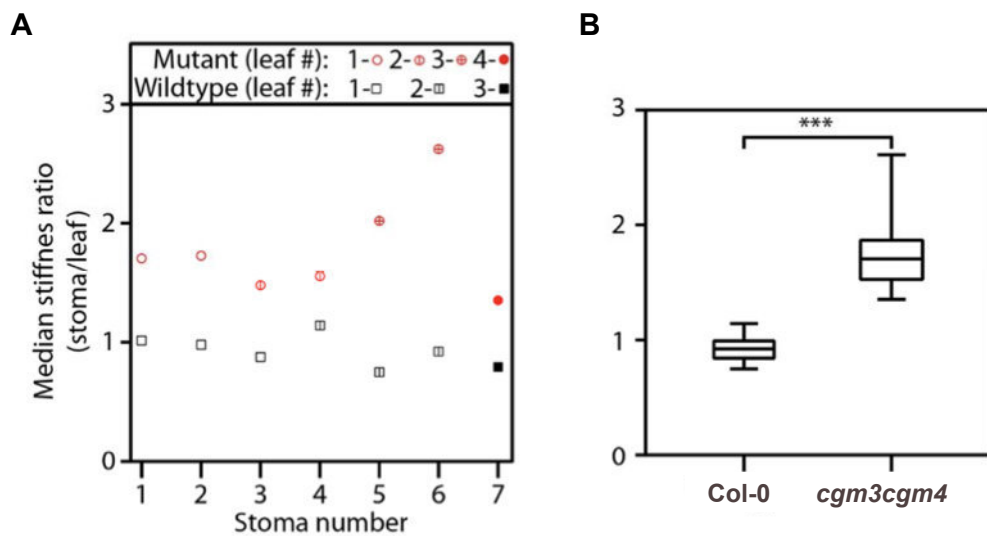


Figure 3.33: Ratio of median stoma stiffness over median surrounding tissues stiffness for wild type Col-0 and *cgm3cgm4*. The data was tested for significance with an unpaired t-test ($p=0.001$). $n=7$. The experiment was done with the help of Prof. Tilman Schäffer and his PhD student Todor Krastev from Institute of Applied Physics, University of Tübingen.

3.19 CGM4 expressed under the guard cell specific promoter GC1 and its effect on stomatal physiology

This study showed that the CGM4 promoter fusion was expressed in the early developmental lineages of the stomata but not in mature stages (Fig.3.2). To investigate the effect of CGM4 in mature stomata, a CGM4-GFP fusion construct expressed under the GC1 promoter (pGC1:CGM4), and thus specifically active in mature guard cells, was used to transform *cgm3cgm4* mutant plants. Expression in the T3 generation, and specifically in mature guard cells, was confirmed by monitoring the GFP signal using confocal microscopy. In the mature cells, GFP signal was observed as unusual dotted structures in the cytoplasm (Fig.3.34).

Gas exchange measurements were performed to analyze the effect of CGM4 on stomatal function when expressed specifically in mature guard cells. The plants were acclimated in dark for 30 min to induce stomatal closure and then exposed to 400 PAR for 60 min to induce stomatal opening, followed by 30 min of dark (0 PAR). In wild-type Col-0 plants, the response of the stomata during the transition from 0 PAR to 400 PAR was fast, causing an increase in the transpiration rate until a plateau was reached at around 60 min of light exposure, followed by a slow decline in the dark. Compared to wild-type Col-0 plants, the transpiration rate in *cgm3cgm4* mutant plants responded slowly upon light induction and the rate remained low. By contrast, the transpiration rate in *cgm3cgm4* plants expressing CGM4 under the guard-cell-specific promoter GC1 responded quickly to light induction, similar to wild type Col-0 (Fig.3.35).

The stomatal aperture index was also measured in the plants expressing pGC1-driven

CGM4 and exposed to stomatal opening solution. In wild type Col-0, the index increased in plants treated with stomatal opening buffer and exposed to 3 hr of constant light whereas under the same conditions the index of *cgm3cgm4* plants was lower. In the *cgm3cgm4* plants expressing pGC1-driven CGM4 the index in treated plants was similar to that of wild-type Col-0 plants (Fig.3.36).

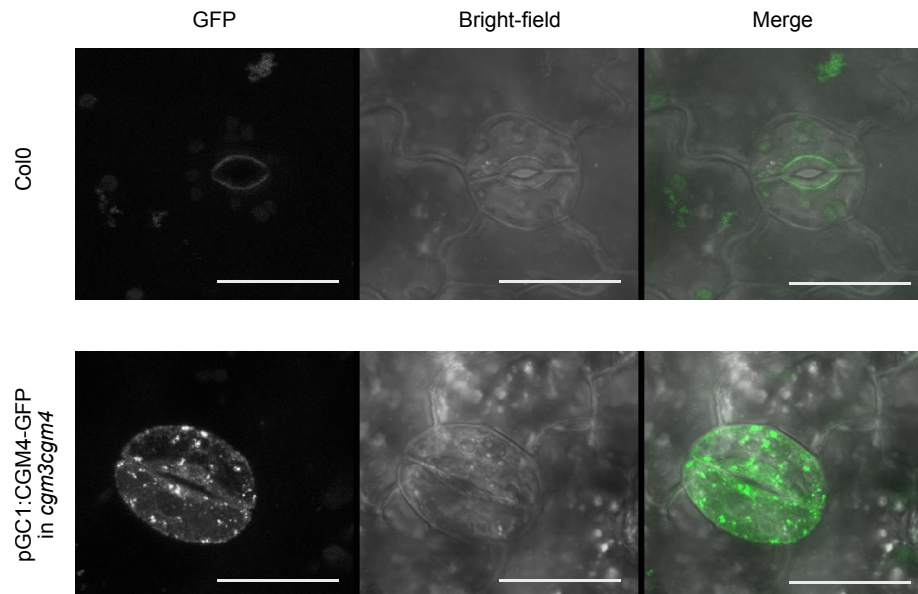


Figure 3.34: Subcellular localization of pGC1:CGM4-eGFP in the cytoplasm (punctate structure) of mature stomata in the *cgm3cgm4*. Scale bar, 20 μ m.

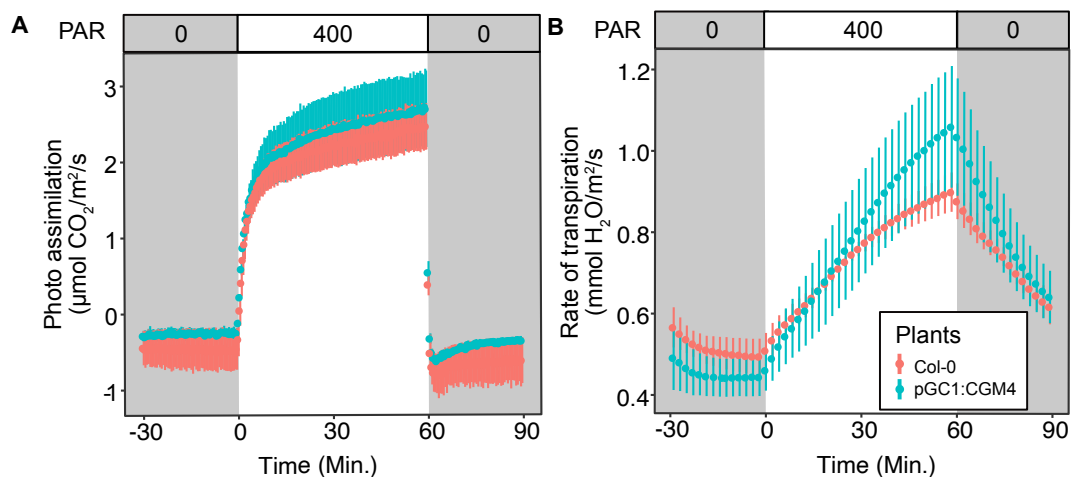


Figure 3.35: Rate of photo assimilation (A) and rate of transpiration (B) measurement of pGC1:CGM4-GFP in *cgm3cgm4* compared to wild type Col-0. The error bars indicate the standard error. n=3.

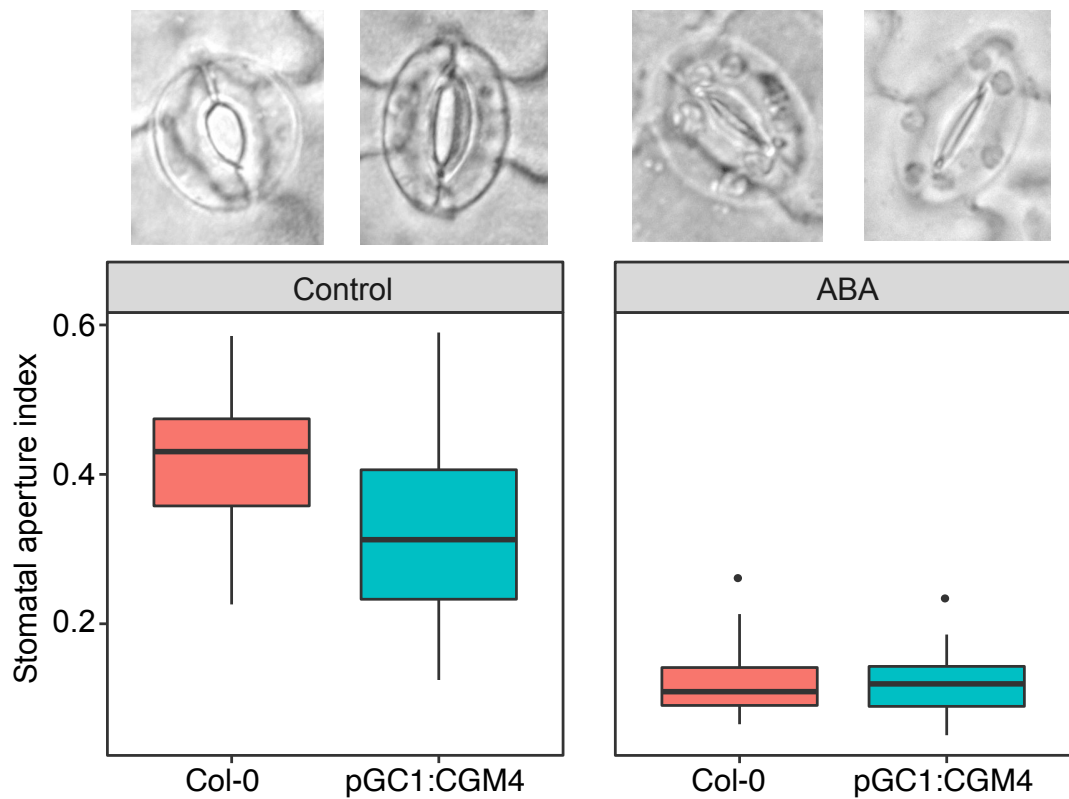


Figure 3.36: Stomatal aperture index measurement of pGC1:CGM4-GFP in *cgm3cgm4* compared to wild type Col-0 under 10 μ M ABA treatment compared to stomatal opening solution as control condition. Boxplots indicate the median (horizontal line) and interquartile range (colored box); whiskers show three times the interquartile range; points indicate values outside this range. n=40.

3.20 Germination of *cgm3cgm4* and CGM4ox

Although CGM3 and CGM4 are paralogous and share 90% protein homology, they are expressed in different tissues: CGM3 in imbibed seeds and CGM4 in leaf stomatal lineages. In the double mutant *cgm3cgm4*, germination was delayed. This trait was analyzed quantitatively by germinating 50–100 seeds each of wild-type Col-0, *cgm3cgm4* and CGM3ox on ½ MS solid plates and then recording the percentage of seed germination every 24 hr for 3 days. After 24 hr of light induction, 75% of wild-type Col-0 and CGM3ox seeds had germinated, compared to 25% of *cgm3cgm4* seeds. In *cgm3cgm4* complemented with the full genomic CGM3 fragment (*cgm3cgm4CGM3*), approximately 60% of the seeds germinated. In *cgm3cgm4* complemented with signal-peptide-mutated CGM3 (*cgm3cgm4CGM3^{dSP}*) the germination rate was approximately 40% after 24 h of light induction. After 72 h of light induction, 100% of wild type, CGM3ox and *cgm3cgm4CGM3* seeds had germinated but only 60% of *cgm3cgm4* seeds. The germination rate of *cgm3cgm4CGM3^{dSP}* after 72 hr was also delayed, by approximately 80% (Fig.3.37).

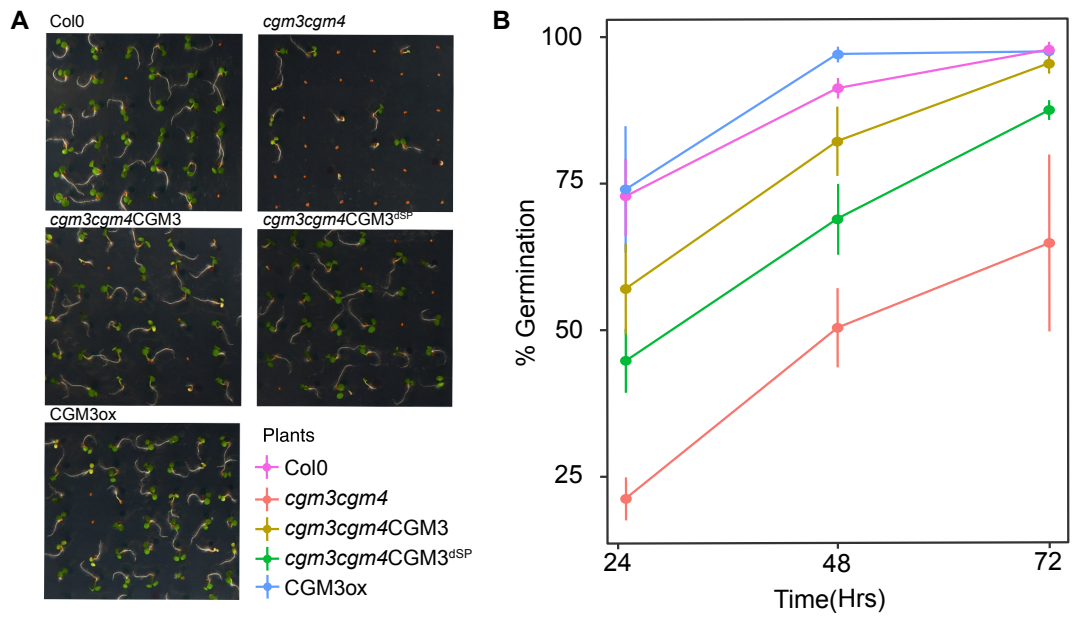


Figure 3.37: (A) Exemplary photographs of germination on 1/2 MS plates for Col-0, *cgm3cgm4*, *cgm3cgm4CGM3*, *cgm3cgm4CGM3^{dSP}* and CGM3ox. (B) Quantification of germination rate over time for Col-0, *cgm3cgm4*, *cgm3cgm4CGM3*, *cgm3cgm4CGM3^{dSP}* and CGM3ox. The error bars indicate the standard error. n=100 seeds.

3.21 Effect of Abscisic Acid (ABA) and Gibberellic acid (GA3) on germination

Seed germination is enhanced by Gibberellic acid (GA3). The effect of GA3 on the studied plant lines was determined using two different concentrations of the phytohormone, 5 μ M and 10 μ M. The germination rate of GA3-treated wild type Col-0, CGM3ox and *cgm3cgm4*CGM3 increased by approximately 10% after 24 h of light induction, whereas no obvious increase was observed in the *cgm3cgm4* mutant. After 72 h of light induction, the germination rate of GA3-treated *cgm3cgm4* was about 55% (Fig.3.38).

ABA is an antagonist of GA3 and inhibits seed germination. Its effect on the studied plant line was investigated by growing the seeds on medium containing 1 μ M and 2 μ M ABA and then quantifying the germination rate. ABA treatment of wild-type seeds caused a 15% decrease in the germination rate compared to the control as measured after 24 h of light induction. After 72 h of light induction, approximately 72% of seeds had germinated, compared to 100% of control seeds. In the ABA-treated CGM3ox line seed germination decreased by 20% after 24 h compared to the control conditions, but after 72 h of light induction 86% of the seeds had germinated. In the *cgm3cgm4* mutant, seed germination decreased by 3% after 24 h of light induction but 72 h only 30% of the seeds had germinated. In the complemented line (*cgm3cgm4*CGM3), after 24 h of light induction, seed germination had decreased by approximately a 16% compared to the control and after 72 h of light induction a total of 72% seeds had germinated (Fig.3.39).

3.21 Effect of Abscisic Acid (ABA) and Gibberellic acid (GA3) on germination

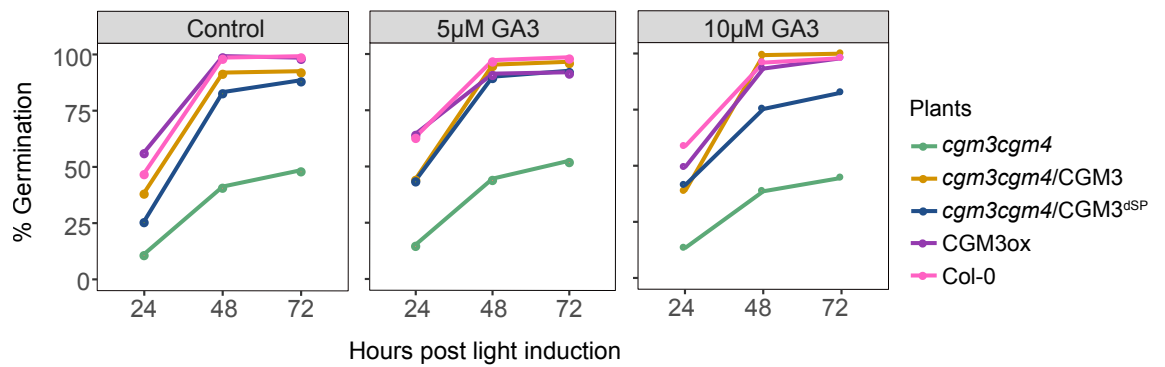


Figure 3.38: Effect of 5 μM and 10 μM GA3 on germination rate of Col-0, *cgm3cgm4*, *cgm3cgm4*CGM3, *cgm3cgm4*CGM3^{dSP} and CGM3ox compared to control conditions without GA3. n=100 seeds.

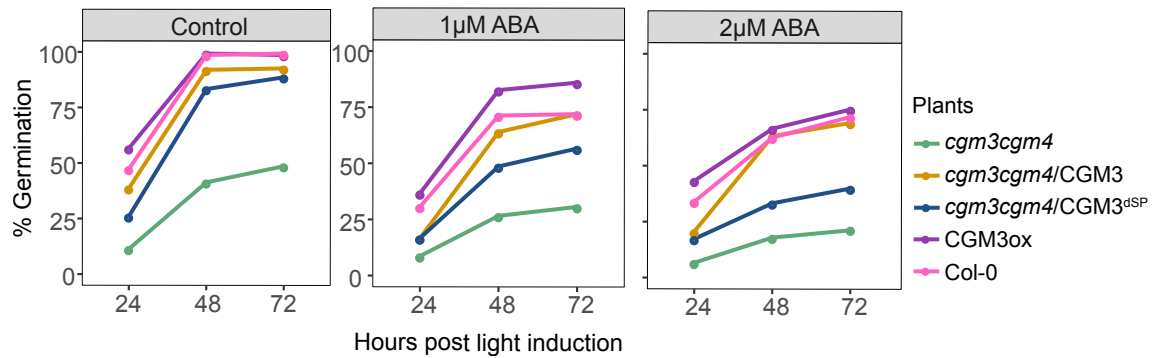


Figure 3.39: Effect of 1 μM and 2 μM ABA on germination rate of Col-0, *cgm3cgm4*, *cgm3cgm4*CGM3, *cgm3cgm4*CGM3^{dSP} and CGM3ox compared to control conditions without ABA. n=100 seeds.

3.22 Co-expression of other GDSL hydrolases with CGM4 in the stomatal lineage

The genome of *A. thaliana* contains roughly 100 members of the GDSL lipase gene family, distributed in all five chromosomes (Tree from Intro). During the plant's life cycle, these genes are expressed with a high spatial and temporal variability. Using available *in-silico* expression data from several resources, a co-expression analysis was performed by ATTED-II to identify genes co-expressed with CGM4 in the stomatal lineage. The analysis identified eight GDSL lipase genes co-expressed with CGM4 in the stomatal lineage (Fig.3.40). Their expression in the stomatal lineage was confirmed using promoter fusions with nls-GFP constructs. Gene fragments of around 2 kb, located 2–3 kb upstream of the respective transcription start sites, were cloned into the vector containing nls-GFP at the C-terminus of the sequence of interest. These constructs were then transformed into *A. thaliana* wild-type Col-0 plants and the T2 seedlings were screened for the nls-GFP signal in the stomatal lineage. Among the eight candidates, six of the fusion constructs were expressed in the stomatal lineage (Fig.3.41).

Multiple T-DNA insertion lines were genotyped for homozygosity of the six putative GDSL candidates for. Of the six candidates, genotyping confirmed that *cgm5* (CRISPR-cas deletion mutant), *cgm19* (SALK 082848c), *cgm21* (SALK 116756), *cgm58* (SAIL-798-c11) were homozygous. The single-mutant lines showed no overall growth or developmental defects under ambient growth conditions compared to wild-type Col-0.

3.22 Co-expression of other GDSL hydrolases with CGM4 in the stomatal lineage

New rank	Average MR to query loci	Average COR to query loci	Locus	Target	CGM	Function
1	0	0.00	At4g18970	S,S	CGM4	GDSL-like Lipase/Acylhydrolase superfamily protein
2	1	0.00	At5g45670	S,S	CGM3	GDSL-like Lipase/Acylhydrolase superfamily protein
4	4	0.00	At3g04290	S,	CGM19	Li-tolerant lipase 1
8	5	0.00	At3g16370	S,S	CGM58	GDSL-like Lipase/Acylhydrolase superfamily protein
9	6	0.00	At4g28780	S,V	CGM22	GDSL-like Lipase/Acylhydrolase superfamily protein
22	14	0.00	At1g33811	S,S	CGM5	GDSL-like Lipase/Acylhydrolase superfamily protein
36	28	0.00	At2g04570	S,S	CGM54	GDSL-like Lipase/Acylhydrolase superfamily protein
74	62	0.00	At1g29660	S,S	CGM2	GDSL-like Lipase/Acylhydrolase superfamily protein
142	117	0.00	At1g29670	S,S	CGM1	GDSL-like Lipase/Acylhydrolase superfamily protein
158	132	0.00	At5g18430	S,S	CGM21	GDSL-like Lipase/Acylhydrolase superfamily protein

Figure 3.40: Co-expression analysis of other GDSL lipase with CGM4 using ATTED-II.

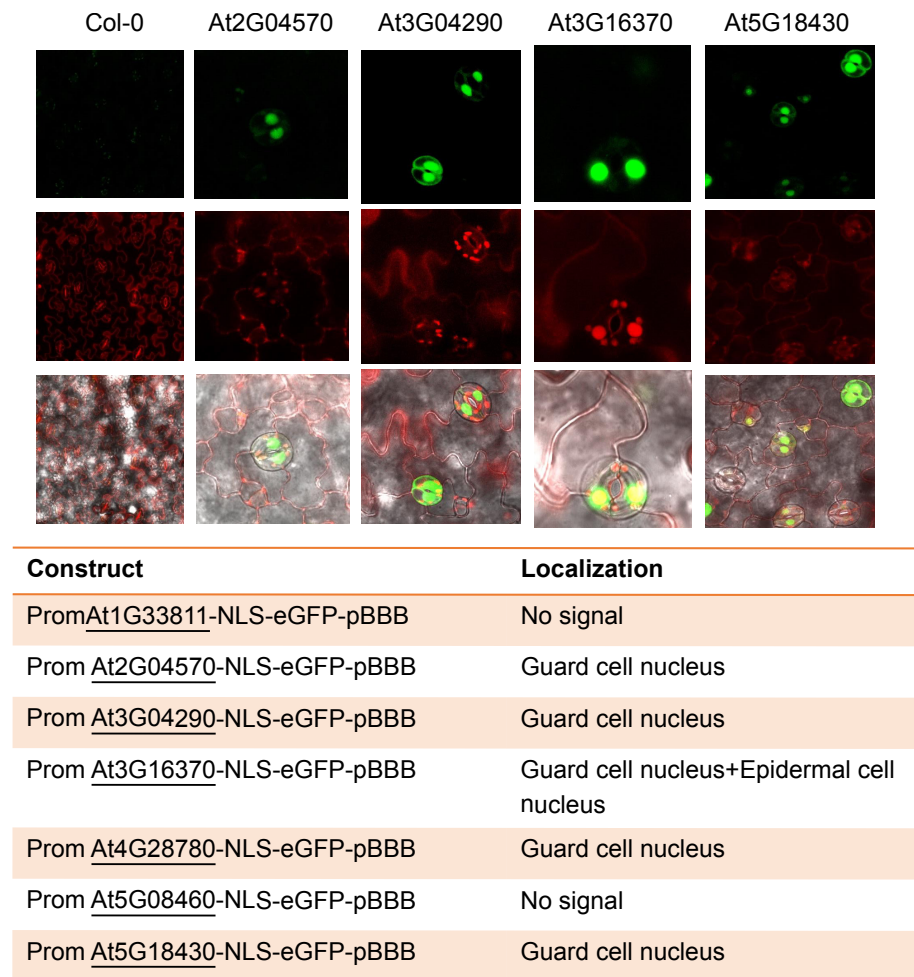


Figure 3.41: Promoter localization of the other GDSL lipases.

Chapter 4

Discussion

4.1 CGM4 and CGM3 are extracellular proteins

Most GDSL hydrolases contain a signal peptide domain at the N-terminal of their sequences (Oh *et al.*, 2005; Ling, 2008; Ding *et al.*, 2019), similar to secretory proteins. These signal peptides are small stretches of amino acids that are recognized by the cytosolic signal recognition particle (SRP) and translocate to the ER for the secretory path-way.

According to the signal peptide analysis tool SignalP v.5.0, CGM3, CGM4 and most of the other GDSL hydrolases in *A. thaliana* should contain a 22- to 27-amino-acid-long signal peptide sequence and peptide cleavage site (Fig.3.1), suggesting that the CGM3 and CGM4 are secreted proteins. When transiently expressed in *N. benthamiana* leaves, mScarlet-tagged CGM4 (p35S-CGM4-mScarlet) was localized in the extracellular space, whereas the signal-peptide-mutated CGM4 (p35S-CGM4^{dSP}-mScarlet) was localized in the cytoplasm (Fig.3.2). A similar localization was found in mature root epidermal cells stably over-expressing CGM4 (pUBQ10-CGM4-GFP) and in CGM4^{dSP}

(pUBQ10-CGM4^{dSP}-GFP) seedlings tagged with GFP (Fig.3.3). However, the GFP and mScarlet signals under confocal microscopy were weak such that apoplastic localization at the protein level remained unclear. To verify the subcellular localization of these proteins will require experiments using different fluorescence tags and protein assays. The absence of ER or Golgi retention motifs in CGM3 and CGM4 sequences suggests that these proteins are not intracellular. Furthermore, the cytoplasmic localization of the signal-peptide-mutated proteins indicated a requirement for the signal peptide to achieve the extracellular localization of these proteins. A study of the *A. thaliana* secretome yielded similar results, demonstrating that the GDSL hydrolase AtGLIP1 was localized in the extracellular space, whereas AtGLIP1 lacking the signal peptide sequence was confined to the cytoplasm (Oh *et al.*, 2005). The rice GDSL hydrolases OsGLIP1 and OsGLIP2 also localized in the apoplast along with ER localization after plasmolysis (Gao *et al.*, 2017), and transient expression of the GDSL hydrolases from *A. thaliana* and *Tanacetum cinerariifolium* was followed by their secretion into the extracellular space (Oh *et al.*, 2005; Kikuta *et al.*, 2012; Gao *et al.*, 2017). However, several GDSL hydrolases from plants were shown to be localized in intracellular organelles, including GER1 from rice, localized in secretory vesicles (Riemann *et al.*, 2007); WDL1 from rice, ESM1 from Arabidopsis, and ZmMs30 from maize, localized in the ER (Zhang *et al.*, 2006; Park *et al.*, 2010; An *et al.*, 2019) and BS1 from rice, localized in the Golgi apparatus (Zhang *et al.*, 2017). Thus, the intracellular localization of the GDSL hydrolases require further study. Many of the studies reported thus far have used protoplast systems to investigate localization and thus did not clearly demonstrate that the respective GDSL hydrolases were not localized in the extracellular space. As described in the Introduction, most secreted proteins are transported to the extracellular space via the conventional secretory pathway which includes the ER, Golgi and secre-

tory vesicles (Chung and Zeng, 2017). Thus, it may be that these GDSL hydrolases are temporarily retained in those organelles while trafficking through the secretory pathway. Furthermore, the functions of most secreted proteins are related to cell wall modification and defense mechanism. Cell wall components are synthesized within intracellular organelles and then transported to the extracellular space (Keegstra, 2010; Lampugnani *et al.*, 2018). While most of their modifications occur primarily in the apoplast, some occur within intracellular organelles (Keegstra, 2010; Lampugnani *et al.*, 2018). Therefore, it may be that some GDSL hydrolases are functional in the intracellular organelles although they are secreted proteins.

This study showed that CGM4 influenced stomatal opening/closing dynamics, as the dynamics of *cgm3cgm4* mutant plants resulted in limited stomatal opening and closing. This effect could be recovered by the transformation using the CGM4 full genomic construct but not the signal-peptide-mutated construct. These results were supported by the stomatal aperture index analysis as well as measurements of the transpiration rate. Moreover, they indicated that the signal peptide domain is necessary for both the localization and the function of CGM3 and CGM4 proteins. Nevertheless, the subcellular localization could not be definitively determined in this study. However, the functional effect of the intracellular localization of CGM3 and CGM4 can be assessed using ER and Golgi retention motifs. Furthermore, when the CGM4 was expressed under a mature guard cell-specific promoter (pGC1) it was localized in the cytoplasm of mature guard cells in a dotted structure (Fig.3.34) instead of extracellular space. The preliminary analysis of transpiration and stomatal opening-closing dynamics with the *cgm3cgm4* plants with pGC1:CGM4 construct showed similar response to wild-type Col-0. Although, more repetitions and detailed analysis of stomatal dynamics and architecture with different stimuli are necessary for these experiments, it might provide

deeper understanding of the question, how CGM4 regulate the stomatal dynamics at the early developmental stages of guard cells and if the deformities of the stomatal pore in *cgm3cgm4* can be overcome when CGM4 is expressed at the later stage of stomatal development.

4.2 CGM4 expressed during the stomatal lineage development

Stomata were one of the key innovations for plants for terrestrial growth (Hetherington and Woodward, 2003; Berry *et al.*, 2010; Chater *et al.*, 2017), and a key step in their development was the basic helix-loop-helix transcription factor SPEECHLESS (SPCH) (MacAlister *et al.*, 2007), which is essential for the establishment of the stomatal lineage (MacAlister *et al.*, 2007; Simmons and Bergmann, 2016). To identify the target genes of SPCH, Lau *et al.* (2014) performed MOBE-ChIPs and profiled the binding events of SPCH over the whole genome of *A. thaliana* (Lau *et al.*, 2014). This study showed that SPCH not only initiates the stomatal lineage but also regulates a broad range of genes, including several GDSL hydrolases. The SPCH binding profile identified several gene regions, mostly promoter regions where SPCH binding induces gene expression. The top-scoring motif, CDCGTG, predominated around 500 bp upstream of the transcription start site (Lau *et al.*, 2014). Among the GDSL hydrolases regulated by SPCH was CGM4 (Fig.3.5) and a nucleotide analysis of the CGM4 sequence identified a SPCH binding motif at the 5' UTR (untranslated region). When the CGM4 promoter construct was expressed in an *spch* mutant, the homozygous seedlings completely lacked cells of the stomatal lineage in the leaf epidermis and there was no pCGM4:nls-GFP

signal in the abundant pavement cells (Fig.3.5). These results provided further evidence that CGM4 is specifically expressed in the stomatal lineage and is likely regulated by the bHLH transcription factor SPCH, as also evidenced by the qPCR (Figs.3.4, 3.5). CGM4 transcript levels were quantified in wild-type Col-0, *spch*, *cgm4* and *cgm3cgm4* plants and normalized to the levels of the house-keeping gene RAN3. The results showed that the transcript levels of CGM4 were down-regulated in *spch*, *cgm4* and *cgm3cgm4* plants compared to wild-type Col-0 (Figs.3.5, 3.9).

The GUS-fused CGM4 promoter construct was expressed in the stomatal lineage but not in the mature stomata (Grefen, 2008). Similarly, nls-GFP tagged CGM4 construct was expressed specifically in the early developmental stages of stomata (Fig.3.4). However, the aim of the experiment was to determine the expression of CGM4 at a distinct stage of the stomatal lineage. The different stages of stomatal development are well characterized and a quantitative analysis of the GFP signal during these stages showed that the promoter fusion construct was strongly expressed during early developmental stages (Fig.3.4). The major limitation to this experiment was the residual fluorescence of the nls-GFP tag. Further expression analyses using an unstable version of the promoter fusion construct may provide a deeper understanding of the expression of CGM4. Phylogenetic analyses have predicted that large gene families including the family of GDSL hydrolases, evolved from gene duplication events, such as segmental duplication (Cannon *et al.*, 2004; Lai *et al.*, 2017). Some of these duplicated genes are retained in the genome (Panchy *et al.*, 2016), with the duplicated gene acquiring a novel function or a sub-functionalization of the ancestral function that becomes evolutionarily important (Pickett and Meeks-Wagner, 1995; Blanc and Wolfe, 2004; Ganko *et al.*, 2007; Panchy *et al.*, 2016). Other studies have shown that duplicate genes have a higher tendency of

divergent expression patterns and encode different biological functions (Ganko *et al.*, 2007; Renny-Byfield and Wendel, 2014; Hu *et al.*, 2015; Panchy *et al.*, 2016). For example, the MADS box transcription factors family belongs to a large gene family of more than 100 members and the paralogous members control different aspects of plant development (McCarthy *et al.*, 2015).

As noted above, the GDSL hydrolase CGM3 is a paralog of CGM4 and shares 90% sequence similarity but according to *in-silico* data CGM3 is expressed in imbibed seeds and CGM4 in stomatal lineages in leaves. CGM3 and CGM4 are examples of duplicated genes retained in the *A. thaliana* genome (Lai *et al.*, 2017). The CGM3 promoter fusion construct was not expressed in the stomatal lineage (Fig.3.8) but it was weakly expressed in the background of *cgm4* single mutant plants (Figs.3.8, 3.9). The weak expression prevented drawing any conclusions, but CGM3 transcript levels were up-regulated in *cgm4* plants compared to wild type Col-0 plants (Fig.3.9), suggesting that CGM3 and CGM4 are functionally redundant.

4.3 CGM4 influences the mature stomatal function

CGM4 is expressed in the developmental lineage of the stomata in *A. thaliana* wild type Col-0 but the *cgm3cgm4* mutant plants showed no obvious phenotypical variation under normal growth conditions (Figs.3.4, 3.10). There were also no abnormalities in stomatal patterning or stomatal distribution in the leaf epidermis of *cgm3cgm4* mutant plants under light microscopy, but stomatal opening and closing were altered (Figs.3.11, 3.12). While there was no obvious difference in the biomass (measured as the fresh weight of the plants) (Fig.3.10) of the *cgm3cgm4* mutant plants vs. wild type Col-0 plants, they showed enhanced drought tolerance (Figs.3.19, 3.20), as a larger number of mutant

plants recovered from drought 14 days after re-watering. Recent studies have shown that genetic modification of stomatal density or stomatal opening-closing dynamics influences the water-use efficiency or drought tolerance of several crop species (Amsbury *et al.*, 2016; Hughes *et al.*, 2017; Bertolino *et al.*, 2019; Dunn *et al.*, 2019), which suggested that drought tolerance is directly dependent on the dynamic range of the stomatal aperture. This may have also been the case in the *cgm3cgm4* mutants, which showed a similar drought tolerance phenotype and altered stomatal opening-closing dynamics under drought stress.

The phytohormone ABA triggers stomatal closure (Munemasa *et al.*, 2015). ABA synthesis is induced by drought stress (Desikan *et al.*, 2004; Fernando and Schroeder, 2016; Daszkowska-Golec, 2016), among other factors, and ABA signaling induces stomatal closure to reduce water loss via transpiration (Desikan *et al.*, 2004; Fernando and Schroeder, 2016; Daszkowska-Golec, 2016). The ABA synthesis and signaling pathway and the mechanism of ABA induced stomatal closure have been well-studied (Desikan *et al.*, 2004; Fernando and Schroeder, 2016; Daszkowska-Golec, 2016). In this study, when epidermal peels were treated with external ABA, a reduced stomatal closure response compared to the wild-type Col-0 was observed in the *cgm3cgm4* mutants whereas peels from plants with constitutive over-expression of CGM4 had a higher width to length ratio of the stomatal pore (Fig.3.12).

To further investigate whether the altered stomatal opening-closing dynamics in the mutant plants was ABA-dependent, the transcriptome analysis of mutant and wild type Col-0 plants treated or not with ABA was performed (Figs.3.12, 3.21, Tables 3.1, 3.2, 3.3). The results showed similar ABA-induced gene up-regulation in mutants and wild type Col-0 under all conditions. These results indicated that the irregularity of the stomatal opening-closing dynamics in the mutant was independent of ABA signaling (Fig.3.21).

Furthermore, when epidermal peels of the mutants were treated with H_2O_2 or the fungal toxin fusicoccin to induce stomatal closure and opening, respectively (Fig.3.12), altered stomatal opening-closing dynamics of the mutants compared to wild type Col-0 were again observed. The production of reactive oxygen species (ROS), such as superoxide anion (O_2^-), hydrogen peroxide H_2O_2 and other free radicals, is triggered by several environmental stresses (Zhang *et al.*, 2001; Neill *et al.*, 2002; Desikan *et al.*, 2004). For example, in response to a water deficit, ABA synthesis and signaling are triggered, which induces H_2O_2 biosynthesis in guard cells. H_2O_2 causes alkalization of the cytoplasm, elevation of the cytosolic calcium level and thus stomatal closure Desikan2004, Neill2002, Zhang2001. ROS, including H_2O_2 , in plant cells can be monitored using the fluorescent dye DCFDA, which showed a higher accumulation of ROS in the stomata of the *cgm3cgm4* mutant than in those of wild type Col-0. These results suggested that the majority of the stomata in the mutant plants were in the closed state (Fig.3.14). When the leaves of the *cgm3cgm4* mutants and wild type Col-0 leaves were treated with external ABA to induce stomatal closure, both showed the accumulation of high ROS levels. Further treatment with the NADPH oxidase inhibitor DPI, a ROS scavenging agent, showed reduced accumulation of ROS in the stomata of wild-type Col-0 whereas in the *cgm3cgm4* mutant there was no change compared to mutant leaves treated only with ABA (Fig.3.15). These results indicated that the altered stomatal opening-closing dynamics in the *cgm3cgm4* mutants involves an ABA- and H_2O_2 -independent mechanism.

The fungal phytotoxin fusicoccin inhibits ABA-induced stomatal closure (Turner and Graniti, 1969; Huang *et al.*, 2014) by promoting cytosolic acidification in the guard cells, which reduces their H_2O_2 levels and thus inhibits stomatal closure (Huang *et al.*, 2014). In *cgm3cgm4* mutants treated with fusicoccin, the width to length ratio of

the stomatal pore was reduced compared to the wild type Col-0 (Fig.3.12). Several pathogens use the stomatal pore as a gate for invasion, with the plant then responding with stomatal closure as a defense strategy (Gudesblat *et al.*, 2009; Zeng *et al.*, 2010; Melotto *et al.*, 2017). The *cgm3cgm4* mutant plants showed moderately higher resistance than the wild type Col-0 when treated with a *Pseudomonas* inoculum (Fig.3.18). However, a limitation of this experiment was the weaker phenotype and the lack of measures of the infection symptoms. Nonetheless, the results indicated that the *cgm3cgm4* mutants better tolerated pathogenic infection.

As stomata are the organs responsible for transpiration, stomatal opening-closing dynamics are influenced by environmental factors such as CO₂ and light (Darwin, 1916). For example, a low CO₂ level induces stomatal opening and an elevated CO₂ stomatal closure, thereby altering the rate of transpiration (Darwin, 1916; Kim *et al.*, 2010). Plants have a higher transpiration rate in a low- CO₂ environment and a lower transpiration rate in the presence of elevated CO₂ levels (Kim *et al.*, 2010; Matrosova *et al.*, 2015; Amsbury *et al.*, 2016). Measurement of the transpiration rate of the *cgm3cgm4* mutants showed a reduced response to different CO₂ concentrations (Fig.3.17). Specifically, under a low CO₂ level (100 mmol), the transpiration rate of the *cgm3cgm4* mutant was lower than that of wild type Col-0, and under a high CO₂ (1000 mmol) level the transpiration rate of wild type Col-0 decreased whereas in the *cgm3cgm4* mutant it remained unchanged. In plants that constitutively over-expressed CGM4, by contrast, the transpiration was higher than that of the wild type Col-0 under both high and low CO₂ conditions.

Stomatal opening-closing dynamics are also influenced by light (Rao and Ander-

son, 1983; Elhaddad *et al.*, 2014; Feng *et al.*, 2019), which induces stomatal opening whereas dark induces stomatal closure, consistent with the circadian clock of plants (Webb, 2003). Under dark conditions, the transpiration rate was lower in the *cgm3cgm4* mutants than in the wild-type (Fig.3.16). The exposure of wild-type Col-0 to 400 PAR light increased the transpiration rate, which immediately dropped when the plants were exposed to dark. By contrast, the transpiration rate of the *cgm3cgm4* mutant plants remain unchanged when they were shifted from dark, to 400 PAR light and then dark again. A similar phenotype was observed when the epidermal peels of the mutants were exposed to light and dark to induce stomatal opening and closing, respectively (Fig.3.12). The width to length ratio of the stomatal pore of wild type Col-0 was higher under light conditions and lower under dark conditions, whereas in the *cgm3cgm4* mutants the ratio remained unchanged. In the plants constitutively over-expressing CGM4, a higher width to length ratio of the stomatal pore compared to the wild type was measured under both dark and light conditions. The *cgm3cgm4* complemented with CGM4 (*cgm3cgm4CGM4*) showed similar response as wild-type Col-0. Together, these results show that the altered stomatal opening-closing dynamics of the mutants influenced both their drought tolerance and transpiration but the growth (in terms of biomass) of the mutants under normal growth conditions was the same as that of wild type Col-0 (Fig.3.10). This raises the question whether the reduced transpiration rate due to the altered stomatal opening-closing dynamics also influenced photosynthetic efficiency, which supports plant growth, given that the growth phenotype of *cgm3cgm4* plants was unaffected under normal growth conditions. Previous studies demonstrated rapid (time scale of seconds) CO₂ assimilation dynamics in sun-exposed plants in natural ecosystems (Percy and Pfitsch, 1995; Vico *et al.*, 2011; Way and Percy, 2012; Papanatsiou *et al.*, 2019). In this study, light intensity under normal growth conditions was 51 $\mu\text{mol}/\text{m}^2/\text{s}$, which was

significantly lower than natural light intensity, which may be as high as $1200 \mu\text{mol}/\text{m}^2/\text{s}$ (Violet-Chabrand *et al.*, 2017; Schumann *et al.*, 2017). To investigate the plant growth under moderately elevated light condition, the mutants and wild type plants were exposed to a light intensity of $190 \mu\text{mol}/\text{m}^2/\text{s}$ (Fig.3.23). While the growth of wild-type and mutant plants increased in response to the higher light intensity, the biomass of the *cgm3cgm4* mutant plants was lower than that of the wild-type Col-0 plants. Although, the fluctuation in natural light was not considered in this experiment, the altered stomatal opening-closing dynamics of the *cgm3cgm4* mutants may have been advantageous only under low light conditions but not under natural growth condition.

A similar phenotype of altered stomatal opening-closing dynamics has been reported for *A. thaliana* with mutations in *PME6*, *PGX3* and arabinans (Jones *et al.*, 2003; Amsbury *et al.*, 2016; Rui *et al.*, 2017). *PME6* is a pectin methyl-esterase that is abundant in the guard cell wall (Amsbury *et al.*, 2016) and plays a key role in the de-methylation of pectin and therefore influences stomatal function. In *pme6* mutant plants, methyl-esterified pectin is enriched in the guard cell wall and mechanical stiffness is increased, causing a decreased dynamic range of the stomata even in the presence of an elevated CO_2 supply. As the altered stomatal function increases stomatal conductance, *pme6* plants have a reduced ability to adjust leaf temperature under drought conditions. Thus, esterification of the pectin and the cell wall properties of stomata influence stomatal function and, in turn, plant physiology (Amsbury *et al.*, 2016). The pectinase *PGX3* regulates guard cell wall mechanics and stomatal development (Rui *et al.*, 2017). In *pgx3* mutant plants, the reduced fluidity of pectin in the cell wall leads to the inhibition of stomatal closure (Rui *et al.*, 2017). These studies highlight the central role of the composition of the guard cell wall in modulating stomatal opening-closing dynamics. While several physiological studies have explored the regulation of stomatal opening-

closing dynamics in response to turgor pressure and ion fluxes (Von Mohl, 1856; Pandey *et al.*, 2007; Jezek and Blatt, 2017), how the mechanical properties of guard cells influence stomatal function is still poorly understood. The altered stomatal opening-closing dynamics of the *cgm3cgm4* mutants and their independence of ABA signaling indicated that the impaired stomatal function might be mechanical.

4.4 CGM4 involved in cell wall biosynthesis of the guard cell

Stomatal opening is promoted by an increased turgor pressure in the guard cells, whereas the reverse mechanism induces stomatal closure. Although, these events involve different sets of signaling cascades and regulatory mechanism, the dynamics are mechanically regulated (Aylor *et al.*, 1973; Woolfenden *et al.*, 2018). The plant cell wall, including the cell wall of guard cells, is a heterogeneous complex of polysaccharides that ensure the mechanical properties of the cell wall, including its flexibility (Doblin *et al.*, 2010; Shtein *et al.*, 2017). The robust and flexible cell wall structure of the stomata facilitates their turgor-driven reversible opening and closing (Meckel *et al.*, 2007; Carter *et al.*, 2017; Woolfenden *et al.*, 2018). Computational modeling and biochemical studies based on stomata have provided substantial information on stomatal mechanics, but experimental studies are limited (Jones *et al.*, 2003; Amsbury *et al.*, 2016; Carter *et al.*, 2017; Rui *et al.*, 2017; Woolfenden *et al.*, 2018). The results of the preliminary biochemical experiments performed in this thesis revealed differences in the cell wall composition of the *cgm3cgm4* mutants compared to wild-type Col-0, including in the polyphenolics content (Figs.3.24, 3.25, 3.26). For example, the amounts of several monosaccharides

were lower in cell wall extracts of the *cgm3cgm4* plants than in those of wild-type Col-0 (Fig.3.24). However, a possible limitation of this experiment was that the cell wall was extracted from whole leaves instead of guard cells alone, resulting in a dilution of guard cell components. Therefore, differences inferred from metabolomic assays cannot be attributed with certainty to differences in guard cell wall composition alone. A possible alternative strategy might be to use laser capture microdissections to pool the stomata and then extract the guard cell wall, but this procedure is highly time-consuming and likely infeasible. Thus, a deeper understanding of the differences in the composition of the guard cell wall of the *cgm3cgm4* mutants vs. that of wild-type Col-0 awaits further methodological advances.

Studies of the ultrastructure of the guard cells in different plants have shown an uneven thickening of the cell wall (Von Mohl, 1856; Zhao and Sack, 1999; Merced and Renzaglia, 2018), with the ventral wall, facing the stomatal pore area, being thicker than the dorsal wall, which faces neighboring epidermal cells. Plant stomata contain cuticular ledges on the upper and lower aspects of the stomatal pore (Von Mohl, 1856; Esau, 1960; Wilkinson, 1979; Hunt *et al.*, 2017; Pautov *et al.*, 2017), but their function is unknown. Stomatal pore formation and the processes giving rise to the unevenly distributed cell wall material in the ventral wall are also poorly understood. Recent biochemical modeling and high-resolution microscopy studies have simulated the mechanics of stomatal structure (Carter *et al.*, 2017; Woolfenden *et al.*, 2018); however, the many different parameters of stomatal structure and stomatal opening-closing dynamics have complicated these efforts. Nonetheless, Rui *et al.* (2016) were able to use their experimentally gained insights into stomatal geometry to model the mechanical stress across the guard cell surface. The scanning electron microscopy study of the individual stomata performed as

part of this thesis showed that the majority of the stomata of *cgm3cgm4* plants were structurally different than those of the wild-type Col-0 (Fig.A.1). Specifically, a large number of stomata were highly wrinkled/deformed/shrunken and the stomatal pores contained visibly thicker cuticular ledges as well as a lack/over-deposition of cuticular material. Similar findings were rarely found in the leaf surface of wild type Col-0 (Figs.A.1, 3.29). Furthermore, AFM showed that the stomata of *cgm3cgm4* were stiffer than those of wild type (Figs.3.31, 3.32, 3.33). A quantification of the relative stiffness of the stomatal pore area vs that of the surrounding cells revealed significantly higher stiffness ratios in the *cgm3cgm4* mutant. However, this finding remains to be confirmed in studies examining a larger number of stoma as well as the induction of stomatal opening-closing by various agents. Although the specific substrate of CGM4 has yet to be identified, these results indicate that the increased stiffness of *cgm3cgm4* stomata were due to biochemical changes in cell wall composition, which would also explain their weaker response to abiotic and biotic stimuli. However, the AFM results are preliminary and the experiments should be replicated along with finite element modeling to analyze the biophysical mechanism underlying stomatal opening-closing dynamics. Galacturonic acid (GalA) residues are the major building blocks of pectin, one of the most abundant components of the plant cell wall (Zabackis *et al.*, 1995; Caffall and Mohnen, 2009). Pectin biosynthesis occurs in the Golgi apparatus and its methyl-esterified components are subsequently transported to the extracellular space. Cell wall pectin exists in several different methyl-esterification states (Caffall and Mohnen, 2009; Hocq *et al.*, 2017; Harholt *et al.*, 2010) that can be identified using different epitopes. This approach can be used to distinguish the guard cell wall from the cell walls of surrounding cells. Three epitopes, LM19, LM20 and 2F4, bind to different esterified forms of pectin: LM19 binds to the unesterified pectin backbone (Verhertbruggen *et al.*, 2009),

LM20 to the highly methyl-esterified form of pectin (Verherbruggen *et al.*, 2009) and 2F4 to the calcium cross-links in pectin (Liners *et al.*, 1989, 1992; Liners and Van Cutsem, 1992). The cell-wall binding pattern of these three epitopes differs in guard cells vs. epidermal cells, in that LM19 binds to the cell wall of both cell types whereas LM20 and 2F4 shows strong binding at the junction between guard cells and epidermal cells (Amsbury *et al.*, 2016). Immunolabeling with different pectin epitopes showed no obvious difference in the spatial distribution of the cell-wall epitopes of the guard cells of *cgm3cgm4* vs. those of the wild type Col-0 (Fig.3.27). Immunolabeling with other cell wall epitopes that recognize different cell wall compounds and their modifications (methylation, acetylation etc.) is therefore needed to understand pectin modification in the guard cell walls of *cgm3cgm4* plants. However, in cell wall extracts of wild type Col-0, *cgm3cgm4* and CGM4ox treated with pectate lyase, a higher amount of unsaturated product was found in the *cgm3cgm4* extract than in the extracts of wild type Col-0 and CGM4ox and a lower amount in the CGM4ox extract compared to that of the wild type (Fig.3.30). At pH 12, demethylated pectin treated with pectate lyase undergoes beta-elimination, during which the double bonds are cleaved by the enzyme, yielding unsaturated polysachharides (Soriano *et al.*, 2006; Sukhumsirchart *et al.*, 2009). Studies of the pectin biogenesis pathway and the involvement of different homogalacturonan modifying enzymes have shown that methylesterified pectin undergoes either block-wise or random de-methylesterification, which determines the cell wall mechanics (Hocq *et al.*, 2017). In block-wise de-methylesterification Ca²⁺-cross-linking is induced, which increases wall stiffness whereas in random de-methylesterification degradation by polygalacturonases or pectate lyase is facilitated, leading to a more flexible cell wall (Hocq *et al.*, 2017). The cell wall of guard cells is characterized by a unique combination of strength and flexibility in which pectin remodeling regulates the opening-closing of the

stomata (Rui and Anderson, 2016; Rui *et al.*, 2017, 2018). Although the immunolabelling and pectate lyase assays did not identify substantial differences in the distribution of the different esterified forms of pectin in the guard cell wall of *cgm3cgm4* and wild-type plants, a difference in the degree of methylation, which would favor pectate lyases activity via the random de-methylesterification of pectin, remains to be explored in additional analytical and cell-biological experiments.

4.5 CGM3 involved in seed germination process

As discussed above, CGM4 shares almost 90% sequence similarity with CGM3, most likely due to gene duplication events (Lai *et al.*, 2017), but they are expressed in different tissues. Fusion of the CGM4 promoter with GUS showed that CGM4 is expressed in the early developmental stages of stomata (Grefen, 2008) whereas an *in-silico* database eFP browser predicted the expression of CGM3 in imbibed seeds (Figs.3.6, 3.7). However, in imbibed seeds ubiquitously over-expressing CGM3 (CGM3ox) and signal-peptide-mutated CGM3 (CGM3^{dSP}ox) did not show convincing CGM3 expression. Nonetheless CGM3 transcript levels were higher in CGM3ox seeds than in wild-type Col-0 and were not detectable in *cgm3* mutant seeds (Fig.3.6). Additionally, the seed germination assay revealed the delayed germination of *cgm3cgm4* plants compared to wild-type Col-0 and CGM3ox plants (Fig.3.37). Conversely, germination rates were higher in the complemented plant lines (*cgm3cgm4CGM3*) than in *cgm3cgm4* plants and in plants complemented with the construct consisting of signal-peptide-mutated CGM3 (*cgm3cgm4CGM3^{dSP}*) a partial recovery of the germination defect was observed. Although an explanation for the *cgm3cgm4CGM3^{dSP}* phenotype is lacking, together these results suggest a role for CGM3 in seed germination.

Many of the developmental processes in plants, especially seed germination (Davies, 1995; Miransari and Smith, 2014), are controlled by GA and ABA (Swain *et al.*, 1997; Fleet and Sun, 2005), and cross-talk between these phytohormones during seed development and germination has been reported (Vishal and Kumar, 2018). Higher levels of ABA accumulate during the unfavorable environmental conditions that lead to seed dormancy whereas GA synthesis is activated during the favorable conditions and induces seed germination (Vishal and Kumar, 2018). In *A. thaliana* GDSL genes are active downstream in the GA pathway and are involved in seed development as well as fatty acid metabolism (Chen *et al.*, 2012). Previous microarray analyses showed that several GDSL hydrolases genes are downregulated by DELLAs, which are key regulators of the GA pathway (Cao *et al.*, 2006; Huang *et al.*, 2015). When *cgm3cgm4* seeds were treated with GA₃, there was no effect on seed germination whereas the germination rates of wild-type Col-0, CGM3ox and *cgm3cgm4*CGM3 seeds increased (Fig.3.38). This suggested that the *cgm3cgm4* is insensitive to GA₃. However, ABA decreased the seed germination in all of the tested genotypes (Fig.3.39). After 72 hr of light induction seeds of the CGM3ox mutants had a higher rate of germination than either wild-type Col-0 seeds or seeds of the other genotypes. Thus, while CGM3 is thought to play a role in *A. thaliana* seed development and germination, its specific target and function in these processes remain unknown. Further studies with high-resolution microscopy and standardized analytical experiments might provide the answers.

4.6 Potential involvement of other GDSL hydrolases in stomatal development and function

There are 100 GDSL hydrolases genes within the GDSL hydrolases gene family in *A. thaliana* (Chepyshko *et al.*, 2012; Lai *et al.*, 2017; Ding *et al.*, 2019) (Fig.1.2). These enzymes show a wide range of functional diversity (Akoh *et al.*, 2004), attributable to their broad substrate specificity. The latter reflects the ability of the active site to undergo a change in conformation depending on the substrate. A search of *in-silico* databases revealed at least eight other GDSL hydrolases co-expressed with CGM4 in stomatal lineages. This was confirmed in the expression assay using the promoter fragment of these candidate GDSL hydrolases in nls-GFP constructs stably expressed in *A. thaliana*, as expression was confined to the stomatal lineage (Fig.3.41). However, single T-DNA insertion lines of these candidate GDSL hydrolases did not show any altered developmental phenotypes. To gain a better understanding the role of GDSL hydrolases in stomatal function, multiple knockout lines have been developed but detailed analysis were not complete at the time of the writing of this thesis. Thus, whether there is indeed a high rate of redundancy among GDSL hydrolases remains to be determined.

Chapter 5

Conclusion and Conceptual Model

Since their characterization in the 19th century (Von Mohl, 1856), stomata, with their unique architectural, developmental and functional characteristics, have captured the attention of plant scientists but also scientists from other disciplines. For example, guard cells have been widely used as a model cell type to study ion transport and cellular signaling. Advances in analytical methods and higher resolution microscopy have revealed the ultrastructure of stomata and the mechanics underlying their opening-closing dynamics, including the roles played by turgor pressure and the mechanical properties of the guard cell wall. Indentation techniques and computational modelling studies have been used to investigate stomatal geometry and the finite element method in detailed studies of stomatal dynamics (Sampathkumar *et al.*, 2014; Carter *et al.*, 2017; Rui *et al.*, 2018). These modelling studies have considered several parameters of stomata, including cell-wall rigidity, guard-cell shape and the mechanics of turgor-driven stomatal movement. In addition to these theoretically based studies, experimental data have been used to predict stomatal geometry, the incorporation of guard cell wall components from the extracellular space during development, and the uneven thickening of

the cell wall of mature stomata. However, much remains to be learned about all of these processes and despite methods that allow the visualization of cell wall components, a specific quantitative determination of stomata cell wall composition is still lacking.

In the current study interdisciplinary approaches were applied to investigate stomatal opening-closing dynamics and the involvement of two GDSL hydrolase genes in the process. The focus was CGM4 and CGM3, two members of the GDSL hydrolase gene family. While their specific substrates have yet to be identified, both are apoplastic proteins with an N-terminal signal peptide sequence that determines their extracellular localization. CGM4 is expressed in the developmental lineages of stomata and is a target of the transcription factor SPCH. Physiological experiments revealed that the stomatal opening-closing dynamics of plants carrying mutated CGM3 and CGM4 genes were severely altered, most likely due to changes in the mechanical properties of the stomata. The analytical data suggested differences in the polyphenolic composition of the cell wall of mutant vs. wild-type stomata. High-resolution microscopy revealed the unusually wrinkled/shrunken ultrastructure of the mutant stomata and that the majority of these stomata had an unusual thickening of their ledges that was absent in the wild-type. The results of this thesis can be synthesized to obtain the following conceptual model (Fig.5.1).

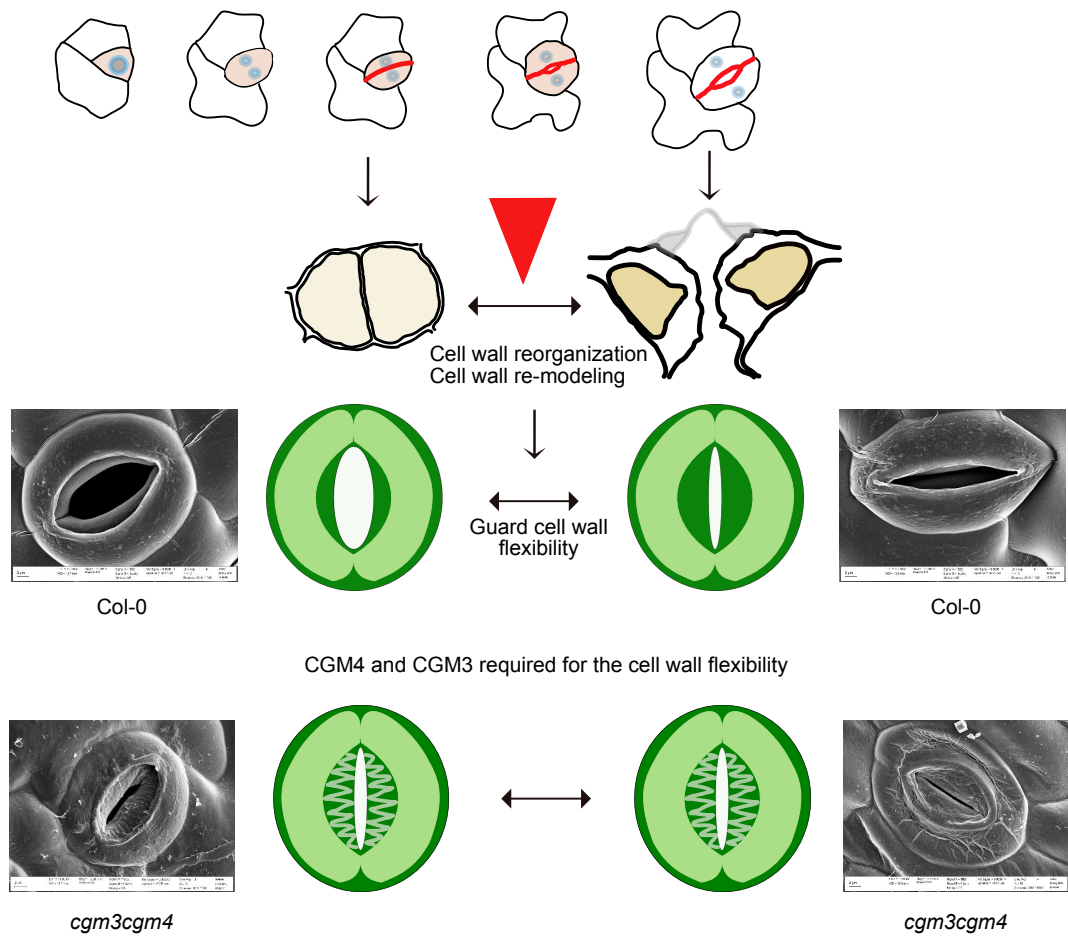


Figure 5.1: Conceptual model of putative function of CGM3 and CGM4 in cell wall biogenesis influencing stomatal opening-closing dynamics. For detailed explanation, refer to main text.

CGM4 is expressed in the developmental lineage of stomata when the meristemoids undergo symmetrical cell division. Later this cell division gives rise to the partition wall for two mature guard cells that is an essential location for subsequent uneven thickening, establishment of the stomatal pore and the development of stomatal ledges. Although the mechanism of pore formation and the functional importance of the uneven thickening at the pore wall as well as the stomatal ledges are poorly understood, this study provided valuable insights into all three. The GDSL lipase gene family includes enzymes

catalyzing xylan de-acetylation, cutinases and alpha-fucosidases. Similar functions of apoplastically localized CGM4 might influence guard cell wall biosynthesis, and specifically the ventral wall facing the stomatal pore. Stomata carrying mutant *cgm4* and *cgm3* had impaired stomatal opening-closing dynamics that could be attributed to limited cell wall flexibility.

The *cgm3cgm4* mutants also showed delayed seed germination, in which cell wall flexibility plays a major role. From a mechanistic standpoint, seed germination reflects two opposing forces. Embryonic growth towards the testa and protrusion through the seed coat is facilitated by a weakening of the seed coat and endosperm cap. Thus, cell wall biosynthesis and remodeling in the embryo and seed coat are necessary prior to seed germination. The delayed germination of the mutant might have been due to defects in either or both of these two mechanistic events. However, whether CGM3, like CGM4, influences cell wall biosynthesis during the seed germination is unknown. Further analytical and structural experiments are required to obtain a deeper understanding of the mechanism and specific role of CGM3 in seed germination.

Chapter 6

Future directions

6.1 Stage-specific expression of CGM4, tagged with the cyclin destruction box sequence in the stomatal lineage

The GUS fusion and nls-eGFP fusions with the CGM4 promoter showed that CGM4 expression occurred during stomatal development but not in mature stomata and the upregulation of CGM4 after SPCH induction. Therefore, while CGM4 expression is clearly initiated during the early developmental stage the stage at which CGM4 expression is terminated remains unclear. To investigate the effect of pCGM4:nls-eGFP protein stability at different stages of stomatal development, an unstable version of the construct can be generated by expressing a fragment of the CYCLINB1;2 gene (*cycD*) (Takada and Jurgens, 2007). When fused at the N-terminus of the nls-eGFP sequence, *cycD* acts as a destruction box. The *cycD* protein is degraded at the anaphase stage of cell division, which creates an instability in the protein fused to it. Therefore, when

cycD is fused at the N-terminus of the nls-eGFP, the pCGM4:cycD-nls-mVenus protein will be synthesized anew after each cell division. The use of this tool would help to identify the specific stage of stomatal development at which CGM4 expression is terminated. Both promoter parts of SPCH and ICE1 can serve as a control in these experiments. The bHLH transcription factor SPCH initiates the stomatal development lineage and is expressed only in the meristemoid stage of stomatal development. By contrast, ICE1, another bHLH transcription factor, is expressed during all stages of stomatal developmental. Therefore, pSPCH fused with cycD-nls-mVenus should be expressed only during the meristemoid stage of stomatal development, and pICE1 fused with cycD-nls-mVenus throughout stomatal development.

6.2 Subcellular localization of CGM3 and CGM4 with an organelle-retaining motif

The N-terminal signal peptide of GDSL hydrolases drives these enzymes to the secretory pathway (Blobel and Dobberstein, 1975). In the early stage of the secretory pathway, the protein is transported from the ER to the Golgi apparatus and then to the trans-Golgi network, from where it is distributed to the plasma membrane, extracellular space or to other endosomal compartments (Cai *et al.*, 2014). Proteins residing in the ER and Golgi possess specific retention signals that ensure structural and functional stability. ER retention is achieved with the KKXX motif and Golgi retention with the KXD/E motif (Gao *et al.*, 2012) towards the C-terminal of the protein sequences (Cosson and Letourneur, 1994; Gao *et al.*, 2012; Montesinos *et al.*, 2013; Gao *et al.*, 2014). GFP and mScarlet fused with the CGM4 protein (under the UBQ10 and 35S promoter) had an ex-

tracellular localization whereas protein lacking the signal peptide region (CGM4^{dSPox}) instead localized in the cytoplasm and was seen as punctate structures. Thus, to gain a deeper understanding of the subcellular localization of CGM4 and its functionality, the protein could be fused with different organelle-retention motifs. The idea would be to monitor the functionality of the proteins when they are forced to localized in the compartments (ER or Golgi) vs. during its normal location in the apoplastic space.

6.3 Standardization of protein extraction protocol from apoplastic sap and development of epitopes for CGM4

Despite the evidence that CGM3 and CGM4 are extracellular proteins and that CGM4 impacts stomatal dynamics, direct evidence of an apoplastic localization of GCM3 and GCM4 in *A. thaliana* is lacking and could not be obtained in this thesis. A first step would be to standardize the protein extraction protocol as applied to the apoplastic sap of the leaf. The greater challenge, however, is to identify the buffer condition allowing the extraction of functional protein in high concentrations. The current protocol does not generate either protein in amounts allowing further analysis. Expressing the recombinant protein in other systems may be advantageous. For example, the *Pichia pastoris* has been used to engineer secreted proteins which can then be extracted from the growth medium without the need to harvest the cells (Li *et al.*, 2007). Other than recombinant expression, the development of antibodies against CGM3 and CGM4 would improve proteomics studies. In this thesis, GFP-tagged proteins were used in the protein analyses but did not yield conclusive results.

6.4 Extensive immunolabeling with multiple cell-wall-related epitopes and high-resolution microscopy

In addition to the three pectin epitopes (LM19, LM20 and 2F4) used in this study to analyze the distribution of the different states of pectin in wild type and mutant plants, many other epitopes are available for targeting cell-wall components and their methylation/acetylation. An extensive study of the composition of the cell wall using immunolabelling with multiple epitopes may provide allow the identification of the targets of CGM3 and CGM4. High-resolution microscopy (TEM, SEM) of transverse sections of wild-type and mutant plants may reveal the cellular deformities that occur in *cgm3cgm4* (stomata and imbibed seeds) but not in wild-type plants.

6.5 Standardization of the cell wall extraction protocol for assays of the cell wall composition

The analysis of the composition of the cell wall in this thesis provided a preliminary understanding of the putative target group of CGM4. In the total metabolome study lower abundances of polyphenolic esters were identified in the cell wall extract from *cgm3cgm4* plants. Thus, polyphenolic compounds may be a putative target of CGM4, but this requires further experimentation. The development of a method to specifically purify the cell wall fraction of guard cells would allow more precise analyses than currently possible using cell wall extracts of whole leaves, which dilutes the guard cell wall fraction. One approach might be to dissect out the guard cells using laser capture

microdissection and then analyze cell wall metabolomics. Alternatively, an extensive targeted metabolomics assay could be conducted for a specific group of cell wall compounds, but this would again benefit from an improved cell wall extraction protocol.

6.6 Atomic Force Microscopy for measuring stomatal stiffness

The use of SEM to examine the ultrastructure of the stomata in *cgm3cgm4* leaves their deformation, wrinkled surface and unconventionally thickened cuticular ledges, none of which were seen in wild-type stomata. These structural alterations may explain the reduced stomatal response of *cgm3cgm4*. A preliminary AFM study of the stiffness of the stomatal pore area showed that *cgm3cgm4* stomata were significantly stiffer (relative to the surrounding cells) than wild-type stomata. Additional studies of stomatal stiffness should include the finite element method (FEM). FEM is used to analyze the deformation of composite structures and to calculate mechanical stress and strain. Thus, when applied to stomatal structure and/or the stomatal ledge FEM can provide valuable information on the structural and functional impairment of the stomata in *cgm3cgm4*.

6.7 Ultrastructure of imbibed seeds and fatty acid content

In addition to altered stomatal opening-closing dynamics, *cgm3cgm4* mutants showed a delay in seed germination. The strength and flexibility that allow the guard cell wall to withstand the high turgor pressure during stomatal opening and engage in stomatal

opening-closing is also required in seed germination. During this process, prior to radicle emergence, the endosperm weakens, with its eventual rupture as well as that of the testa/seed coat (Groot and Karssen, 1987; Sechet *et al.*, 2016). Endosperm weakening involves xyloglucan biosynthesis as well as PME and PMEI. However, the biophysical and biochemical changes that occur during the final stage of seed germination are still unknown. Five GDSL hydrolases have been shown to participate in fatty acid degradation in seeds and thus influence the seed germination process. Accordingly, studies of the fatty acid content of the *cgm3cgm4* mutants as well as ultrastructural studies of imbibed seeds will provide insights into the involvement of GDSL hydrolases in seed germination.

6.8 Multiple knock-out lines of other GDSL candidates with *cgm3cgm4*

According to *in-silico* data and promoter analysis, four putative GDSL candidates, CGM5, CGM19, CGM21 and CGM58, are co-expressed with CGM4 in the stomatal lineage (Figs.3.40, 3.41). To further investigate their importance in stomatal development and/or function, multiple knock-out lines of GDSL lipases have been developed by conventional crossing. The initial crosses were made between *cgm4* and, respectively, *cgm5*, *cgm19* and *cgm21*. Plants homozygous for double mutants were selected from the T3 generation. Triple knockout lines were then developed by crossing *cgm3cgm4* with, respectively, *cgm4cgm5*, *cgm4cgm19* and *cgm4cgm21*. Homozygous triple mutant plants were selected from the T3 generation by genotyping. Quadruple mutants were also developed, by crossing *cgm3cgm4cgm19* with *cgm3cgm4cgm219* and

6.8 Multiple knock-out lines of other GDSL candidates with *cgm3cgm4*

cgm3cgm4cgm19 with *cgm5*. The quadruple mutant *cgm3cgm4cgm19cgm21* (Fig.6.1) was assessed for homozygosity by genotyping from the T4 generation. The quadruple mutant *cgm3cgm4cgm5cgm19* is currently being genotyped for homozygosity for T-DNA insertions in all candidate genes. These multiple knock-out plants can be further utilized in physiological, biochemical, analytical and biophysical investigations aimed at a detailed understanding of the involvement of GDSL hydrolases in cell-wall biogenesis during dynamic processes such as stomatal development and seed germination.

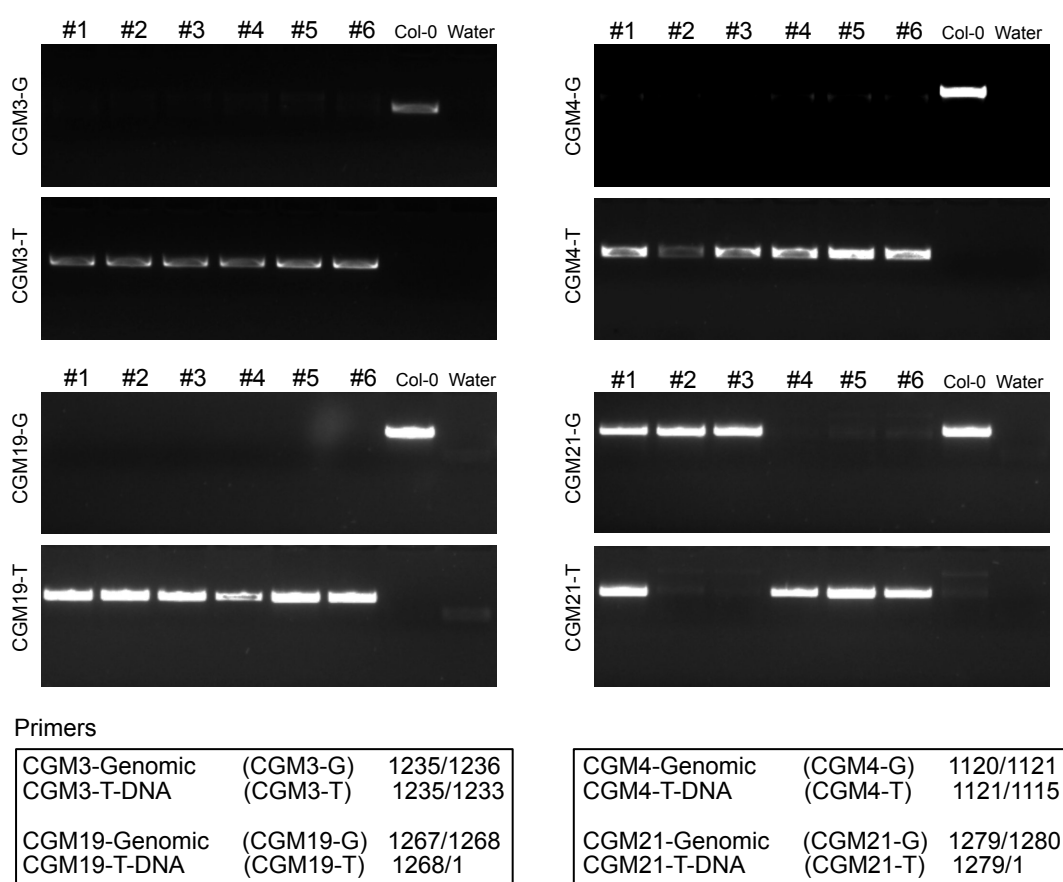


Figure 6.1: Genotyping of *cgm3cgm4cgm19cgm21*.

Appendix A

Appendices

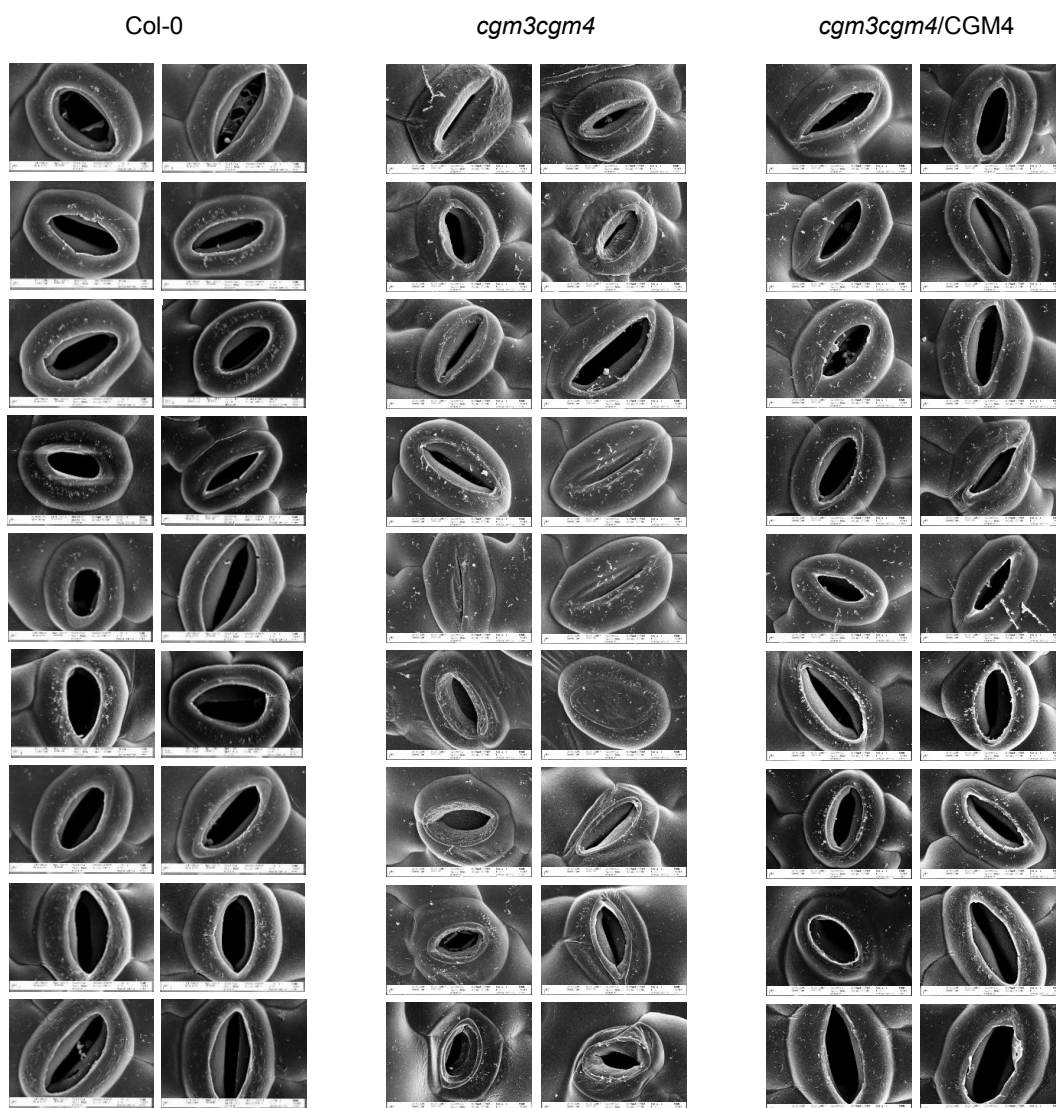


Figure A.1: Scanning electron microscopy of individual stomate of wild type Col-0, *cgm3cgm4* and *cgm3cgm4CGM4*.

Table A.1: Entry clones

S.No	Name	Selection marker	Vector
E042	pENTR/SD-CGM3prom	Kan	pENTR/SD-TOPO
E043	pENTR/SD-CGM4prom	Kan	pENTR/D-TOPO
E050	pDONR207-CGM3(FG)	Gen	pDONR207
E051	pDONR207-CGM4(FG)	Gen	pDONR207
E058	pDONR207-CGM3 ^{dSP} (FG)	Gent	pDONR207
E059	pDONR207-CGM4 ^{dSP} (FG)	Gent	pDONR207
E189	pDONR207-CGM3-st (CDS)	Gent	pDONR207
E190	pDONR207-CGM3 ^{dSP} (CDS)	Gent	pDONR207
E191	pDONR207-CGM3 ^{S36A} (CDS)	Gent	pDONR207
E192	pDONR207-CGM4-st (CDS)	Gent	pDONR207
E193	pDONR207-CGM4 ^{dSP} (CDS)	Gent	pDONR207
E194	pDONR207-CGM4 ^{S35A} (CDS)	Gent	pDONR207
E343	pDONR207-pAt1g33811	Gen	pDONR207
E344	pDONR207-pAt2g04570	Gen	pDONR207
E345	pDONR207-pAt3g04290	Gen	pDONR207
E346	pDONR207-pAt3g16370	Gen	pDONR207
E347	pDONR207-pAt4g28780	Gen	pDONR207
E348	pDONR207-pAt5g08460	Gen	pDONR207
E349	pDONR207-pAt5g45950	Gen	pDONR207
E350	pDONR207-pAt5g18430	Gen	pDONR207
E357	pDONR207-35Sprom	Gen	pDONR207
E429	pDONR221-L3L2-CGM4	Kan	pDONR221-P3P2
E430	pDONR221-L3L2-CGM4(FG)dSP	Kan	pDONR221-P3P2
E455	pDONR207- pAt1G33811(4kb)	Gen	pDONR207
E456	pDONR207- pAt1G33811(6kb)	Gen	pDONR207
E671	pDONR221-P1P4-pSPCH	Kan	pDONR221-P1P4
E672	pDONR221-P3P2-pCGM4	Kan	pDONR221-P3P2
E673	pDONR221-P1P4-pICE1	Kan	pDONR221-P1P4

Table A.2: Destination clones

S.No	Name	Selection marker (<i>E.coli</i> , Plant)
D0340	pUB-Dest-CGM3-st (CDS)	Spec, Cm, BASTA
D0341	pUB-Dest-CGM3 ^{dSP} (CDS)	Spec, Cm, BASTA
D0342	pUB-Dest-CGM3 ^{S36A} (CDS)	Spec, Cm, BASTA
D0343	pUB-Dest-CGM4-st (CDS)	Spec, Cm, BASTA
D0344	pUB-Dest-CGM4 ^{dSP} (CDS)	Spec, Cm, BASTA
D0345	pUB-Dest-CGM4 ^{S35A} (CDS)	Spec, Cm, BASTA
D0383	pUBQ10C-GFP:CGM3-woST	Spec, Cm, Basta
D0384	pUBQ10C-GFP:CGM4-woST	Spec, Cm, Basta
D0385	pUBQ10C-GFP:CGM3 ^{S36A} -woST	Spec, Cm, Basta
D0386	pUBQ10C-GFP:CGM4 ^{S35A} -woST	Spec, Cm, Basta
D0387	pUBQ10C-GFP:CGM3 ^{dSP} -woST	Spec, Cm, Basta
D0388	pUBQ10C-GFP:CGM4 ^{dSP} -woST	Spec, Cm, Basta
D0564	pMDC123-CGM3 ^{dSP}	Kan, Cm, Basta
D0565	pMDC123-CGM4 ^{dSP}	Kan, Cm, Basta
D0792	pAt1G33811-NLS-eGFP-pBBB	Spec, Basta
D0793	pAt2G04570-NLS-eGFP-pBBB	Spec, Basta
D0794	pAt3G04290-NLS-eGFP-pBBB	Spec, Basta
D0795	pAt3G16370-NLS-eGFP-pBBB	Spec, Basta
D0796	pAt4G28780-NLS-eGFP-pBBB	Spec, Basta
D0797	pAt5G08460-NLS-eGFP-pBBB	Spec, Basta
D0798	pAt5G18430-NLS-eGFP-pBBB	Spec, Basta
D0799	CGM3Prom-NLS-eGFP-pBBB	Spec, Basta
D0800	CGM4Prom-NLS-eGFP-pBBB	Spec, Basta
D0982	pAt1G33811(4Kb)-NLS-eGFP-pBBB	Spec, Basta
D1180	pBBB-35S-CGM4-3xHA	Spec, Basta
D1296	PromCGM3-NLS-eGFP-PBBK	Spec, Kan
D1297	PromCGM3-NLS-eGFP-PBBH	Spec, Hyg
D1298	PromCGM4-NLS-eGFP-PBBK	Spec, Kan
D1299	PromCGM4-NLS-eGFP-PBBH	Spec, Hyg
D1573	pGC1-CGM4-GFP	Spec, Basta
D1574	pGC1(Tr)-CGM4-GFP	Spec, Basta
D1587	pCGM2-CGM4-GFP	Spec, Basta
D1695	p35S-CGM4-mScarlet-3xHA	Spec, Basta
D1696	p35S-CGM4 ^{dSP} -mScarlet-3xHA	Spec, Basta
D1697	pCGM4-cycD-nls-mVenus	Spec, Basta
D1698	pICE1-cycD-nls-mVenus	Spec, Basta

Table A.3: Chemicals

Chemicals	Company
2-(N-morpholino)ethanesulfonic acid (MES)	Duchefa Biochemie
2',7'- Dichlorofluorescin diacetate (DCFDA)	Sigma Aldrich
Abscisic acid (ABA)	Duchefa Biochemie
Acetone	Carl Roth
Acetosyringon	Sigma Aldrich
Agar	Serva
Agarose	Genaxxon
BP Clonase	Thermo Fisher
Calcium chloride (CaCl ₂)	Carl Roth
cDNA synthesis kit	NEB Biolab
Chloroform	Carl Roth
CO ₂ cartridges (12gm)	Liss
Cooloidal graphite	Agar Scientific
Dimethylsulfoxide (DMSO)	Carl Roth
Diphenyleneiodonium chloride (DPI)	Sigma Aldrich
Drierite	Thermo Fisher
Ethanol	Carl Roth
Ethidiumbromide	Carl Roth
Ethylendiamintetraacetate (EDTA)	Carl Roth
Fusicoccin	Sigma Aldrich
Gibberellic acid (GA ₃)	Duchefa Biochemie
Glacial acetic acid	Carl Roth
Glass beads	Carl Roth
Glucose	Carl Roth
Hydrochloric acid (HCl)	Carl Roth
Hydrogen peroxide (H ₂ O ₂)	Sigma Aldrich
Isopropanol	Carl Roth
KOD hotstart	Novagen
LR Clonase	Thermo Fisher
Luria-Bertani media (LB)	Carl Roth
Magnesium chloride (MgCl ₂)	Carl Roth
Mannitol	Duchefa Biochemie
Methanol	Carl Roth
Murashige Skoog media (MS)	Duchefa Biochemie
PCR gel purification kit	Invitrogen
Pectin Antibiotics	Plant probes
Pectin identification kit	Megazyme
Plant agar	Duchefa Biochemie

Chemicals	Company
Plasmid isolation kit	Invitrogen
Potassium acetate	Carl Roth
Potassium chloride (KCl)	Carl Roth
Propidium Iodide	Sigma Aldrich
Real-time PCR kit (qRT-PCR)	NEB Biolab
Restriction enzymes	NEB Biolab/Therm Fisher
RNA extraction kit	Roboklon
SCRI Renaissance SR2200	Renaissance Chemicals
Silwet	Sigma Aldrich
Sodium Chloride	Carl Roth
Sodium dodecyl sulphate (SDS)	Carl Roth
Sodium hydroxide (NaOH)	Carl Roth
Sodium hypochloride (Bleach solution)	Carl Roth
Sucrose	Carl Roth
Taq polymerase	Ampliqon
Tissue Tek OCT	Sakura Europe
Tris-Cl	Carl Roth

Table A.4: Primer sequences

S.No	Name	Sequence
1	CG-LBb1.3-SALK	ATTTTGCCGATTTTCGGAAC
3	CG-LB-SAIL	GCCTTTTCAGAAATGGATAAATAGCCTTGCTTCC
1388	RK-CGM4dSP-S-attB3	ggggacaactttgtataataaagttagtataaaacaagggttctttctt
1389	RK-CGM4dSP-A-attB2wo	ggggaccactttgtacaagaaagctgggtgGAGATCCAAATGAATTTAGT
1390	RK-CGM4-S-attB3	ggggacaactttgtataataaagttagtataaaacaagggttctttctt
1391	RK-CGM4-A-attB2wo	ggggaccactttgtacaagaaagctgggtgGAGCCGAGCAAGCTG
1393	RK-Geno-GK-492D11-LP	ACTCGGGAATGGGAAGTAACG
1394	RK-Geno-GK-492D11-RP	CAACAACCTTTGTCCACAACCTC
1395	RK-Geno-GK-552A03-LP	GCATGGGAAGACAAGTGGAGAACT
1396	RK-CGM4cds-A-attB2wo	ggggaccactttgtacaagaaagctgggtgGATTTTGTATGGAACGCAA
1396	RK-Geno-GK-552A03-RP	GCCTCGACACATTCACCTGGCAG
1397	RK-Geno-SALK-002060-LP	ATCATTCCCTTGGACTACCAG
1398	RK-Geno-SALK-002060-RP	TCCACCGACCGTGATTAATAC
1399	RK-Geno-SALK-012570-LP	GCCCCATCATTTTTTTGTACG
1400	RK-Geno-SALK-012570-RP	GATTTCTCAATGAAAACCAGTG
1401	RK-Geno-SALK-082848-LP	CGTCATCTAGTCCCATTCTCTG
1402	RK-Geno-SALK-082848-RP	TAGCTTCTGGTCCGATCAATG
1403	RK-Geno-SALK-091361-LP	CTTATGGCCGTGATTTTCGCTA
1404	RK-Geno-SALK-091361-RP	TTGCAGCGGGAAGACATCCTG
1405	RK-Geno-SALK-094557-LP	CCACTGATTGCGATTGTAGTC
1406	RK-Geno-SALK-094557-RP	GAGAGCATTGGCCATGATG
1407	RK-Geno-SALK-116756-LP	CGACGTACCTGATCTCGCCA
1408	RK-Geno-SALK-116756-RP	ACCGTATGGAATCGATTTTCC
1409	RK-Geno-SALK-129661-LP	AGCAAAACCCTGATGATCACAAC
1410	RK-Geno-SALK-129661-RP	TGGTAATGTAGGCTCAGATCC
1411	RK-Geno-SALK-141771-LP	ATTTGCTTCTTGTACAGACCG

S.No	Name	Sequence
1412	RK-Geno-SALK-141771-RP	GCCGTAAGGGAGATAGTTGGA
1413	RK-Geno-SALK-150917-LP	TGCCCTATTTTTCAAACGATG
1414	RK-Geno-SALK-150917-RP	CTGCAGAAGCGAAATTAGCAC
1468	RK-GWS-PrAt1g33811(6kb)-2	ggggacaagttgtacaaaaaagcaggctGTAGAGGATTCACGCAAACG
1475	RK-Oec-mChe	AGCTCTAGAGGAGGAGGATCCATGGTGTAGCAAGGGCG
1476	RK-Oed-mChe-NdeI	AAAAC TAGTTTACTTGTACAGCTCGTCCATGC
1477	RK-A-XbaI-3HA	AGCTtctagaGCACTGAGCAGCGTAATCTG
1477	RK-OePa-NdeI-CGM4	AAACATATGGTTCCTCTGAAGACAAC
1478	RK-OePa-SpeI-CGM3	TCCTAGAATGAGAGGAACATGTAATGCA
1479	RK-OePb-Pr-CGM3	GTAACATGGCATCTTTTTCTAGGAGCAAGA
1480	RK-OePb-Pr-CGM4	GTAACATGGCATCTCTACCCTTATCCG
1481	RK-OePc-ATG-CGM3	AAAAAGATGCCATGTTACTTCATATTTGGT
1482	RK-OePc-ATG-CGM4	GTAGAGATGCCATGTTACTTCATATTCGGT
1483	RK-OePd-MfeI-CGM3	AACAGAGGATATAGAAGTGTGTATACGAACC
1484	RK-OePd-MfeI-CGM4	ACTGAAGTCTAAATGATATCTCATGACATCA
1485	RK-PC(II)-seq1	TCCGCTTTTACATCTGCGAG
1486	RK-PC(III)-seq1	CACTAGTTACGAATGCACAGA
1487	RK-PC(III)-seq2	ATCAAGACAAATGAAAAGTC
1488	RK-S-BspHI-PsiI-FR	GCtcatgattataaGGCCCTTCAAGTGTATGTAG
1489	RK-A-FspI-FR	ATtgcgcaCAATCTTAAGAACTTTATTGCC
1490	RK-LTL1-RT1	CGCATCTCACCGGAGAAAATCT
1491	RK-LTL1-RT2	GTAACGCGTATTGGCGAGAACG
1492	RK-LTL1-RT3	ATGAATATCAATTGTTCTCCATTA
1493	RK-LTL1-RT4	TCAGTTATTGAGGATGATCTTATG
1494	RK-A-XbaI-3HA	AGCTtctagaCATAATCTGGAACATCG
1495	RK-CGM1prom-seq-primer	CCGCGGCCGCCTTGTTTAAAC
1495	RK-S-SpeI-3HA	GCactagtTACCCTTATGATGTTCCCT
1535	RK-GWA-attB2-HA	ggggaccactttgtacaagaaagctgggttGCACTGAGCAGCGTAATCTG

S.No	Name	Sequence
1536	RK-GWA-CGM1prom-attB2wo	ggggaccactttgtacaagaaagctgggtgCAACAACACAAGCACTACACACCA
1541	RK-GWS-35Sp	ggggacaagtttgtaaaaaagcaggctGACTAGAGCCAAGCTGATCT
1544	RK-GWS-CGM1prom-attB3	ggggacaactttgtataataaagtgaCTGATGTTATGTGTGTACCCAAAG
1564	RK-V428-Seq1	CAAGGACGACGGCAACTACAAG
1565	RK-V429-Seq1	GCCGTTTGCCTCGTGGCGTAACT
1639	RK-At5g18430-RT1	CAACTCGATTACTTCCAACAATACC
1640	RK-At5g18430-RT2	TCATAGGGCAAGAGCAGAG
1641	RK-At5g18430-RT3	ATGACGATATCAACGGTTATAGCA
1715	RK-S-CGM3-RT	ATGGCGAGAATGAGTTTGTATGA
1716	RK-A-CGM3-RT	TTAGAGAGATGCTAGCTGCTGA
1717	RK-S-CGM4-RT	ATGGCTAGAGTTTGTGTAATGATGA
1718	RK-A-CGM4-RT	CTAGAGCCGAGCAAGCTG
1745	RK_CGM3dSP_Seq_Fwd	GAGCTTGGCCGTTAGATTTG
1746	RK_CGM3dSP_Seq_Rev	GCTATTCGACCTCCCTGAGG
1747	RK_CGM4dSP_Seq_Fwd	CCCAACTGTCTCATCCCTTG
1748	RK_CGM4dSP_Seq_Rev	TGATTAGCTACTTGCCCTGC
1771	RK-CGM4-S-qRT	AACATTATCACCGCGTGACA
1772	RK-CGM4-A-qRT	AGCTATGTTTCATAGCCATAGCTAT
1795	RK-pCGM3-NLS-seq	GACAGAAGTAATAACTCTCC
1796	RK-pCGM4-NLS-seq	CTCCACATAATTATACAGTTA
1845	CG-GWS-PrAt1g33811	ggggacaagtttgtaaaaaagcaggctAACTGATAATTGGTCATAAGGTCAT
1846	CG-GWS-PrAt2g04570	ggggacaagtttgtaaaaaagcaggctAACTCTGAAAGAGTGAAAGTGACGT
1847	CG-GWA-PrAt1g33811	ggggaccactttgtacaagaaagctgggtgCGCCATTGTTAGCCAATCC
1847	CG-GWS-PrAt3g04290	ggggacaagtttgtaaaaaagcaggctATTCTAACATGCCATGGCATGT
1848	CG-GWA-PrAt2g04570	ggggaccactttgtacaagaaagctgggtgTCCCATAGTGTGTTTGTGTTTGTGG
1848	CG-GWS-PrAt3g16370	ggggacaagtttgtaaaaaagcaggctTAAGAGAGAAAGAGAGAGACAGAGAT
1849	CG-GWA-PrAt3g04290	ggggaccactttgtacaagaaagctgggtgATTCATTGTTATGGACAGAGAATGG
1849	CG-GWS-PrAt4g28780	ggggacaagtttgtaaaaaagcaggctGACTGAAAAGATAGACAACCACTTA

S.No	Name	Sequence
1850	CG-GWA-PrAt3g16370	ggggaccactttgtacaagaaagctgggtgATCCATGTTTTTGCTTTGGTATG
1850	CG-GWS-PrAt5g08460	ggggacaagtttgtacaaaaaagcaggctATCTTTAGGCCCAACCTCAGT
1851	CG-GWA-PrAt4g28780	ggggaccactttgtacaagaaagctgggtgGGACATGATCTAGAAAGCGAAAC
1851	CG-GWS-PrAt5g18430	ggggacaagtttgtacaaaaaagcaggctTATGAAGGATTTTGCTCAGCTTAG
1852	CG-GWA-PrAt5g08460	ggggaccactttgtacaagaaagctgggtgATGCATGGTTCGCTTGAGATATATA
1852	CG-GWS-PrAt5g45950	ggggacaagtttgtacaaaaaagcaggctTTAAGTGAACCTCGAACCCATAATT
1853	CG-GWA-PrAt5g18430	ggggaccactttgtacaagaaagctgggtgCGTCATAAAAGCGTTTTGTTTAAAT
1854	CG-GWA-PrAt5g45950	ggggaccactttgtacaagaaagctgggtgCAACATGTTTAAATTAATAGAGAGAATGTG
1881	RK-GFP-rev-seq-primer	CGAGAGATCCACCGCCGGCC
1882	RK-GWA-35Sp	ggggaccactttgtacaagaaagctgggtTCGACTAGAATAGTAAATTGTAATG
1882	RK-MGD1-S-qPCR	CAGGATGAGGAAATGCCGGA
1883	RK-GWA-attB2-EPF1-wo	ggggaccactttgtacaagaaagctgggttAGGGACAGGGTAGGACTTATTG
1883	RK-MGD1-A-qPCR	AACGCCAAACCAAACAGCA
1884	RK-CGM3-S-qPCR	TACAAACCCTGCTCGCTACG
1884	RK-GWA-attB2-EPF2-wo	ggggaccactttgtacaagaaagctgggttAGCTCTAGATGGCACGTGATAG
1885	RK-CGM3-A-qPCR	GACATGGTGCTTGACCTGGA
1886	RK-CGM4-S-qPCR	TTGTCTTCCGGGTCAAGCTC
1887	RK-CGM4-A-qPCR	AACTAGAGCCGAGCAAGCTG
1898	RK-CGM3-S-Seq	AACATTAGCTCAGCTTTTGG
1899	RK-CGM3-A-Seq	GAAGATGCCATAAGCGTTG
1943	RK-CGM4-5'UTR-S-qPCR	CTGTCTAAAGCTCAAAACTTGT
1944	RK-CGM4-5'UTR-A-qPCR	TACTGGAAGTCGATACCGTA
1945	RK-CGM3-5'UTR-S-qPCR	cgttaaaaaactttataaaataacagt
1946	RK-CGM3-5'UTR-A-qPCR	GTAAGGAAAGTAATTAGCTCTAGCT
1947	RK-LTL1-5'UTR-S-qPCR	ACACACACTCTCCATATGCTCT
1948	RK-LTL1-5'UTR-A-qPCR	GCATGCCTATAGCCTCACTGAT
1951	RK-CGM4-S-qPCR	CTGGTCGACAATTGGGAGCTA
1952	RK-CGM4-A-qPCR	TTGCTCGGTGTAGCGGTTTA

S.No	Name	Sequence
1969	RK-S-SALK-qPCR	CTGTAGCGCGTTTTTCATCGG
1970	RK-A-SALK-qPCR	TAGATCGGGCCTCCTGTCAA
1971	RK-S-GK-qPCR	AATGGTCTTGCCTTGGCGTA
1972	RK-A-GK-qPCR	TTGAATCAGAACCCGAGGGC
1985	RK-PP2CA- qPCR-F	GAAGACGAGACATGGAAGACG
1986	RK-PP2CA- qPCR-R	CTTAACCATCGTCTCTGTCCAC
1987	RK-NCED3-qPCR-F	GAGTGTCTGTCTGAAATCCG
1988	RK-NCED3-qPCR-R	CGAATCCTGAGACTTTAGGCC
1989	RK-ABA3-qPCR-F	AGTGGATATTGAAGAGGCAGC
1989	RK-nPCR-A-EPF2	cgccgccagccaaaactgata
1990	RK-ABA3-qPCR-R	CACCAGATCTAGATTAAACCTCAGG
1990	RK-nPCR-A-PrAt1g33811	GCAGAGAGGAGCAAATTCAC
1991	RK-nPCR-A-PrAt2G04570	TCGCCAAACACGATGATCGC
1991	RK-S-mScarlet-I-XhoI	TCCctcagagATGGTGTCTAAGGGAGAAG
1992	RK-nPCR-A-PrAt3G04290	GTCGGGTAGTCGATACCATA
1992	RK-S-mScarlet-I-SpeI	TCCactagtATGGTGTCTAAGGGAGAAGCAGT
1993	RK-A-mScarlet-I-SpeI	GCCactagtTTTGTAGAGTTCATCCATACCAC
1993	RK-nPCR-A-PrAt3G16370	GTTGCCGACATCAACTACAG
1994	RK-nPCR-A-PrAt4G28780	CAGGGAGGTTCAAGCCG
1994	RK-S-CGM4gen-PvuII	TCTcagctgGTAAAACAAGGTTCTTTCTTCCC
1995	RK-A-CGM4gen-SpeI	AAAactagtGAGCCGAGCAAGCTGCTG
1995	RK-nPCR-A-PrAt5G08460	TCGGATGAGTCTTCTCCAC
1996	RK-nPCR-A-PrAt5G18430	TTGTTGTTGCCACTGTGCGAC
1997	RK-nPCR-A-PrAt5G45950	GCTGCAAAGCTACTGCTAC
1997	RK-S-CGM4gen-SacI	TCTgagctcGTAAAACAAGGTTCTTTCTTCCC
1998	RK-A-CGM4gen-BglII	AAAagatctGAGCCGAGCAAGCTGCTG
1998	RK-nPCR-A-PrAt5G45950-ii	GTAACCCATGGCCTCCGCTGTA
1999	RK-mScarlet(C-term)-seq-For	GTCTGCAGGTCGACCATAGTGAC

S.No	Name	Sequence
2000	RK-mScarlet(C-term)-seq-Rev	GCTCAACACATGAGCGAAACCC
2000	RK-nPCR-S-PrAt1g33811	GTGGACATTGAAGGACTTGC
2001	RK-mScarlet(N-term)-seq-For	TCCGATTTGTTCAAATAATTTG
2001	RK-nPCR-S-PrAt2G04570	CGCCGGAGACGATGAAAAC
2002	RK-mScarlet(N-term)-seq-Rev	GCCTAATGCGGCCGCCATAGTG
2002	RK-nPCR-S-PrAt3G04290	CAAGTTTGGCTGCTTCCTCA
2003	RK-nPCR-S-PrAt3G16370	CCAGGCGAGCCAATAATCAA
2003	RK-S-fama_1-geno	GTCTTCTTCTACTATCTTGCATGTCTTG
2004	RK-A-fama_1-geno	TTTTCGTAACATTCTTGTCTCCCTATC
2004	RK-nPCR-S-PrAt4G28780	GGTCAGGAAAGCTCATTGTG
2005	RK-nPCR-S-PrAt5G08460	GGTTCATCATGACACTACC
2005	RK-S-spch_3-geno	ATCTAAAACATAAATGAGACACGAAAAC
2006	RK-A-spch_3-geno	AGAACTTGTTGTAACCTCGTTATGTACTC
2006	RK-nPCR-S-PrAt5G18430	GCAGATGGCAAAGCAAACAC
2007	RK-nPCR-S-PrAt5G45950	GATTGGTTTGAAACCGAACCAA
2008	RK-nPCR-S-PrAt5G45950-ii	CGCGTAGCTCGTTTTTGTCTTCTC
2011	RK-A-mScarlet-I-FspI	GCctgcgcaTTTGTAGAGTTCATCCATACCAC
2071	RK-RT-F-FAMA	GCTCGAGCAACTCCTACAATG
2072	RK-RT-R-FAMA	GGAAGTTGCTATGTCTTCTGC
2073	RK-RT-F-SPCH	AAAATCGGCTTTGGCTGATGTGGAAG
2074	RK-RT-R-SPCH	AGAAAGTGAGTACGTACTGC
2083	RK-D1482-seq1	ACGCAATTAATGTGAGTTAGCTC
2084	RK-D1482-seq2	TTTATGAGTCACTGACTCCAAAC
2085	RK-D1482-seq3	TCACCGCGTGACATTTAATGCTT
2086	RK-D1482-seq4	GCTAATTACCTAAGTAAATGCAT
2087	RK-D1482-seq5	ATATCCAGCAGCTTGCTCGGCTC
2114	RK-AAO3-1F	ttgcgattgaacactccttc
2115	RK-AAO3-1R	tcgtgttccaagaccttcag

S.No	Name	Sequence
2116	RK-ABA1-1F	GGCATTGTTGGTCTAAGGTGAGAA
2117	RK-ABA1-1R	CAGACTCGATATCCGCTGGTA
2118	RK-ABF1-qF	TGCAGAAGAAACAGGCTGAA
2119	RK-ABF1-qR	GACCGGTAAGGGTTCTTCTCA
2120	RK-ABF3-qF	CGTTCTCAACCTGCAACACA
2121	RK-ABF3-qR	TCATAGGATGGTTATGAATTCCAAG
2122	RK-PYR1-qF	GCGAACACATCAACGGAAAG
2123	RK-PYR1-qR	CCAGATCCGATTCTCTTTCTCG
2124	RK-PYL1-qF	ACAGCCAGAGAATCTCAACAC
2125	RK-PYL1-qR	TTGATTGGGAGAGTTGGGTG
2194	RK-S-SacI-pGC1	GGCAGAGCTCgagtaaagattcagtaaccg
2195	RK-S-SacI-pGC1(Tr)	TATTGAGCTCatggttgcaacagagaggatga
2196	RK-A-pGC1-NcoI	CATGCCATGGatttcttgagtagtgatttgaag
2225	RK-D1573-seq1	CACACAGGAAACAGCTATGACCA
2226	RK-D1573-seq2	tatacaatcaatctttaggaatt
2227	RK-D1573-seq3	actgtttgcatatcaaactcca
2228	RK-D1573-seq4	TGTCGACCAGTTTCTTCTCGG
2230	RK-S-SacI-pCGM2	TATTGAGCTAACACGGACCCGATCC
2231	RK-A-pCGM2-NcoI	CATGCCATGGCCACACAGAAACTA
2243	RK-D1587 seq2	TAAGTGATGTATGCAAAATTACC
2244	RK-D1587 seq3	GTCTATGTGTAACAAGACTTAAG
2245	RK-D1587 seq4	CGATAGGATCGATCGTGTTTGAC
2246	RK-E343-seq1	CGATCTGCTTCTCCATTAGCGT
2247	RK-E344-seq1	GATACTTGTTTAGGAGACAGTG
2248	RK-EcoICRI-NLS-PsiI-For	ccGAGCTCATGATTGCTGCAGCGGCCGA
2249	RK-EcoICRI-NLS-PsiI-Rev	ggcgTTATAACTACTCTTCTTCTTGATCAGCTTCTG
2253	RK-S-CycD-GB	tctgcagctagatgtaaacactagtATGGCGACGAGAGCAAAC
2254	RK-A-CycD-GB	atcatactagATCAACATACTCCACCGC

S.No	Name	Sequence
2254	RK-SDM-A-V292repair	TGGCCGCTTATAATCACTTGTACAGCTCGTCCATG
2255	RK-SDM-S-V292repair	ACGAGCTGTACAAGTGATTATAAGCGGCCATGC
2255	RK-S-NLS-GB	gtatgtgatCTAGTATGATTGCTGCAG
2256	RK-A-NLS-GB	tgctcaccatACTCTTCTTCTTGATCAGC
2256	RK-seq-GFP-rev	CTTGTACAGCTCGTCCATGCCG
2256	RK-SpeI-NLSwo-XbaI-For	ccACTAGTATGATTGCTGCAGCGGCCGA
2257	RK-Seq-NLS-For	CACAGCCAGTCTGCAGG
2257	RK-S-mVenus-GB	gaagaagagtATGGTGAGCAAGGGCGAG
2257	RK-SpeI-NLSwo-XbaI-Rev	ggcgTCTAGACTCTTCTTCTTGATCAGCTTCTGTG
2258	RK-A-mVenus-GB	gactctagcatggccgctataaTTATTTGTACAGCTCGTCCATGC
2258	RK-S-PmlI-Get3b(Pr)	AAGAGCACGTGGCCAAGCCCTACT
2259	RK-S-mTrq-GB	gaagaagagtATGGTGAGCAAGGGCGAG
2260	RK-A-mTrq-GB	gactctagcatggccgctataaCTTGTACAGCTCGTCCATGC
2261	RK-pSPCH-attB1	ggggacaagttgtacaaaaaagcaggctCACCAGATCATCACTGCGATAAGG
2262	RK-pSPCH-attB4	ggggacaactttgtatagaaaagttgggtgGCGGCCGCGTGATTAGAGATATATCCT
2263	RK-pICE1-attB1	ggggacaagttgtacaaaaaagcaggctACCACCGTCAATAACATCG
2264	RK-pICE1-attB4	ggggacaactttgtatagaaaagttgggtgGCCAAAGTTGACACC
2265	RK-pCGM4-attB3	ggggacaactttgtataataaagttGTAAAACAAGGTTCTTTCTT
2266	RK-pCGM4-attB2	ggggaccactttgtacaagaagctgggtgAGCCATCATCATTACACAAA
2267	RK-V486-Seq1	gagaaaataccgcatcagg
2268	RK-V486-Seq2	AGGAATTAGAAATTTTATTGA
2270	RK-V488-GB1	gcacgtgcggagctccgtacgtACAAGTTTGTACAAAAAAGCTG
2271	RK-V488-GB2	agcatggccgctataaCTTGTACAGCTCGTCCATG
2272	RK-V488-GB3	gctgtacaagttataagcggccatgctattataagcggccGCAACTTTGTATAATAAAGTTGAAC
2273	RK-V488-GB4	attctccgctcatgatctacTTATTTGTACAGCTCGTC
2284	RK-V488-seq1	tacacagccagtctcaggtc
2285	RK-V488-seq2	GCCGCTTATAATAGCATGG
2286	RK-V488-seq3	gctgatgcagacggggctt

S.No	Name	Sequence
2287	RK-V488-seq4	TTCAACGTTGCGGTTCTGTCAGT
2288	RK-D1482-seq-rev	TTGCGGACTCTAGCATGGCC
2309	RK-S-V487-SacI	tcaGAGCTCcagggtttccagt
2310	RK-A-V487-Ecl136II	TTctcgagCCAAGCTTAGGCCTTC
2310	RK-V392-Seq primer-for	GCATCAGAGCAGATTGTACTG
2311	RK-V392-Seq primer-rev	ACCATACTAGTGCCTAACCTA
2363	RK-pSPCH-attB3	ggggacaactttgtataataaagtgCACCAGATCATCACTGCGATAAGG
2364	RK-pSPCH-attB2	ggggaccactttgtacaagaaagctgggtgGCGGCCGCGTGATTAGAGATATATCCT
2365	RK-pICE1-attB3	ggggacaactttgtataataaagtgACCACCGTCAATAACATCG
2366	RK-pICE1-attB2	ggggaccactttgtacaagaaagctgggtgGCCAAAGTTGACACC
2367	RK-pSPCH-SacI	tcaGAGCTCCACCAGATCATCACTGCGATAAGG
2368	RK-pSPCH-SpeI	TTtgatcaGCGGCCGCGTGATTAGAGATATATCCT
2369	RK-pICE1-SacI	tcaGAGCTCACCACCGTCAATAACATCG
2370	RK-pICE1-SpeI	TTtgatcaGCCAAAGTTGACACC

Bibliography

- Adrian, J., Chang, J., Ballenger, C. E., Bargmann, B. O., Alassimone, J., Davies, K. A., Lau, O. S., Matos, J. L., Hachez, C., Lanctot, A., Vatén, A., Birnbaum, K. D., and Bergmann, D. C. (2015). Transcriptome dynamics of the stomatal lineage: Birth, amplification, and termination of a self-renewing population. *Developmental Cell*, **33**(1), 107–119.
- Akoh, C. C., Lee, G. C., Liaw, Y. C., Huang, T. H., and Shaw, J. F. (2004). GDSL family of serine esterases/lipases. *Progress in Lipid Research*, **43**(6), 534–552.
- Amsbury, S., Hunt, L., Elhaddad, N., Baillie, A., Lundgren, M., Verhertbruggen, Y., Scheller, H. V., Knox, J. P., Fleming, A. J., and Gray, J. E. (2016). Stomatal Function Requires Pectin De-methyl-esterification of the Guard Cell Wall. *Current Biology*, **26**(21), 2899–2906.
- An, X., Dong, Z., Tian, Y., Xie, K., Wu, S., Zhu, T., Zhang, D., Zhou, Y., Niu, C., Ma, B., Hou, Q., Bao, J., Zhang, S., Li, Z., Wang, Y., Yan, T., Sun, X., Zhang, Y., Li, J., and Wan, X. (2019). Zmms30 encoding a novel gdsl lipase is essential for male fertility and valuable for hybrid breeding in maize. *Molecular plant*, **12**(3), 343–359.
- Anderson, C. T. (2019). *Pectic Polysaccharides in Plants: Structure, Biosynthesis*,

- Functions, and Applications*, pages 487–514. Springer International Publishing, Cham.
- Avci, U., Pattathil, S., and Hahn, M. G. (2012). Immunological approaches to plant cell wall and biomass characterization: immunolocalization of glycan epitopes. In *Biomass Conversion*, pages 73–82. Springer.
- Aylor, D. E., Parlange, J.-Y., and Krikorian, A. D. (1973). Stomatal mechanics. *American Journal of Botany*, **60**(2), 163–171.
- Barlowe, C. K. and Miller, E. A. (2013). Secretory protein biogenesis and traffic in the early secretory pathway. *Genetics*, **193**(2), 383–410.
- Beisson, F., Gardies, A., Teissere, M., Ferte, N., and Noat, G. (1997). An esterase neosynthesized in post-germinated sunflower seeds is related to a new family of lipolytic enzymes. *Plant Physiology and Biochemistry (France)*, **35**(10), 761–765.
- Beljaars, A. C., Viterbo, P., Miller, M. J., and Betts, A. K. (1996). The anomalous rainfall over the united states during july 1993: Sensitivity to land surface parameterization and soil moisture anomalies. *Monthly Weather Review*, **124**(3), 362–383.
- Berry, J. A., Beerling, D. J., and Franks, P. J. (2010). Stomata: key players in the earth system, past and present. *Current opinion in plant biology*, **13**(3), 232–239.
- Bertolino, L. T., Caine, R. S., and Gray, J. E. (2019). Impact of stomatal density and morphology on water-use efficiency in a changing world. *Frontiers in plant science*, **10**, 225.
- Bethke, G., Thao, A., Xiong, G., Li, B., Soltis, N. E., Hatsugai, N., Hillmer, R. A., Katagiri, F., Kliebenstein, D. J., Pauly, M., and Glazebrook, J. (2016). Pectin biosynthesis

- is critical for cell wall integrity and immunity in *arabidopsis thaliana*. *The Plant Cell*, **28**(2), 537–556.
- Bhatia, R., Gallagher, J. A., Gomez, L. D., and Bosch, M. (2017). Genetic engineering of grass cell wall polysaccharides for biorefining. *Plant biotechnology journal*, **15**(9), 1071–1092.
- Binnig, G., Quate, C. F., and Gerber, C. (1986). Atomic force microscope. *Physical review letters*, **56**(9), 930.
- Blanc, G. and Wolfe, K. H. (2004). Functional divergence of duplicated genes formed by polyploidy during *arabidopsis* evolution. *The Plant Cell*, **16**(7), 1679–1691.
- Blatt, M. R. (1990). Potassium channel currents in intact stomatal guard cells: rapid enhancement by abscisic acid. *Planta*, **180**(3), 445–455.
- Blobel, G. and Dobberstein, B. (1975). Transfer of proteins across membranes. i. presence of proteolytically processed and unprocessed nascent immunoglobulin light chains on membrane-bound ribosomes of murine myeloma. *The Journal of cell biology*, **67**(3), 835–851.
- Brick, D. J., Brumlik, M. J., Buckley, J. T., Cao, J.-X., Davies, P. C., Misra, S., Tranbarger, T. J., and Upton, C. (1995). A new family of lipolytic plant enzymes with members in rice, *arabidopsis* and maize. *FEBS letters*, **377**(3), 475–480.
- Brzozowski, A., Derewenda, U., Derewenda, Z., Dodson, G., Lawson, D., Turkenburg, J., Bjorkling, F., Huge-Jensen, B., Patkar, S., and Thim, L. (1991). A model for interfacial activation in lipases from the structure of a fungal lipase-inhibitor complex. *Nature*, **351**(6326), 491.

- Burton, R. A., Gidley, M. J., and Fincher, G. B. (2010). Heterogeneity in the chemistry, structure and function of plant cell walls. *Nature Chemical Biology*, **6**(10), 724–732.
- Caffall, K. and Mohnen, D. (2009). The structure, function, and biosynthesis of plant cell wall pectic polysaccharides. *Carbohydrate research*, **344** **14**, 1879–900.
- Cai, Y., Zhuang, X., Gao, C., Wang, X., and Jiang, L. (2014). The arabidopsis endosomal sorting complex required for transport iii regulates internal vesicle formation of the prevacuolar compartment and is required for plant development. *Plant physiology*, **165**(3), 1328–1343.
- Cannon, S. B., Mitra, A., Baumgarten, A., Young, N. D., and May, G. (2004). The roles of segmental and tandem gene duplication in the evolution of large gene families in arabidopsis thaliana. *BMC plant biology*, **4**(1), 10.
- Cao, D., Cheng, H., Wu, W., Soo, H. M., and Peng, J. (2006). Gibberellin mobilizes distinct della-dependent transcriptomes to regulate seed germination and floral development in arabidopsis. *Plant physiology*, **142**(2), 509–525.
- Carrière, F., Withers-Martinez, C., van Tilbeurgh, H., Roussel, A., Cambillau, C., and Verger, R. (1998). Structural basis for the substrate selectivity of pancreatic lipases and some related proteins. *Biochimica et Biophysica Acta (BBA)-Reviews on Biomembranes*, **1376**(3), 417–432.
- Carter, R. (2015). *In viva analysis of plant mechanics using atomic force microscopy and modelling*. Ph.D. thesis, Department of animal and plant sciences, University of Sheffield.

- Carter, R., Woolfenden, H., Baillie, A., Amsbury, S., Carroll, S., Healicon, E., Sovatzoglou, S., Braybrook, S., Gray, J. E., Hobbs, J., Morris, R. J., and Fleming, A. J. (2017). Stomatal Opening Involves Polar, Not Radial, Stiffening Of Guard Cells. *Current Biology*, **27**(19), 2974–2983.e2.
- Cavalier, D. M., Lerouxel, O., Neumetzler, L., Yamauchi, K., Reinecke, A., Freshour, G., Zabolina, O. A., Hahn, M. G., Burgert, I., Pauly, M., Raikhel, N. V., and Keegstra, K. (2008). Disrupting two arabidopsis thaliana xylosyltransferase genes results in plants deficient in xyloglucan, a major primary cell wall component. *The Plant Cell*, **20**(6), 1519–1537.
- Chater, C. C., Caine, R. S., Fleming, A. J., and Gray, J. E. (2017). Origins and evolution of stomatal development. *Plant Physiology*, **174**(2), 624–638.
- Chen, F., Nonogaki, H., and Bradford, K. J. (2002). A gibberellin-regulated xyloglucan endotransglycosylase gene is expressed in the endosperm cap during tomato seed germination. *Journal of Experimental Botany*, **53**(367), 215–223.
- Chen, M., Du, X., Zhu, Y., Wang, Z., Hua, S., Li, Z., Guo, W., Zhang, G., Peng, J., and Jiang, L. (2012). Seed Fatty Acid Reducer acts downstream of gibberellin signalling pathway to lower seed fatty acid storage in Arabidopsis. *Plant, Cell and Environment*, **35**(12), 2155–2169.
- Chepyshko, H., Lai, C.-P., Huang, L.-M., Liu, J.-H., and Shaw, J.-F. (2012). Multifunctionality and diversity of GDSL esterase/lipase gene family in rice (*Oryza sativa* L. japonica) genome: new insights from bioinformatics analysis. *BMC Genomics*, **13**(1), 309.

- Chung, K. P. and Zeng, Y. (2017). An overview of protein secretion in plant cells. In *Plant Protein Secretion*, pages 19–32. Springer.
- Clauß, K., Baumert, A., Nimtz, M., Milkowski, C., and Strack, D. (2008). Role of a gdsI lipase-like protein as sinapine esterase in brassicaceae. *The Plant Journal*, **53**(5), 802–813.
- Cooke, J. R., De Baerdemaeker, J. G., Rand, R. H., and Mang, H. A. (1976). A finite element shell analysis of guard cell deformations. *Transactions of the ASAE*, **19**(6), 1107–1121.
- Coque, L., Neogi, P., Pislariu, C., Wilson, K. A., Catalano, C., Avadhani, M., Sherrier, D. J., and Dickstein, R. (2008). Transcription of *enod8* in medicago truncatula nodules directs *enod8* esterase to developing and mature symbiosomes. *Molecular plant-microbe interactions*, **21**(4), 404–410.
- Cosgrove, D. J. (2005). Growth of the plant cell wall. *Nature reviews molecular cell biology*, **6**(11), 850.
- Cosson, P. and Letourneur, F. (1994). Coatamer interaction with di-lysine endoplasmic reticulum retention motifs. *Science*, **263**(5153), 1629–1631.
- Cowan, I. and Troughton, J. (1971). The relative role of stomata in transpiration and assimilation. *Planta*, **97**(4), 325–336.
- Darwin, F. (1916). IX. on the relation between transpiration and stomatal aperture. *Philosophical Transactions of the Royal Society of London. Series B, Containing Papers of a Biological Character*, **207**(335-347), 413–437.

- Daszkowska-Golec, A. (2016). The role of abscisic acid in drought stress: how aba helps plants to cope with drought stress. In *Drought Stress Tolerance in Plants, Vol 2*, pages 123–151. Springer.
- Daszkowska-Golec, A. and Szarejko, I. (2013). Open or close the gate—stomata action under the control of phytohormones in drought stress conditions. *Frontiers in plant science*, **4**, 138.
- Davies, P. J. (1995). The plant hormone concept: concentration, sensitivity and transport. In *Plant hormones*, pages 13–38. Springer.
- de la Torre, F., Sampedro, J., Zarra, I., and Revilla, G. (2002). Atfxg1, an arabidopsis gene encoding α -l-fucosidase active against fucosylated xyloglucan oligosaccharides. *Plant Physiology*, **128**(1), 247–255.
- Desikan, R., Cheung, M.-K., Bright, J., Henson, D., Hancock, J. T., and Neill, S. J. (2004). ABA, hydrogen peroxide and nitric oxide signalling in stomatal guard cells. *Journal of experimental botany*, **55**(395), 205–212.
- Dickstein, R., Prusty, R., Peng, T., Ngo, W., and Smith, M. E. (1993). Enod8, a novel early nodule-specific gene, is expressed in empty alfalfa nodules. *Molecular plant-microbe interactions*, **6**(6), 715–721.
- Ding, L.-N., Li, M., Wang, W.-J., Cao, J., Wang, Z., Zhu, K.-M., Yang, Y.-H., Li, Y.-L., and Tan, X.-L. (2019). Advances in plant gDSL lipases: from sequences to functional mechanisms. *Acta Physiologiae Plantarum*, **41**(9), 151.
- Doblin, M. S., Pettolino, F., and Bacic, A. (2010). Plant cell walls: the skeleton of the plant world. *Functional Plant Biology*, **37**(5), 357–381.

- Dunn, J., Hunt, L., Afsharinafar, M., Al Meselmani, M., Mitchell, A., Howells, R., Wallington, E., Fleming, A. J., and Gray, J. E. (2019). Reduced stomatal density in bread wheat leads to increased water-use efficiency. *Journal of experimental botany*, **70**(18), 4737–4748.
- Elhaddad, N. S., Hunt, L., Sloan, J., and Gray, J. E. (2014). Light-induced stomatal opening is affected by the guard cell protein kinase *apk1b*. *PLoS One*, **9**(5).
- Esau, K. (1960). Anatomy of seed plants. *Soil Science*, **90**(2), 149.
- Feng, L., Raza, M. A., Li, Z., Chen, Y., Khalid, M. H. B., Du, J., Liu, W., Wu, X., Song, C., Yu, L., Zhang, Z., Yuan, S., W, Y., and F, Y. (2019). The influence of light intensity and leaf movement on photosynthesis characteristics and carbon balance of soybean. *Frontiers in plant science*, **9**, 1952.
- Fernando, V. D. and Schroeder, D. F. (2016). Role of *aba* in *arabidopsis* salt, drought, and desiccation tolerance. In *Abiotic and Biotic Stress in Plants-Recent Advances and Future Perspectives*, chapter 22, pages 507–524. IntechOpen.
- Finch-Savage, W. E. and Leubner-Metzger, G. (2006). Seed dormancy and the control of germination. *New phytologist*, **171**(3), 501–523.
- Fleet, C. M. and Sun, T.-p. (2005). A delicate balance: the role of gibberellin in plant morphogenesis. *Current opinion in plant biology*, **8**(1), 77–85.
- Fojan, P., Jonson, P. H., Petersen, M. T. N., and Petersen, S. B. (2000). What distinguishes an esterase from a lipase: A novel structural approach. *Biochimie*, **82**(11), 1033–1041.

- Fry, S. C., Aldington, S., Hetherington, P. R., and Aitken, J. (1993). Oligosaccharides as signals and substrates in the plant cell wall. *Plant Physiology*, **103**(1), 1.
- Ganko, E. W., Meyers, B. C., and Vision, T. J. (2007). Divergence in expression between duplicated genes in arabidopsis. *Molecular biology and evolution*, **24**(10), 2298–2309.
- Gao, C., Christine, K., Qu, S., San, M. W. Y., Li, K. Y., Lo, S. W., and Jiang, L. (2012). The golgi-localized arabidopsis endomembrane protein12 contains both endoplasmic reticulum export and golgi retention signals at its c terminus. *The Plant Cell*, **24**(5), 2086–2104.
- Gao, C., Cai, Y., Wang, Y., Kang, B.-H., Aniento, F., Robinson, D. G., and Jiang, L. (2014). Retention mechanisms for er and golgi membrane proteins. *Trends in plant science*, **19**(8), 508–515.
- Gao, M., Yin, X., Yang, W., Lam, S. M., Tong, X., Liu, J., Wang, X., Li, Q., Shui, G., and He, Z. (2017). Gdsl lipases modulate immunity through lipid homeostasis in rice. *PLoS pathogens*, **13**(11), e1006724.
- Gawkowska, D., Cybulska, J., and Zdunek, A. (2018). Structure-related gelling of pectins and linking with other natural compounds: A review. *Polymers*, **10**(7), 762.
- Graham, I. A. (2008). Seed storage oil mobilization. *Annu. Rev. Plant Biol.*, **59**, 115–142.
- Grefen, C. (2008). *Charakterisierung von vier GDSL-lipasen aus Arabidopsis thaliana*. Ph.D. thesis, Eberhard Karls Universität Tübingen.

- Grefen, C., Donald, N., Hashimoto, K., Kudla, J., Schumacher, K., and Blatt, M. R. (2010). A ubiquitin-10 promoter-based vector set for fluorescent protein tagging facilitates temporal stability and native protein distribution in transient and stable expression studies. *The Plant Journal*, **64**(2), 355–365.
- Groot, S. and Karssen, C. (1987). Gibberellins regulate seed germination in tomato by endosperm weakening: a study with gibberellin-deficient mutants. *Planta*, **171**(4), 525–531.
- Gudesblat, G. E., Torres, P. S., and Vojno, A. A. (2009). Stomata and pathogens: warfare at the gates. *Plant signaling & behavior*, **4**(12), 1114–1116.
- Günl, M., Neumetzler, L., Kraemer, F., de Souza, A., Schultink, A., Pena, M., York, W. S., and Pauly, M. (2011). Axy8 encodes an α -fucosidase, underscoring the importance of apoplastic metabolism on the fine structure of arabidopsis cell wall polysaccharides. *The Plant Cell*, **23**(11), 4025–4040.
- Hara, K., Kajita, R., Torii, K. U., Bergmann, D. C., and Kakimoto, T. (2007). The secretory peptide gene EPF1 enforces the stomatal one-cell-spacing rule. *Genes and Development*, **21**(14), 1720–1725.
- Hara, K., Yokoo, T., Kajita, R., Onishi, T., Yahata, S., Peterson, K. M., Torii, K. U., and Kakimoto, T. (2009). Epidermal cell density is autoregulated via a secretory peptide, EPIDERMAL PATTERNING FACTOR 2 in arabidopsis leaves. *Plant and Cell Physiology*, **50**(6), 1019–1031.
- Harholt, J., Suttangkakul, A., and Vibe Scheller, H. (2010). Biosynthesis of pectin. *Plant Physiology*, **153**(2), 384–395.

- Hetherington, A. M. and Woodward, F. I. (2003). The role of stomata in sensing and driving environmental change. *Nature*, **424**(6951), 901.
- Hocq, L., Pelloux, J., and Lefebvre, V. (2017). Connecting Homogalacturonan-Type Pectin Remodeling to Acid Growth. *Trends in Plant Science*, **22**(1), 20–29.
- Hong, J. K., Choi, H. W., Hwang, I. S., Kim, D. S., Kim, N. H., Choi, D. S., Kim, Y. J., and Hwang, B. K. (2008). Function of a novel gdsI-type pepper lipase gene, caglip1, in disease susceptibility and abiotic stress tolerance. *Planta*, **227**(3), 539–558.
- Hoth, S., Morgante, M., Sanchez, J.-P., Hanafey, M. K., Tingey, S. V., and Chua, N.-H. (2002). Genome-wide gene expression profiling in arabidopsis thaliana reveals new targets of abscisic acid and largely impaired gene regulation in the abi1-1 mutant. *Journal of cell science*, **115**(24), 4891–4900.
- Hu, G., Koh, J., Yoo, M.-J., Chen, S., and Wendel, J. F. (2015). Gene-expression novelty in allopolyploid cotton: a proteomic perspective. *Genetics*, **200**(1), 91–104.
- Huang, A.-X., She, X.-P., Zhao, J.-L., and Zhang, Y.-Y. (2014). Inhibition of aba-induced stomatal closure by fusicoccin is associated with cytosolic acidification-mediated hydrogen peroxide removal. *Botanical studies*, **55**(1), 33.
- Huang, L.-M., Lai, C.-P., Chen, L.-F. O., Chan, M.-T., and Shaw, J.-F. (2015). Arabidopsis sfar4 is a novel gdsI-type esterase involved in fatty acid degradation and glucose tolerance. *Botanical Studies*, **56**(1), 33.
- Huang, Y.-C., Wu, H.-C., Wang, Y.-D., Liu, C.-H., Lin, C.-C., Luo, D.-L., and Jinn, T.-L. (2017). Pectin methylesterase34 contributes to heat tolerance through its role in promoting stomatal movement. *Plant physiology*, **174**(2), 748–763.

- Hughes, J., Hepworth, C., Dutton, C., Dunn, J. A., Hunt, L., Stephens, J., Waugh, R., Cameron, D. D., and Gray, J. E. (2017). Reducing stomatal density in barley improves drought tolerance without impacting on yield. *Plant Physiology*, **174**(2), 776–787.
- Hunt, L. and Gray, J. E. (2009). The signaling peptide epf2 controls asymmetric cell divisions during stomatal development. *Current Biology*, **19**(10), 864–869.
- Hunt, L., Bailey, K. J., and Gray, J. E. (2010). The signalling peptide EPFL9 is a positive regulator of stomatal development. *New Phytologist*, **186**(3), 609–614.
- Hunt, L., Amsbury, S., Baillie, A., Movahedi, M., Mitchell, A., Afsharinifar, M., Swarup, K., Denyer, T., Hobbs, J. K., Swarup, R., Fleming, A. J., and Gray, J. E. (2017). Formation of the Stomatal Outer Cuticular Ledge Requires a Guard Cell Wall Proline-Rich Protein. *Plant Physiology*, **174**(2), 689–699.
- Jezek, M. and Blatt, M. R. (2017). The Membrane Transport System of the Guard Cell and Its Integration for Stomatal Dynamics. *Plant Physiology*, **174**(2), 487–519.
- Jones, L., Milne, J. L., Ashford, D., and McQueen-Mason, S. J. (2003). Cell wall arabinan is essential for guard cell function. *Proceedings of the National Academy of Sciences*, **100**(20), 11783–11788.
- Kanaoka, M. M., Pillitteri, L. J., Fujii, H., Yoshida, Y., Bogenschutz, N. L., Takabayashi, J., Zhu, J.-K., and Torii, K. U. (2008). SCREAM/ICE1 and SCREAM2 Specify Three Cell-State Transitional Steps Leading to Arabidopsis Stomatal Differentiation. *the Plant Cell Online*, **20**(7), 1775–1785.
- Karunarathna, N. L., Wang, H., Harloff, H.-J., Jiang, L., and Jung, C. (2020). Elevating

- seed oil content in a polyploid crop by induced mutations in seed fatty acid reducer genes. *Plant Biotechnology Journal* (DOI: 10.1111/pbi.13381).
- Kearns, E. V. and Assmann, S. M. (1993). The guard cell-environment connection. *Plant Physiology*, **102**(3), 711.
- Keegstra, K. (2010). Plant cell walls. *Plant physiology*, **154**(2), 483–486.
- Kikuta, Y., Ueda, H., Takahashi, M., Mitsumori, T., Yamada, G., Sakamori, K., Takeda, K., Furutani, S., Nakayama, K., Katsuda, Y., Hatanaka, A., and Matsuda, K. (2012). Identification and characterization of a gdsl lipase-like protein that catalyzes the ester-forming reaction for pyrethrin biosynthesis in *tanacetum cinerariifolium*—a new target for plant protection. *The Plant Journal*, **71**(2), 183–193.
- Kim, H. G., Kwon, S. J., Jang, Y. J., Nam, M. H., Chung, J. H., Na, Y.-C., Guo, H., and Park, O. K. (2013). Gdsl lipase1 modulates plant immunity through feedback regulation of ethylene signaling. *Plant physiology*, **163**(4), 1776–1791.
- Kim, H. G., Kwon, S. J., Jang, Y. J., Chung, J. H., Nam, M. H., and Park, O. K. (2014). Gdsl lipase 1 regulates ethylene signaling and ethylene-associated systemic immunity in *arabidopsis*. *FEBS letters*, **588**(9), 1652–1658.
- Kim, T.-H., Böhmer, M., Hu, H., Nishimura, N., and Schroeder, J. I. (2010). Guard cell signal transduction network: advances in understanding abscisic acid, co₂, and ca²⁺ signaling. *Annual review of plant biology*, **61**, 561–591.
- Knox, J. P. (2008). Revealing the structural and functional diversity of plant cell walls. *Current opinion in plant biology*, **11** 3, 308–13.

- Kwon, S. J., Jin, H. C., Lee, S., Nam, M. H., Chung, J. H., Kwon, S. I., Ryu, C.-M., and Park, O. K. (2009). Gdsl lipase-like 1 regulates systemic resistance associated with ethylene signaling in arabidopsis. *The Plant Journal*, **58**(2), 235–245.
- Lai, C.-P., Huang, L.-M., Chen, L.-F. O., Chan, M.-T., and Shaw, J.-F. (2017). Genome-wide analysis of gdsl-type esterases/lipases in arabidopsis. *Plant molecular biology*, **95**(1-2), 181–197.
- Lampard, G. R., MacAlister, C. A., and Bergmann, D. C. (2008). Arabidopsis stomatal initiation is controlled by mapk-mediated regulation of the bhlh speechless. *Science*, **322**(5904), 1113–1116.
- Lampugnani, E. R., Khan, G. A., Somssich, M., and Persson, S. (2018). Building a plant cell wall at a glance. *Journal of Cell Science*, **131**(2), jcs207373.
- Larkin, J. C., Marks, M. D., Nadeau, J., and Sack, F. (1997). Epidermal cell fate and patterning in leaves. *The Plant Cell*, **9**(7), 1109.
- Lau, O. S. and Bergmann, D. C. (2012). Stomatal development : a plant ' s perspective on cell polarity , cell fate transitions and intercellular communication. **3692**, 3683–3692.
- Lau, O. S., Davies, K. A., Chang, J., Adrian, J., Rowe, M. H., Ballenger, C. E., and Bergmann, D. C. (2014). Direct roles of SPEECHLESS in the specification of stomatal self-renewing cells. *Science*, **345**(6204), 1605–1609.
- Lawson, T. and Morison, J. I. (2004). Stomatal function and physiology. In *The evolution of plant physiology*, pages 217–242. Elsevier.

- Lee, D. S., Kim, B. K., Kwon, S. J., Jin, H. C., and Park, O. K. (2009). Arabidopsis gds1 lipase 2 plays a role in pathogen defense via negative regulation of auxin signaling. *Biochemical and biophysical research communications*, **379**(4), 1038–1042.
- Levasseur, A. and Pontarotti, P. (2011). The role of duplications in the evolution of genomes highlights the need for evolutionary-based approaches in comparative genomics. *Biology direct*, **6**(1), 11.
- Li, P., Anumanthan, A., Gao, X.-G., Ilangovan, K., Suzara, V. V., Düzgüneş, N., and Renugopalakrishnan, V. (2007). Expression of recombinant proteins in pichia pastoris. *Applied biochemistry and biotechnology*, **142**(2), 105–124.
- Li, Y., Beisson, F., Pollard, M., and Ohlrogge, J. (2006). Oil content of arabidopsis seeds: the influence of seed anatomy, light and plant-to-plant variation. *Phytochemistry*, **67**(9), 904–915.
- Linder, B. and Raschke, K. (1992). A slow anion channel in guard cells, activating at large hyperpolarization, may be principal for stomatal closing. *FEBS letters*, **313**(1), 27–30.
- Liners, F. and Van Cutsem, P. (1992). Distribution of pectic polysaccharides throughout walls of suspension-cultured carrot cells. *Protoplasma*, **170**(1-2), 10–21.
- Liners, F., Letesson, J.-J., Didembourg, C., and Van Cutsem, P. (1989). Monoclonal antibodies against pectin: recognition of a conformation induced by calcium. *Plant physiology*, **91**(4), 1419–1424.
- Liners, F., Thibault, J.-F., and Van Cutsem, P. (1992). Influence of the degree of

- polymerization of oligogalacturonates and of esterification pattern of pectin on their recognition by monoclonal antibodies. *Plant physiology*, **99**(3), 1099–1104.
- Ling, H. (2008). Sequence analysis of gds1 lipase gene family in arabidopsis thaliana. *Pakistan Journal of Biological Sciences*, **11**(5), 763.
- MacAlister, C. A., Ohashi-Ito, K., and Bergmann, D. C. (2007). Transcription factor control of asymmetric cell divisions that establish the stomatal lineage. *Nature*, **445**(7127), 537–540.
- Matrosova, A., Bogireddi, H., Mateo-Peñas, A., Hashimoto-Sugimoto, M., Iba, K., Schroeder, J. I., and Israelsson-Nordström, M. (2015). The ht 1 protein kinase is essential for red light-induced stomatal opening and genetically interacts with ost 1 in red light and co 2-induced stomatal movement responses. *New Phytologist*, **208**(4), 1126–1137.
- McCarthy, E. W., Mohamed, A., and Litt, A. (2015). Functional divergence of *apetala1* and *fruitfull* is due to changes in both regulation and coding sequence. *Frontiers in plant science*, **6**, 1076.
- Meckel, T., Gall, L., Semrau, S., Homann, U., and Thiel, G. (2007). Guard cells elongate: relationship of volume and surface area during stomatal movement. *Biophysical journal*, **92**(3), 1072–1080.
- Melotto, M., Zhang, L., Oblessuc, P. R., and He, S. Y. (2017). Stomatal defense a decade later. *Plant Physiology*, **174**(2), 561–571.
- Merced, A. and Renzaglia, K. S. (2018). Contrasting pectin polymers in guard cell walls

- of arabidopsis and the hornwort phaeoceros reflect physiological differences. *Annals of botany*, **123**(4), 579–585.
- Miklešević, G., Salopek-Sondi, B., and Luić, M. (2009). Arab-1, a GDSL Lipase from the Model Plant, *Arabidopsis thaliana* (L.) Heynh. *Croatica chemica acta*, **82**(2), 439–447.
- Miransari, M. and Smith, D. (2014). Plant hormones and seed germination. *Environmental and Experimental Botany*, **99**, 110–121.
- Mølgaard, A., Kauppinen, S., and Larsen, S. (2000). Rhamnogalacturonan acylesterase elucidates the structure and function of a new family of hydrolases. *Structure*, **8**(4), 373–383.
- Montesinos, J. C., Langhans, M., Sturm, S., Hillmer, S., Aniento, F., Robinson, D. G., and Marcote, M. J. (2013). Putative p24 complexes in arabidopsis contain members of the delta and beta subfamilies and cycle in the early secretory pathway. *Journal of experimental botany*, **64**(11), 3147–3167.
- Müller, K., Levesque-Tremblay, G., Bartels, S., Weitbrecht, K., Wormit, A., Usadel, B., Haughn, G., and Kermode, A. R. (2013). Demethylesterification of cell wall pectins in arabidopsis plays a role in seed germination. *Plant Physiology*, **161**(1), 305–316.
- Munemasa, S., Hauser, F., Park, J., Waadt, R., Brandt, B., and Schroeder, J. I. (2015). Mechanisms of abscisic acid-mediated control of stomatal aperture. *Current opinion in plant biology*, **28**, 154–162.
- Naranjo, M. Á., Forment, J., Roldán, M., Serrano, R., and Vicente, O. (2006). Overex-

- pression of *Arabidopsis thaliana* LTL1 , a salt-induced gene encoding a GDSL-motif lipase , increases salt tolerance in yeast and transgenic plants. **29**(10), 1890–1900.
- Neill, S., Desikan, R., and Hancock, J. (2002). Hydrogen peroxide signalling. *Current opinion in plant biology*, **5**(5), 388–395.
- Nonogaki, H. (2019). Seed germination and dormancy: The classic story, new puzzles, and evolution. *Journal of integrative plant biology*, **61**(5), 541–563.
- Oh, I. S., Park, A. R., Bae, M. S., Kwon, S. J., Kim, Y. S., Lee, J. E., Kang, N. Y., Lee, S., Cheong, H., and Park, O. K. (2005). Secretome analysis reveals an arabidopsis lipase involved in defense against *alternaria brassicicola*. *The Plant Cell*, **17**(10), 2832–2847.
- Ohashi-Ito, K. and Bergmann, D. C. (2006). *Arabidopsis fama* controls the final proliferation/differentiation switch during stomatal development. *The Plant Cell*, **18**(10), 2493–2505.
- Panchy, N., Lehti-Shiu, M., and Shiu, S.-H. (2016). Evolution of gene duplication in plants. *Plant physiology*, **171**(4), 2294–2316.
- Pandey, S., Zhang, W., and Assmann, S. M. (2007). Roles of ion channels and transporters in guard cell signal transduction. *FEBS Letters*, **581**(12), 2325–2336.
- Papanatsiou, M., Petersen, J., Henderson, L., Wang, Y., Christie, J., and Blatt, M. (2019). Optogenetic manipulation of stomatal kinetics improves carbon assimilation, water use, and growth. *Science*, **363**(6434), 1456–1459.
- Park, J.-J., Jin, P., Yoon, J., Yang, J.-I., Jeong, H. J., Ranathunge, K., Schreiber, L., Franke, R., Lee, I.-J., and An, G. (2010). Mutation in wilted dwarf and lethal 1

- (wd11) causes abnormal cuticle formation and rapid water loss in rice. *Plant molecular biology*, **74**(1-2), 91–103.
- Pauly, M., Gille, S., Liu, L., Mansoori, N., de Souza, A., Schultink, A., and Xiong, G. (2013). Hemicellulose biosynthesis. *Planta*, **238**(4), 627–642.
- Pautov, A., Yakovleva, O., Krylova, E., and Gussarova, G. (2016). Large lipid droplets in leaf epidermis of angiosperms. *Flora*, **219**, 62–67.
- Pautov, A., Bauer, S., Ivanova, O., Krylova, E., Sapach, Y., and Gussarova, G. (2017). Role of the outer stomatal ledges in the mechanics of guard cell movements. *Trees*, **31**(1), 125–135.
- Pearcy, R. and Pfitsch, W. A. (1995). The consequences of sunflecks for photosynthesis and growth of forest understory plants. In *Ecophysiology of photosynthesis*, pages 343–359. Springer.
- Pickett, F. B. and Meeks-Wagner, D. R. (1995). Seeing double: appreciating genetic redundancy. *The Plant Cell*, **7**(9), 1347.
- Pillitteri, L. J., Sloan, D. B., Bogenschutz, N. L., and Torii, K. U. (2007). Termination of asymmetric cell division and differentiation of stomata. *Nature*, **445**(7127), 501.
- Rao, I. M. and Anderson, L. E. (1983). Light and stomatal metabolism: I. possible involvement of light modulation of enzymes in stomatal movement. *Plant physiology*, **71**(3), 451–455.
- Raschke, K. (1975). Stomatal action. *Annual Review of Plant Physiology*, **26**(1), 309–340.

- Ren, C. and Kermode, A. R. (2000). An increase in pectin methyl esterase activity accompanies dormancy breakage and germination of yellow cedar seeds. *Plant Physiology*, **124**(1), 231–242.
- Renny-Byfield, S. and Wendel, J. F. (2014). Doubling down on genomes: polyploidy and crop plants. *American journal of botany*, **101**(10), 1711–1725.
- Riemann, M., Gutjahr, C., Korte, A., Danger, B., Muramatsu, T., Bayer, U., Waller, F., Furuya, M., and Nick, P. (2007). Ger1, a gds1 motif-encoding gene from rice is a novel early light-and jasmonate-induced gene. *Plant Biology*, **9**(01), 32–40.
- Rose, J. K. and Lee, S.-J. (2010). Straying off the highway: trafficking of secreted plant proteins and complexity in the plant cell wall proteome. *Plant Physiology*, **153**(2), 433–436.
- Rui, Y. and Anderson, C. T. (2016). Functional analysis of cellulose and xyloglucan in the walls of stomatal guard cells of *Arabidopsis thaliana*. *Plant Physiology*, **170**(3), 1398–1419.
- Rui, Y., Xiao, C., Yi, H., Kandemir, B., Wang, J. Z., Puri, V. M., and Anderson, C. T. (2017). POLYGALACTURONASE INVOLVED IN EXPANSION3 Functions in Seedling Development, Rosette Growth, and Stomatal Dynamics in *Arabidopsis thaliana*. *The Plant Cell*, **29**(10), 2413–2432.
- Rui, Y., Chen, Y., Kandemir, B., Yi, H., Wang, J. Z., Puri, V. M., and Anderson, C. T. (2018). Balancing Strength and Flexibility: How the Synthesis, Organization, and Modification of Guard Cell Walls Govern Stomatal Development and Dynamics. *Frontiers in Plant Science*, **9**, 1202.

- Sampathkumar, A., Krupinski, P., Wightman, R., Milani, P., Berquand, A., Boudaoud, A., Hamant, O., Jönsson, H., and Meyerowitz, E. M. (2014). Subcellular and supra-cellular mechanical stress prescribes cytoskeleton behavior in arabidopsis cotyledon pavement cells. *Elife*, **3**, e01967.
- Scheler, C., Weitbrecht, K., Pearce, S. P., Hampstead, A., Büttner-Mainik, A., Lee, K. J., Voegelé, A., Oracz, K., Dekkers, B. J., Wang, X., Wood, A. T., Bentsink, L., King, J. R., Knox, J. P., Holdsworth, M. J., Müller, K., and Leubner-Metzger, G. (2015). Promotion of testa rupture during garden cress germination involves seed compartment-specific expression and activity of pectin methylesterases. *Plant Physiology*, **167**(1), 200–215.
- Scheller, H. V. and Ulvskov, P. (2010). Hemicelluloses. *Annual review of plant biology*, **61**, 263–289.
- Schindelin, J., Arganda-Carreras, I., Frise, E., Kaynig, V., Longair, M., Pietzsch, T., Preibisch, S., Rueden, C., Saalfeld, S., Schmid, B., *et al.* (2012). Fiji: an open-source platform for biological-image analysis. *Nature methods*, **9**(7), 676–682.
- Schrag, J. D., Li, Y., Wu, S., and Cygler, M. (1991). Ser-his-glu triad forms the catalytic site of the lipase from *geotrichum candidum*. *Nature*, **351**(6329), 761.
- Schultink, A., Naylor, D., Dama, M., and Pauly, M. (2015). The Role of the Plant-Specific ALTERED XYLOGLUCAN9 Protein in Arabidopsis Cell Wall Polysaccharide *O*-Acetylation. *Plant Physiology*, **167**(4), 1271–1283.
- Schumann, T., Paul, S., Melzer, M., Dörmann, P., and Jahns, P. (2017). Plant growth under natural light conditions provides highly flexible short-term acclimation properties toward high light stress. *Frontiers in plant science*, **8**, 681.

- Schwendener, S. (1881). *Über Bau und Mechanik der Spaltöffnungen*. Buchdr. d. Königl. Akad. d. Wiss.
- Sechet, J., Frey, A., Effroy-Cuzzi, D., Berger, A., Perreau, F., Cueff, G., Charif, D., Rajjou, L., Mouille, G., North, H. M., and Marion-Poll, A. (2016). Xyloglucan metabolism differentially impacts the cell wall characteristics of the endosperm and embryo during arabidopsis seed germination. *Plant physiology*, **170**(3), 1367–1380.
- Shtein, I., Shelef, Y., Marom, Z., Zelinger, E., Schwartz, A., Popper, Z. A., Bar-On, B., and Harpaz-Saad, S. (2017). Stomatal cell wall composition: distinctive structural patterns associated with different phylogenetic groups. *Annals of botany*, **119**(6), 1021–1033.
- Simmons, A. R. and Bergmann, D. C. (2016). Transcriptional control of cell fate in the stomatal lineage. *Current Opinion in Plant Biology*, **29**, 1–8.
- Somerville, C. R., Bauer, S., Brininstool, G., Facette, M. R., Hamann, T., Milne, J., Osborne, E., Paredez, A., Persson, S., Raab, T., Vorwerk, S., and Youngs, H. (2004). Toward a systems approach to understanding plant cell walls. *Science*, **306** 5705, 2206–11.
- Soriano, M., Diaz, P., and Pastor, F. I. J. (2006). Pectate lyase c from bacillus subtilis: a novel endo-cleaving enzyme with activity on highly methylated pectin. *Microbiology*, **152**(3), 617–625.
- Sticklen, M. B. (2008). Plant genetic engineering for biofuel production: towards affordable cellulosic ethanol. *Nature Reviews Genetics*, **9**(6), 433–443.

- Sugano, S. S., Shimada, T., Imai, Y., Okawa, K., Tamai, A., Mori, M., and Hara-Nishimura, I. (2010). Stomagen positively regulates stomatal density in Arabidopsis. *Nature*, **463**(7278), 241–244.
- Sukhumsirchart, W., Kawanishi, S., Deesukon, W., Chansiri, K., Kawasaki, H., and Sakamoto, T. (2009). Purification, characterization, and overexpression of thermophilic pectate lyase of bacillus sp. rn1 isolated from a hot spring in thailand. *Bio-science, biotechnology, and biochemistry*, **73**(2), 268–273.
- Swain, S. M., Reid, J. B., and Kamiya, Y. (1997). Gibberellins are required for embryo growth and seed development in pea. *The Plant Journal*, **12**(6), 1329–1338.
- Takada, S. and Jurgens, G. (2007). Transcriptional regulation of epidermal cell fate in the Arabidopsis embryo. *Development*, **134**(6), 1141–1150.
- Takahashi, K., Shimada, T., Kondo, M., Tamai, A., Mori, M., Nishimura, M., and Hara-Nishimura, I. (2009). Ectopic expression of an esterase, which is a candidate for the unidentified plant cutinase, causes cuticular defects in arabidopsis thaliana. *Plant and cell physiology*, **51**(1), 123–131.
- Turner, N. C. and Graniti, A. (1969). Fusicoccin: a fungal toxin that opens stomata. *Nature*, **223**(5210), 1070–1071.
- Updegraff, E. P., Zhao, F., and Preuss, D. (2009). The extracellular lipase exl4 is required for efficient hydration of arabidopsis pollen. *Sexual plant reproduction*, **22**(3), 197–204.
- Upton, C. (1995). A new family of lipolytic enzymes? *Trends Biochem. Sci.*, **20**, 178–179.

- Verger, R. (1997). 'Interfacial activation' of lipases: facts and artifacts. *Trends in Biotechnology*, **15**(1), 32–38.
- Verhertbruggen, Y., Marcus, S. E., Haeger, A., Ordaz-Ortiz, J. J., and Knox, J. P. (2009). An extended set of monoclonal antibodies to pectic homogalacturonan. *Carbohydrate Research*, **344**(14), 1858–1862.
- Violet-Chabrand, S. R., Matthews, J. S., McAusland, L., Blatt, M. R., Griffiths, H., and Lawson, T. (2017). Temporal dynamics of stomatal behavior: modeling and implications for photosynthesis and water use. *Plant physiology*, **174**(2), 603–613.
- Vico, G., Manzoni, S., Palmroth, S., and Katul, G. (2011). Effects of stomatal delays on the economics of leaf gas exchange under intermittent light regimes. *New Phytologist*, **192**(3), 640–652.
- Vishal, B. and Kumar, P. P. (2018). Regulation of seed germination and abiotic stresses by gibberellins and abscisic acid. *Frontiers in plant science*, **9**, 838.
- Volokita, M., Rosilio-Brami, T., Rivkin, N., and Zik, M. (2010). Combining comparative sequence and genomic data to ascertain phylogenetic relationships and explore the evolution of the large gDSL-lipase family in land plants. *Molecular biology and evolution*, **28**(1), 551–565.
- Von Mohl, H. (1856). Welche Ursachen bewirken die Erweiterung und Verengung der Spaltöffnungen. *Botanische Zeitung*, **14**, 697–704.
- Way, D. A. and Pearcy, R. W. (2012). Sunflecks in trees and forests: from photosynthetic physiology to global change biology. *Tree physiology*, **32**(9), 1066–1081.

- Webb, A. A. (2003). The physiology of circadian rhythms in plants. *New Phytologist*, **160**(2), 281–303.
- Wilkinson, H. (1979). The plant surface (mainly leaf). *Anatomy of the Dicotyledons*, **1**, 97–165.
- Winkler, F., d’Arcy, A., and Hunziker, W. (1990). Structure of human pancreatic lipase. *Nature*, **343**(6260), 771.
- Wolf, S., Rausch, T., and Greiner, S. (2009). The n-terminal pro region mediates retention of unprocessed type-i pme in the golgi apparatus. *The Plant Journal*, **58**(3), 361–375.
- Wolf, S., Mravec, J., Greiner, S., Mouille, G., and Höfte, H. (2012). Plant cell wall homeostasis is mediated by brassinosteroid feedback signaling. *Current Biology*, **22**(18), 1732–1737.
- Woolfenden, H. C., Baillie, A. L., Gray, J. E., Hobbs, J. K., Morris, R. J., and Fleming, A. J. (2018). Models and Mechanisms of Stomatal Mechanics. *Trends in Plant Science*, **23**(9), 1–11.
- Yi, H., Chen, Y., Wang, J. Z., Puri, V. M., and Anderson, C. T. (2019). The stomatal flexoskeleton: How the biomechanics of guard cell walls animate an elastic pressure vessel. *Journal of experimental botany*, **70**(14), 3561–3572.
- Zablackis, E., Huang, J., Muller, B., Darvill, A. G., and Albersheim, P. (1995). Characterization of the cell-wall polysaccharides of arabidopsis thaliana leaves. *Plant physiology*, **107**(4), 1129–1138.

- Zeiger, E., Farquhar, G. D., and Cowan, I. (1987). *Stomatal function*. Stanford University Press.
- Zeng, W., Melotto, M., and He, S. Y. (2010). Plant stomata: a checkpoint of host immunity and pathogen virulence. *Current opinion in biotechnology*, **21**(5), 599–603.
- Zhang, B., Zhang, L., Li, F., Zhang, D., Liu, X., Wang, H., Xu, Z., Chu, C., and Zhou, Y. (2017). Control of secondary cell wall patterning involves xylan deacetylation by a gds1 esterase. *Nature plants*, **3**(3), 17017.
- Zhang, X., Zhang, L., Dong, F., Gao, J., Galbraith, D. W., and Song, C.-P. (2001). Hydrogen peroxide is involved in abscisic acid-induced stomatal closure in vicia faba. *Plant physiology*, **126**(4), 1438–1448.
- Zhang, Z., Ober, J. A., and Kliebenstein, D. J. (2006). The gene controlling the quantitative trait locus epithiospecifier modifier1 alters glucosinolate hydrolysis and insect resistance in arabidopsis. *The Plant Cell*, **18**(6), 1524–1536.
- Zhao, H., Ma, B., Duan, K.-X., Li, X.-K., Lu, X., Yin, C.-C., Tao, J.-J., Wei, W., Zhang, W.-K., Xin, P., *et al.* (2020). The gds1 lipase mhz11 modulates ethylene signaling in rice roots. *The Plant Cell*.
- Zhao, L. and Sack, F. D. (1999). Ultrastructure of stomatal development in Arabidopsis (Brassicaceae) leaves. *American Journal of Botany*, **86**(7), 929–939.
- Zhu, J., Lou, Y., Shi, Q.-S., Zhang, S., Zhou, W.-T., Yang, J., Zhang, C., Yao, X.-Z., Xu, T., Liu, J.-L., *et al.* (2020). Slowing development restores the fertility of thermo-sensitive male-sterile plant lines. *Nature Plants*, pages 1–8.

Zoulias, N., Harrison, E. L., Casson, S. A., and Gray, J. E. (2018). Molecular control of stomatal development. *Biochemical Journal*, **475**(2), 441 LP – 454.

Curriculum Vitae

Ritwika Kar

Balduin-Helm-Str.81
D-82256 Fürstfeldbruck
Email: ritwika.bot2012@gmail.com

Currently

2015– **PhD Biology**, Eberhard Karls University, Tübingen.

Thesis: Functional characterization of two genes of the GDSL hydrolase gene family. (Under supervision of Prof. Dr. Christopher Grefen, Molecular and cellular botany, Ruhr-University, Bochum.)

Education

2012-2014 MPhil Botany, Department of Botany, University of Delhi, India.
Thesis: A novel strategy for specific silencing of multiple loci using artificial miRNA

2010-2012 MSc Botany, Department of Botany, University of Delhi, India.
Thesis: RNA Editing: an overview

2007-2010 BSc (Hons.) Botany, Department of Botany, Visva-Bharati University, India.

Selected research skills

Molecular Biology Techniques. Gateway system of gene cloning, Gibson assembly cloning techniques, CRISPR-Cas technology, Transformation of *E.coli* and *A. tumefaciens*, Site-directed mutagenesis

Tissue culture tools and techniques. Maintenance of aseptic conditions and handling of laminar airflow, knowledge of different media used in tissue culture studies

Protein chemistry. PAGE, Co-immunoprecipitation assay (Co-IP), Yeast-2-hybrids,

mating-based split-ubiquitin system (mbSUS)

RNA chemistry. RNA isolation techniques, real-time quantitative reverse transcription PCR (qRT-PCR), co-infiltration assay

Microscopy. Differential interference contrast (DIC) microscope, confocal laser scanning microscope (Leica TCS SP8), scanning electron microscopy (Zeiss Sigma VP FE-SEM)

Dry lab. ImageJ (Fiji), Leica, LICOR, JMP, Affinity Designer, biostatistics, **R**, LaTeX, Microsoft Office

Conferences and meeting

Plant Growth and Form Symposium, Heidelberg (2019)

Regio-Plant-Science Meeting, Tübingen (2018)

Dynamics of Plant Development and Evolution, PSC Symposium, ETH, Zurich (2017)

3rd Summer academy in plant molecular biology, ZMBP, University of Tuebingen (2017)

2nd Summer academy in plant molecular biology, ZMBP, University of Tuebingen (2015)

Miscellaneous

2015 **Research assistance**, Center for Plant Molecular Biology (ZMBP), Tübingen, Germany

2014 **Research assistance**, Indian Institute of Science Education and Research (IISER), Kolkata, India

2011 **Summer-school Internship**, School of Life Science, Jawaharlal Nehru University, Delhi, India

Scholarships

Non-net MPhil scholarship (UGC)

Indira Gandhi Single Girl-child scholarships for post-graduation study (UGC)

Languages

Bengali (mother tongue), English (fluent), German (intermediate), Hindi (fluent)

Publications

Franz-Sebastian Krah, Ulf Büntgen, Hanno Schäfer, Jörg Müller, Carrie Andrew, Lynne Boddy, Jeffrey Diez, Simon Egli, Robert Freckleton, Alan C Gange, Rune Halvorsen, Einar Heegaard, Antje Heideroth, Christoph Heibl, Jacob Heilmann-Clausen, Klaus Høiland, **Ritwika Kar**, Håvard Kauserud, Paul M Kirk, Thomas W Kuyper, Irmgard Krisai-Greilhuber, Jenni Norden, Phillip Papastefanou, Beatrice Senn-Irlet, Claus Bässler. European mushroom assemblages are darker in cold climates. 2019:10(1):2890 *Nature Communications*.

Shuping Xing, Dietmar Gerald Mehlhorn, Niklas Wallmeroth, Lisa Yasmin Asseck, **Ritwika Kar**, Alessa Voss, Philipp Denninger, Vanessa Aphaia Fiona Schmidt, Markus Schwarzländer, York-Dieter Stierhof, Guido Grossmann and Christopher Grefen. Loss of GET pathway orthologs in *Arabidopsis thaliana* causes root hair growth defects and affects SNARE abundance. 2017:114:E1544–E1553 *Proceedings of the National Academy of Sciences*.